Wettability/surface potential control on different interfaces and their applications on optical and electrochemical devices

異種界面における濡れ性と表面エネルギーの制御と

光学および電気化学素子への応用

July 2016

DOCTOR OF ENGINEERING

WEI XING

TOYOHASHI UNIVERSITY OF TECHNOLOGY

別紙４ （課程博士）

Department 電気・電子情報 工学 専攻	Student ID Number 学籍番号	第 115406 号	Supervisors 指導教員	松田　厚範 教授 武藤　浩行 教授
Applicant's name 氏名	Wei Xing			

Abstract
論文内容の要旨　（博士）

Title of Thesis 博士学位論文名	Wettability/surface potential control on different interfaces and their applications on optical and electrochemical devices （異種界面における濡れ性と表面エネルギーの制御と光学および電気化学素子への応用）

(Approx. 800 words)
(要旨　1,200 字程度)

Being an attractive topic, surface wettability/potential has been well studied in the last two decades. Controlling of the wettability and surface potential has many areas of applications such as bio-fouling, liquid lens fabrication and the electrophoretic deposition. In this work, by analyzing and using different principles, controllability of surface wettability/potential by physical and chemical methods has been studied. The applications of surface wettability/potential control were expanded to make optical and electrical devices with higher performances.

In the first study, the wettability of Nafion film was found to have a time dependent: contact angle (CA) of a water droplet on the Nafion film was reduced from 149° to 134° within one minute. The change in CA could be explained from the molecular structure of Nafion, which is a fluoropolymer material containing long branches with sulfonic group endings. When the interface changed from air/Nafion into water/Nafion, according to the surface potential, these branches became upright or bent over. This causes a "flip-flop" wettability change phenomenon. To study the effect of the applied voltage on this phenomenon, we used multilayered thin films of 67 nm Nafion / 150 nm TiO_2 / 110 nm Pt coated on silicon wafer. The results showed that when a water droplet was biased by positive DC voltage higher than 2V, owing to the strong attraction force towards the sulfonic top groups, the unwinding of the branched chains in the polymer film becomes enhanced. A decrease in CA to a minimum level of 20° can be obtained in two minutes. Conversely, a negative DC voltage inhibits the "flip-flop" property by giving repulsive force towards the sulfonic groups.

In the second study, electrowetting property on dielectric multilayered thin films was investigated. Similar to "flip-flop" wetting, electrowetting is a modification of the wetting properties on a solid surface by using an applied voltage. Teflon was used as the hydrophobic layer in this study, owing to its remarkable CA reversibility. Multilayered thin films of 50 nm Teflon / 160 nm TiO_2 / 80 nm Al_2O_3 / on ITO glass were used as the solid phase. The TiO_2 layer was added to increase dielectric constant for a larger CA changing range. Meanwhile, the Al_2O_3 layer was used to give high dielectric strength to prevent breakdown. Sol-gel and chemical solution dip coating processes were used to prepare each layer. By measuring the CAs with different applied voltages,

we found that the case of negative DC is more stable than the positive DC. In addition, by testing the leakage current during the electrowetting, the most suitable working voltage was obtained to be -10 V DC. In dodecane atmosphere, the CA of a water droplet on Teflon surface was controlled from 155° to 67° by biasing with -10 V DC without any electric breakdown. Furthermore, when the same multilayers were coated on the inside of a glass tube, the curvature of the water-oil interface could be adjusted by the applied voltage and due to the different refractive indices of water and oil, light passing through the interface can be converged or diverged depending on the curvature. By this principle we designed and assembled a liquid focusing lens driven by electrowetting with a diameter of 4 mm. The performance of the liquid lens was tested based on its range of focusing lengths, response time, and life time. The results showed that by increasing the voltage from 0 V to -10 V, the focal length changed from -2 mm to +10 mm, with its numerical aperture changed from 0.21 to 1.38. The lens had a quick response time of less than 100 ms and it was still stable after 1800 loading periods.

In the final study, on dye-sensitized solar cells (DSSCs), we prepared silver nanoparticles (Ag NPs) with high Zeta-potential and improved a method of making Ag NPs / TiO_2 nanotubes (TNTs) composite, by electrophoretic deposition (EPD). Ag NPs with an average size of 25 nm were modified by carboxy methylcellulose on their surfaces to obtain a high Zeta-potential of -43.3 mV. TNT arrays with a thickness of 13 μm were grown by anodizing Ti foils. EPD was employed to fill the TNT arrays with Ag NPs. A combination of +2 V DC and square waved 4 V AC with a frequency of 1 Hz proved to be the most effective applied voltage for EPD according to the results obtained by quantitative analysis of deposited Ag NPs. Also, an acetone vapor pretreatment was invented to replace the air in the TNTs before the EPD process. Back illuminated DSSCs were fabricated with the TNT arrays with different EPD time. After the TNT arrays were filled by Ag NPs using 30 min EPD time, the efficiency of DSSCs increased from 3.70% to 5.01% due to the surface plasmon resonance effect. However, the efficiency decreased to 4.62% with excess Ag NPs deposition when the EPD time was increased to 60 min.

The results obtained in this thesis are useful for controlling the wettability of the solid surfaces, which contributes for the designing and fabricating new optical and electrochemical devices.

Tables of Contents

Acknowledgement

Foremost, I would like to express my sincere gratitude to my advisor Prof. Atsunori Matsuda for the continuous support of my master study and research, for his patience, motivation, enthusiasm, and immense knowledge. His guidance helped me all the time of research and study. I could not have imagined having a better advisor and mentor for my doctor study.

Besides my advisor, I would like to thank other two instructors in our laboratory: Prof. Hiroyuki Muto and Dr. Go Kawamura for their encouragement, insightful comments, and kind supports.

Also I would like to thank all the members in our laboratory, not only for the help in study and research but also for treating me as a family member. I would like to thank all the professors and staff members in Toyohashi University of Technology, for every exciting lecture and kind guidance.

During three years, my wife always supports me overseas. It is from her where I got power to overcome every difficulty in a foreign country.

Last but not the least, I would like to thank my parents, for giving birth to me at the first place and supporting me spiritually throughout my life.

Dedication

My respect and thanks go to all the scientific and technical workers. It is because of their selfless contributions and sacrifices, that our lives are getting better and better day by day.

Chapter 1
General Introduction

Study on surface/interface science started serval decades ago. It is a study on phenomena at the interface between two or three phases (gas, solid, and liquid). It is also an interdisciplinary field containing applied physics, material science and chemical engineering. By discovering the theory of interface phenomena such as wettability, surface tension/energy, adsorption and reunite/coagulation, many new technologies have been developed and being severed in our everyday life like detergent, artificial rainfall, painting, and wastewater treatment. The most convictive example is a polymer named polytetrafluoroethylene, also being called PTFE. Depending on its unique fluorinated polymer structure which provides a quite low surface energy, PTFE is now widely used as a waterproof coating. Overall, the research on interface science has important meanings for all industry fields.

As an attractive topic, a study on wettability and surface potential has been well improved in the last two decades. Controlling technologies for of the wettability and surface-potential can be served in lots of applications such as bio-fouling, liquid lens fabrication, and the electrophoretic deposition (EPD). In this study, some phenomena of wettability change were discussed. A "flip-flop" function on a fluoropolymer with sulfo groups (Nafion) film has been demonstrated and

investigated Furthermore, this function was controlled by an applied DC voltage. Then, a focus-adjustable liquid lens was prepared using this wettability controllable function. On the other hand, by giving silver nanoparticles (Ag NPs) with high surface-potential, the NPs became suitable for EPD process to fill in TiO_2 nanotubes (TNTs). Owing to that, the performance of Dye-Sensitized Solar Cells (DSSCs) was obviously improved.

The topics of this thesis are summarized as follows:

1. Observation and characterization of the "flip-flop" effect of the Nafion film were carried out. By measuring the water contact angles on the film, the "flip-flop" phenomenon was proved to be controllable by an applied electric field.

2. Electrowetting on dielectric was studied with sol-gel coated multilayered films. By monitoring the leakage current, the stable working voltage was decided. A focal liquid lens driven by electrowetting was fabricated and its performance has been investigated.

3. By making silver nanoparticles with high Zeta potential, they were deposited into TiO_2 nanotubes with EPD to form a nano-composite layer. This nano-composite layer showed improved optic-electric performance in DSSCs.

This thesis is divided into 4 chapters as a follows:

Chapter 1:

Background and contents of this thesis

Chapter 2:

In this chapter, the wettability of Nafion film was found to have a time dependence. In air, contact angle of a water droplet on Nafion film reduced from 101° to 62° in one minutes. When being immersed in water, the film showed a remarkable oleophobicity. The reason could be explained from the structure of Nafion, which is a sulfonated tetrafluoroethylene based fluoropolymer-copolymer. When the film is moved to air from water surrounding, or to water from air surrounding, these branches became upright by bending. So that the wettability changed by the flip-flop phenomenon. What's more, by giving an applied voltage lower than -3 V DC the flip-flop could be completely prohibited.

Chapter 3:

In this chapter, similar to the flip-flop phenomenon, the wettability could be controlled by an applied voltage, even on a Teflon surface. Here, multilayered thin films of 50 nm Teflon / 160 nm TiO_2 / 80 nm Al_2O_3 / on an ITO (indium tin oxide) glass have been used as the solid surface, to both

increase the dielectric strength and dielectric constant. The contact angle of a water droplet on that surface could be controlled from 155° to 67° by -10 V DC without breakdown. Using the same multilayer coated inside a glass tube (inner diameter: 4 mm), the curvature of the water-oil interface could be controlled by an applied voltage. Due to the different refractive indices of water and oil, light passing through the interface could be focused like a lens. When the voltage increased from 0 V to -10 V, the focal length changed from -2 mm to infinity then to 10 mm.

Chapter 4:

In this chapter, by using stabilizing agent of carboxy methylcellulose during the preparation, Ag NPs with strong surface potential of -43 mV were prepared. As high surface potential provides high driving force during the EPD, by using DC 2V + AC 4V as an applied voltage, Ag NPs with such a high surface potential were successfully filled into TiO_2 nanotube arrays. These nano-composite material showed good performance on light harvest. DSSCs made by the Ag NPs filled TiO_2 nanotube arrays gave 5.01% efficiency while it was only 3.07% without Ag NPs.

Finally, the general conclusion is described.

Chapter 2
Controllable Flip-flop phenomenon on Nafion film

2.1 Introduction

2.1.1 Wettability and Young's Equation

As mentioned in the 1st chapter, there are many nature phenomena which can be explained by the study of surface wettability. First systematic study on the surface wetting situation can be traced back to year 1805 when Young's equation was first announced by Thomas Young, an English polymath and physician. Now it is the most fundamental and important theory on wettability. In the theory, the wettability of a liquid droplet on a solid surface is characterized by its contact angle (CA=θ), which is the angle at where the liquid–vapor interface meets the solid–liquid interface [2-1]. Depending on CAs, wetting states are classified to two situations: When $0° < \theta < 90°$, the droplet can spread on the solid surface, indicating that this kind of solid is wettable by this liquid; meanwhile; when $90° \leq \theta < 180°$, the droplet holds the shape of an over half-spherical. It means the solid surface has poor wettability on this kind of liquid. For water, wettable surfaces are called hydrophilic surface. Non-wettable surfaces are called hydrophobic surface. [Fig. 2-1]. For extreme conditions, super hydrophobic surfaces have water contact angles greater than 150°. Meanwhile, super hydrophilic surfaces have water contact angles less than 10° [2-2~5].

On the dynamics analysis, the wetting process can be considered as the gas phase attached on the solid surface being replaced by the liquid phase. The driving force during the wetting is deemed to be the work of adhesion (W_a). It is defined as the loss of Helmholtz free energy caused by the contacting of two surfaces and the interaction between them:

$$W_a = \gamma_1 + \gamma_2 - \gamma_{12}$$

-Eq. 2-1

Here γ_1 and γ_2 are different surface tension respectively, γ_{12} is surface tension between two phases. When a droplet on a solid surface in gas atmosphere, the work of adhesion between solid-liquid is:

$$W_a = \gamma_s + \gamma_{lv} - \gamma_{sl} = W_{slv}$$

-Eq.2-2

Here γ_s, γ_{lv} and γ_{sl} are surface tensions of solid phase, liquid-gas phase and solid-liquid phases, respectively.

Using the work of adhesion to evaluate the wettability is absolute strict. However, the surface tension of solid phase cannot be easily measured by common ways. So, as follows, another method on deductive calculation of CAs became widely used, showing in [Fig. 2-2]: When a solid surface is wetted by a droplet at state conditions, there is a contact angle, (CA=θ). Then if the droplet has a tiny movement, making the area where the solid is covered by liquid phase increased:

$$\Delta A = 2\pi R dR$$

Thus there comes another CA, θ'. The surface free energy changes:

$$\Delta G^s = 2\pi R dR(\gamma_{sl} - \gamma_{sv}) + 2\pi R dR\gamma_{lv}\cos\theta'$$

Because: $\theta' = \theta - \Delta\theta$:

$$\Delta G^s = 2\pi R dR[\gamma_{sl} - \gamma_{sv} + \gamma_{lv}\cos(\theta - \Delta\theta)]$$

-Eq.2-3

When it reached equilibrium:

$$\lim_{dR \to 0} \frac{\Delta G^s}{2\pi R dR} = 0$$

Here: $dR \to 0$, $\Delta\theta \to 0$, $\theta' \to \theta$. So it becomes:

$$\gamma_{sl} - \gamma_{sv} + \gamma_{lv}\cos\theta = 0$$

Or:

$$\cos\theta = \frac{\gamma_{sl} - \gamma_{sv}}{\gamma_{lv}}$$

-Eq.2-4

Eq.2-4 is the famous **Young's equation**. γ_{sl}, γ_{sv} and γ_{lv} are surface tensions of solid-liquid, solid-gas and liquid-gas interface, respectively. It exposits the relationship between CA and surfaces tensions when an ideal solid surface is wetting by a liquid droplet. When different kinds of liquids were dripped on a certain solid surface, the one which has higher γ_{lv} shows higher CA. For example, the mercury droplets always

show sphere shape even on a piece of glass while glass can be easily wetted by water (Surface tension against air, mercury: 485.2, H_2O: 71.97, dyn/cm, 20°C). On the other hand, for the same liquid droplets, it means a solid surface with lower surface tension always has a higher CA. Such as some fluoropolymer, like polytetrafluoroethylene (PTFE), water droplets slip off from it easily. Nowadays, it is widely used on the waterproofing work such as non-stick cooking spray, self-cleaning windows, etc.

2.1.2　Nafion film and its "flip-flop" phenomenon

Our wettability study in this chapter is mainly on a material named "Nafion". Being known as a typical ion exchange material, Nafion is a kind of sulfonated tetrafluoroethylene based fluoropolymer-copolymer. It was first discovered by Du Pont© in 1960s. The full name of Nafion is called "tetrafluoroethylene-perfluoro-3, 6-dioxa-4-methyl-7-octenesulfonic acid copolymer". Fig.2-3 gives the molecular structure of Nafion. Its "fluoropolymer-copolymer" structure can be considered that a long mean chain of tetrafluoroethylene carrying lots of branches of fluoropolymer. Meanwhile, at each top of the branch, there is a top group of sulfonate. This special structure gives Nafion many unique properties such as high conductivity on protons and many other cations. The chains of fluorinated polymer provide a commendable chemical corrosion resistance. Also, as one of fluoric polymer family, Nafion has a relatively high working temperature around 190 °C. According to its remarkable properties, Nafion is now widely serving in the area of fuel cells, surface treatment of metals, and batteries [2-6~9].

On the other hand, Nafion has special tunable wettability which can be changed under different conductions, this phenomenon was named "flip-flop type coating" [2-10~12]. In general, it means that a water droplet would have a high CA at the moment when it was dripped on the Nafion film. However, as time goes on, the CA decreased which means that the

surface turns from hydrophobic into hydrophilic. This unique phenomenon can be explained by its fluoric- sulfonate structure. As showing in Fig 2-4, naturally, when being exposed in the air, the branches in the polymer were banded and messy crossed, so that the sulfonic groups are curling down inside the chains. Thus, the surface exposed on the air is almost fluorinated alkyl groups. It exhibits that surface is hydrophobic, Fig.2-4 (a). So as a water droplet just drips on the surface, the droplet has a high contact angle at that moment, Fig.2-4 (b). However, as time goes on, the sulfonic top groups are being ionized. As we know, comparing with fluorinated main chain, the ionized sulfonic top groups have stronger affinity to water. Thus, the negative charges make the top of branched chains become hydrophilic. Because of the attractive force to the water molecules, the branched chains are disengaged from crossed condition and lifted up. Thereupon, the surface energy increases and the contact angle accordingly decreases, Fig.2-4 (c).

Theoretically, sulfonic top groups in Nafion are anionic in water. That means the "flip-flop" phenomenon might be controllable by some external effects such as electro field. This chapter is a study by using an applied voltage loading to the droplet on Nafion film to control the "flip-flop" property. By giving different voltage to the water droplet, the phenomenon can be enhanced of even counteracted.

2.2 Experimental

2.1.1 Thin films coating

Si wafer <101> was used to be the substrate. Before being used, all the pieces of Si wafer substrates have to be cleaned to remove the organic residue and inclusion on the surface. They were immersed into hot Radio Corporation of America(RCA) solution at 70°C for 15min. RCA solution is one kind of common washing liquor made of H_2O_2 (30 wt% aqueous solution) : NH_3 (28 wt% aqueous solution) : IEW(ion exchanged water) = 1:1:5 in vol ratio. After that, the substrates have been washed by IEW and blow-dried by nitrogen gas for further use.

To apply an electric field on the droplet, we need a conductive base layer to be the counter electrode. Pt layer with a thickness of 110 nm has been deposited by magnetron sputtering at working current of 15 mA for 10 min. Then the sputtered specimens were heated at 400°C for 1h to remove the inner force of the metal layer and enhance the adhesion to the Si substrate for the coming coating procedures.

Since its difficult to form a thick Nafion layer by dip coating from its aqueous solution (10wt%). If just coating directly on the Pt conductive layer, electric breakdown would occur easily and the film would be unrecoverable damaged. So that, dielectric inner layer is necessary to be the insulator inside. Titanium oxide (TiO_2) was finally decided to be the inner layer for its superior dielectric properties and easy preparation by sol-

gel method[Fig.2-5] [2-13,14]. In order to make TiO_2 sol, titanium tetraisopropoxide (TTIP) and ethyl alcohol (EtOH) are used to be the starting material and solvent, respectively. First of all, TTIP was mixed with EtOH for 10 min by an electromagnetic stirrer. Then, EtOH with 3.6 wt% hydrochloric acid (HCl) mixture was added into the solution drop by drop. Because TTIP is very sensitive to water, it would precipitate easily at high pH level. The existence of acid would raise the stability of the sol, so that it can be kept as liquid form for enough time. After stirring for 1h, stable and homogeneous sol was prepared. The total molar ratio of each chemicals was $TTIP : HCl : EtOH : H_2O = 1: 0.4 : 24 : 0.75$. The dip coating was carried out on the Pt-coated Si wafer, with a withdraw speed of 1 mm/s. After that, heat treatment was taken in air atmosphere at 450°C for 1h, with a step preheat treatment of 10°C/min. All of the chemicals were produced from Wako©, Japan.

Above the as-coated films, a top layer of Nafion was formed from its 10wt% aqueous solution by dip coating at a with draw speed of 1 mm/s. Finally, the multilayered films were created after dried at 70°C for 1 h to remove all the solvent[Fig.2-6].

The thickness of each layer has been measured by field emission scanning electron microscope (FE-SEM, SU-8000, Hitachi©). Their crystal structures were tested by X-ray diffraction (XRD, UltimaIV   R185, Rigaku©). The surface roughness was measured by atomic force

microscope (AFM, OLS3500, Olympus©).

2.2.2　Contact angles measurements with applied voltage

To measure the contact angles during the droplet in being loaded by applied voltage, set-up of analyzers is showing in Fig.2-7: multilayered thin films coated on Si wafer was immersed into a dodecane filled transparent tank. Instead of gas phase of the air, we used dodecane to form an oil atmosphere. That was to prevent the evaporation of the water droplet because the tests needed a relatively long time. Then, a water droplet was dripped onto the Nafion film, followed by a thin Pt wire touched into the droplet to be the electrode. Meanwhile, the Pt layer underneath and the Pt wire were connected to a DC power supply. Then DC voltage was loaded to the droplet and the Pt layer by the AC/DC power source (EC750S, NF©). During the voltage applying, images of the droplet were taken by a CCD camera. The contact angles were finally measured by an analyzer named Drop Master 200, Kyowa©. To test the time dependence of "flip-flop" property, the measurement was set of taking photo for every second automatically.

We applied DC voltage of from 1 V to 2.5 V. Because we found when the voltage is higher than 2.5 V, water electrolysis occurred and hydrogen and oxygen bubbles appeared inside the droplet. The water electrolysis hints that the current is very high and the films are already being electric breakdown. That would destroy the multilayered films and should be prevented[2-18,19].

2.3 Results and discussion

2.3.1 Nafion films and nature flip-flop phenomenon

Cross section SEM image of coated multilayered thin films is given in Fig. 2-8. A Pt layer with thickness of 110 nm and a TiO_2 layer with thickness of 150 nm coated on Si wafer can be observed. The Nafion top layer is not clear from the image. The reason can be explained that Nafion is a polymer which is not electro-conductive. So that, when being illumined by the electron beam, it shrinks a lot or even be decomposed. In order to test the real thickness of Nafion layer, we directly coated it on the Si wafer by the same steps and measured it by ellipsometer (WVASE32, Woollam[©]). The result shows that our Nafion top layer should have a thickness of 67 nm.

Since the SEM is not available to test the roughness and surface morphology of the Nafion top layer, AFM was used instead and the result is given in Fig.2-10. With a scan area of 1 μm by 1 μm, the average roughness Ra is around 5.6 nm. At this low roughness level, the soild surface can be considered to be an ideal smooth surface. So that the effect of surface roughness to contact angle can be omitted [2-15~17].

In Fig.2-10, the CAs changing along time have been tested without any voltage applying. Inset images are the photos of droplet at different time. At the moment when a water droplet was just dripped on to the film, the contact angle was 149˚. Then, it decreases very fast at the beginning.

After 30 s, it decreased down to 136˚. That may because the branch chains of Nafion extended when being attached to water and the sulfonate top groups becomes ionized into $-SO_3^-$ which are hydrophilic. Due to the "flip-flop" effect, the ionized top groups make the surface become more wettable, so that the droplet extended on the solid Nafion film. New area where the water attached Nafion film would have the same "flip-flop" effect. That is why the CA needs around 60 s to reach stable level. However, the speed of contact angle changing becomes slow after 30 s. It has only decreased 2˚ after another 30 s. In this case, without any applied voltage loaded, the driving force is just the attraction between the sulfonic groups and the water molecules. By contrast, this interaction is not strong enough to lift up all the sulfonic groups. Much more driving energy is necessary to unwind all the branched chains to attract all the hydrophilic sulfonic groups on to the top of the Nafion surface.

2.3.2　Application voltage effects

　　We also studied how the "filp-flop" phenomenon expressed under different applied voltage. Fig.2-11(a) gives the contact angle changing during positive DC voltage loaded to the droplet. When the voltage is lower than 1.5V (filled circle and square), the contact angle decreasing is still very slow. However, when the voltage has been increased to 2V (empty rhombus), the contact angle has a sharp decrease from 124˚ to 60˚ in 60 s. Then it has been finally decreased to 20˚ after another minute. Afterwards, when the positive DC voltage rises to 2.5V (empty circle), the sharply dropping point has been brought forward to 20 s. Then as the loading goes on, the contact angle reduced to 20˚ in 120 s, too. As a result, it can be proved that when the positive voltage is being loaded, the "flip-flop" property of Nafion can be amplified [Fig.2-12. (a,b)]. The positive pole inside droplet supports a very strong attractive force to the sulfonic groups which are electronegative inside the water. The higher the voltage becomes, the faster the branched chains unwind and lift up.　At last, if all the sulfonic top groups have been attracted on to the surface, the surface energy reached its maximum. No possibility remains for the wettability to change more. Thus, the contact angle decreased down to the same value even the applied voltage is different. By contrast, when being loaded by negative DC voltage, Fig.2-11(b), the contact angle does not change a lot even the voltage increased to 2.5 V. Because the negative DC gives a repulsive force

to the sulfonic top groups. The free "flip-flop" has been inhibited [Fig.2-12. (c)]. When the voltage has been increased to 3V, the aqueous droplet becomes bubbling. That means the water is electrolyzed due to the dielectric breakdown of the films.

Another notice is that we found in this case, even the possitive polarity was being loaded at 1 V or 1.5 V [Fig.2-11(a)], the CAs did not change a lot. But according to the result of Fig.2-10, CA should decrease around 10 ˚ even without the possitive voltage to enhance the "flip-flop" phenomenon. We attribute the reason to the different branching condition of the Nafion layer. As a ploymer material, during it was being heated in the coating process, the branches and the main chains intertwine with each other. This effect would be very sensitive to the temprature, so that the error during the heat treatment such as non-uniform heating inside the oven may give the polymer with different crosslinking. Strong crosslink of the branches can not be easily unfasten by only the attraction from ionic sulfonic groups and water. So that higher driving energy such as applied voltage over 2V is necessary to unfasten the crosslinked branches and attract the sulfonic groups on to the surface to show "flip-flop" phenomenon.

2.4 Conclusion

On a multilayered thin films of Nafion/TiO$_2$/Pt/Si, free "flip-flop" property has been proved to be able to reduce the water contact angle from 149˚ to 134˚ in dodecane atmosphere. When the droplet is loaded by negative DC voltage higher than 2V, owing to the strong attraction force to the sulfonic top groups, the unwinding work of branched chains in the polymer film is being enhanced. The minimum contact angle can be decreased down to 20˚. Being the opposite, a negative DC voltage can inhibit the "flip-flop" property by giving repulsive force to the sulfonic top groups.
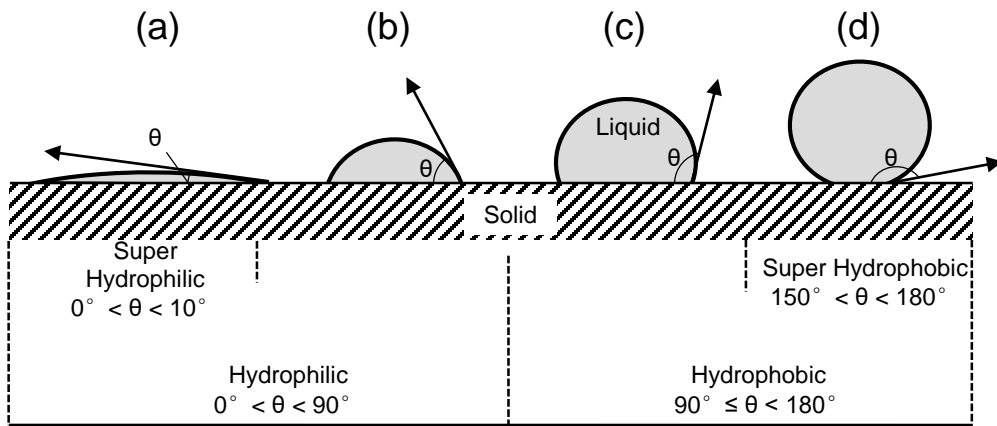
Fig. 2-1: Different wetting situations: (a) Super Hydrophilic, (b) Hydrophilic, (c) Hydrophobic, (d) Super Hydrophobic.
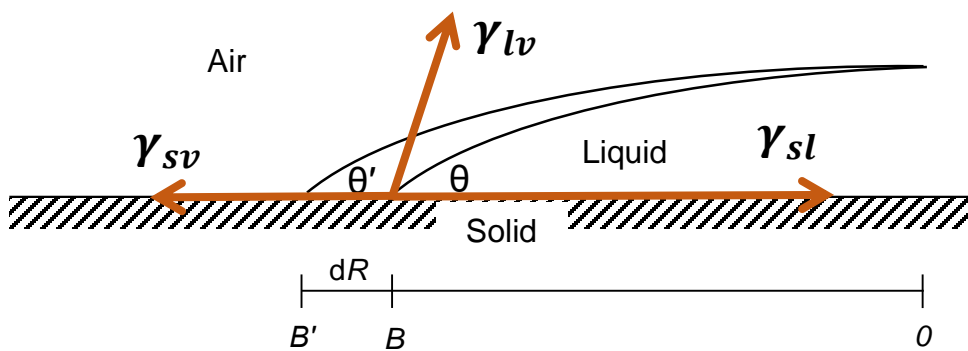

Fig. 2-2: Contact angle and surface tension.

Top sulfo group (hydrophilic)

branch (hydrophobic)

Main chain (hydrophobic)

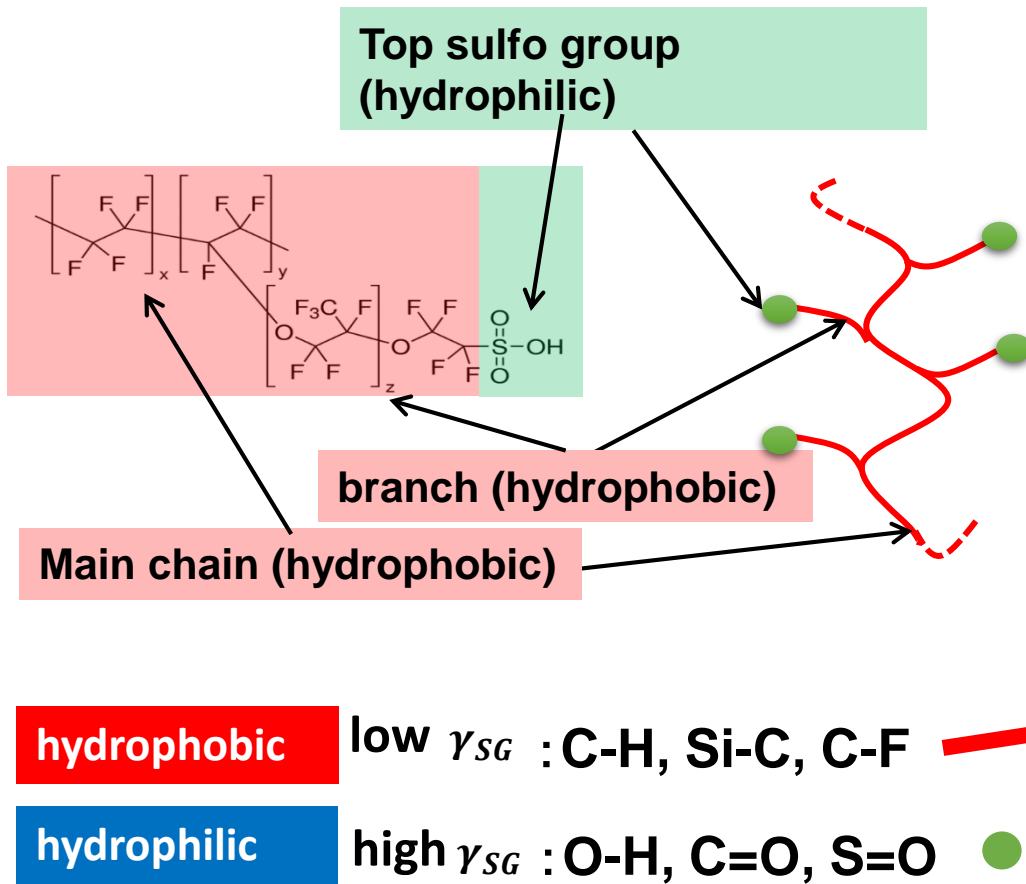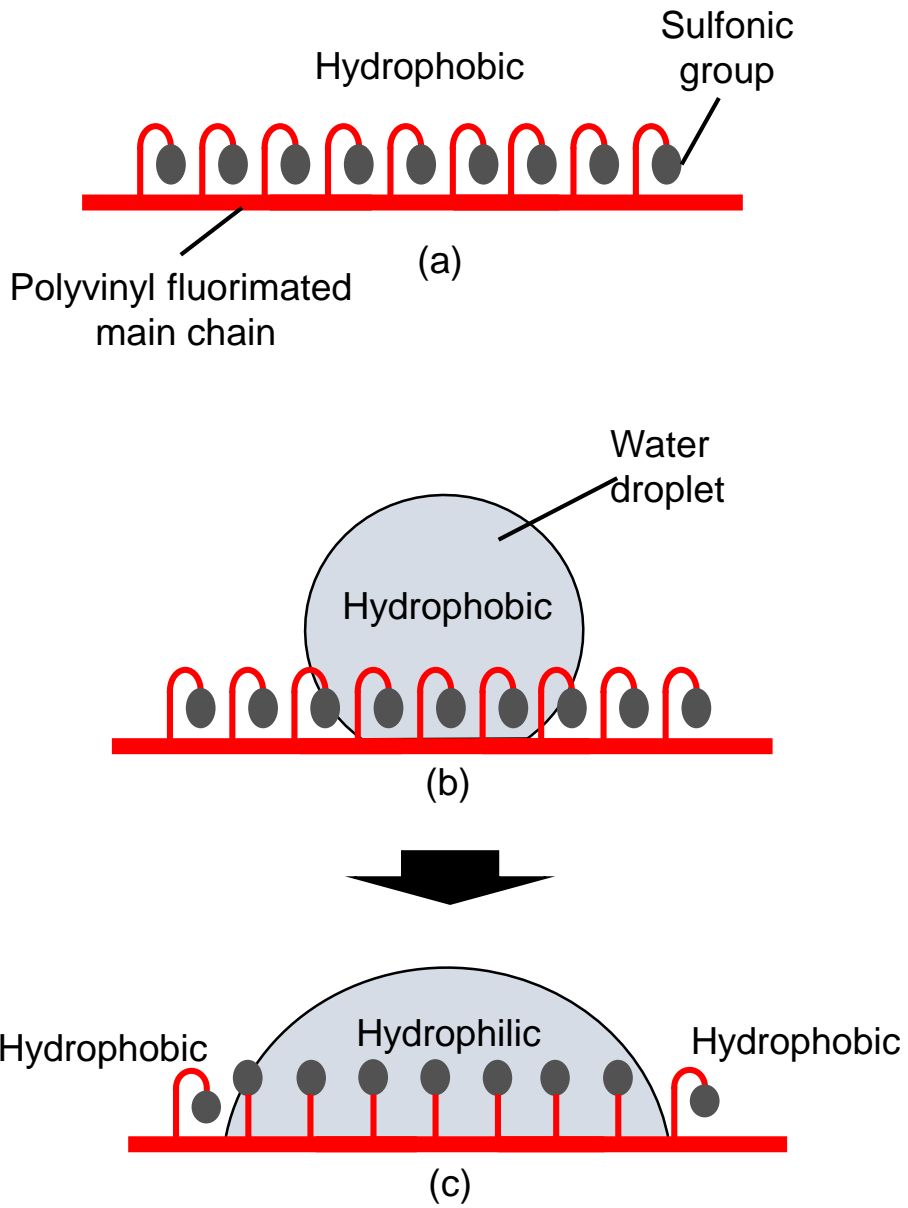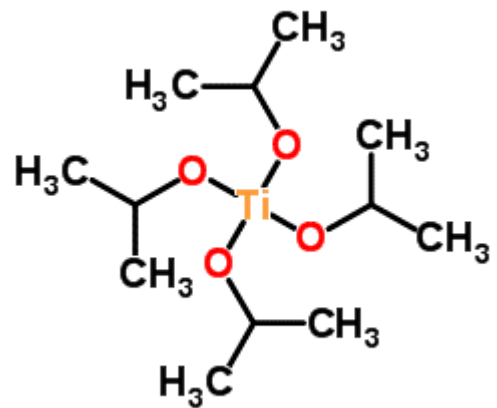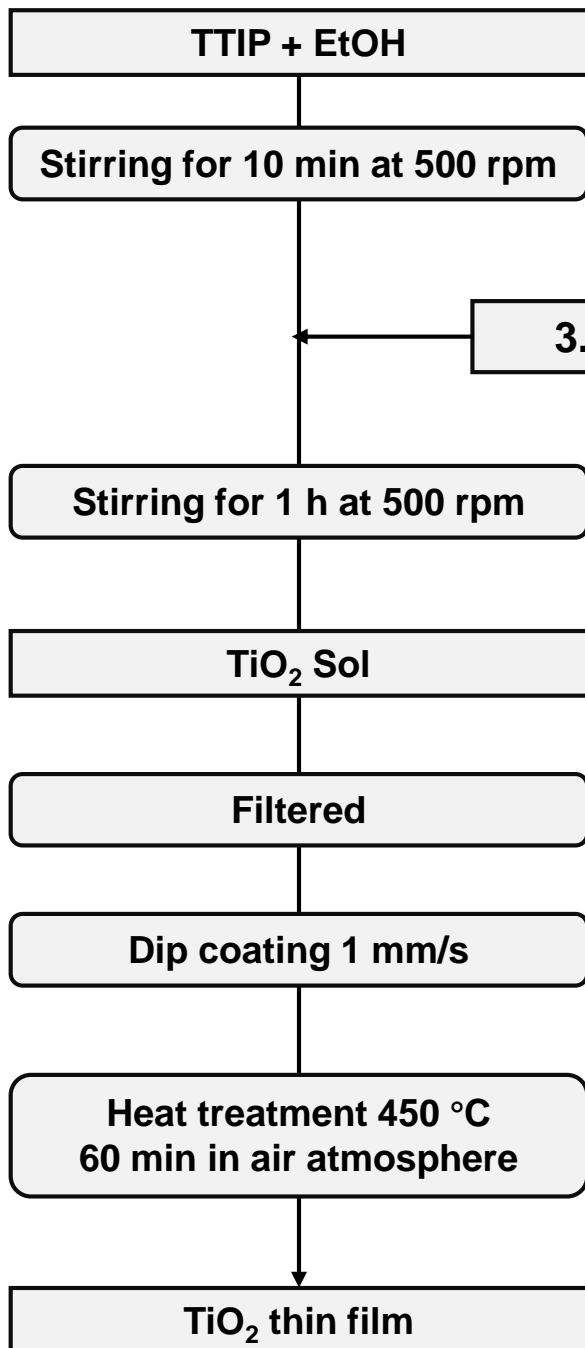| hydrophobic | low γ_{SG} : C-H, Si-C, C-F |
| hydrophilic | high γ_{SG} : O-H, C=O, S=O |

Fig. 2-3: Molecular structure of Nafion.

Fig.2-4: Schematic of flip-flip property, (a) in air; (b) upon water dropping; and (c) a moment after water dropping.

Fig. 2-5: Flow-chart of TiO$_2$ thin films formation prepared by sol-gel dip coating process with the molar ratio of TTIP : HCl : EtOH : H$_2$O = 1: 0.4 : 24 : 0.75.

```
┌─────────────────────────────────────────────┐
│          TiO₂ / Pt / Si wafer               │
└─────────────────────────────────────────────┘
                     │
╭─────────────────────────────────────────────╮
│          Dip coating 1 mm/s from            │
│     10 wt% Nafion aqueous solution          │
╰─────────────────────────────────────────────╯
                     │
╭─────────────────────────────────────────────╮
│   Dried at 70°C for 1 h in air atmosphere   │
╰─────────────────────────────────────────────╯
                     │
                     ▼
┌─────────────────────────────────────────────┐
│          Multilayered thin films            │
└─────────────────────────────────────────────┘
```
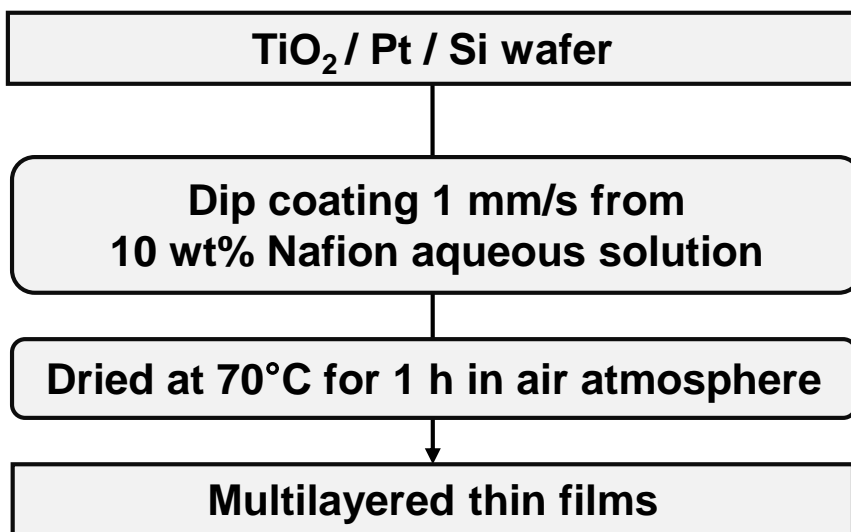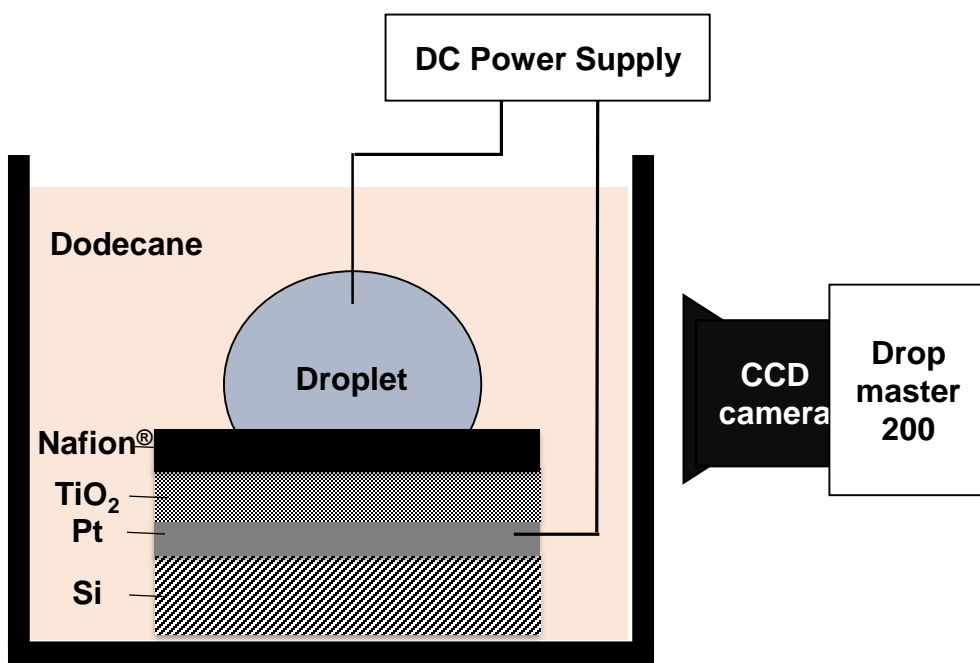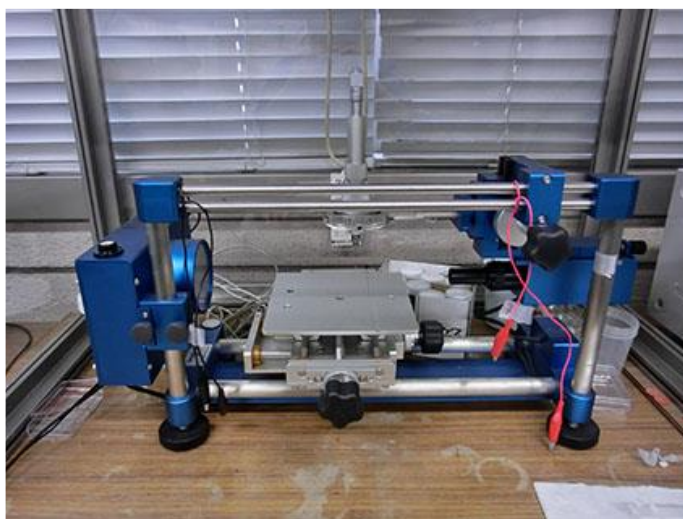
Fig. 2-6: Flow chart of the Nafion thin films preparation
coating on the top of TiO$_2$/Pt/Si wafer

(a)

(b)

Fig.2-7: (a) schematic of the contant angle analyzer set-up for a
water droplet in dodecane;
(b) Photo of Drop Master 200, Kyowa©.
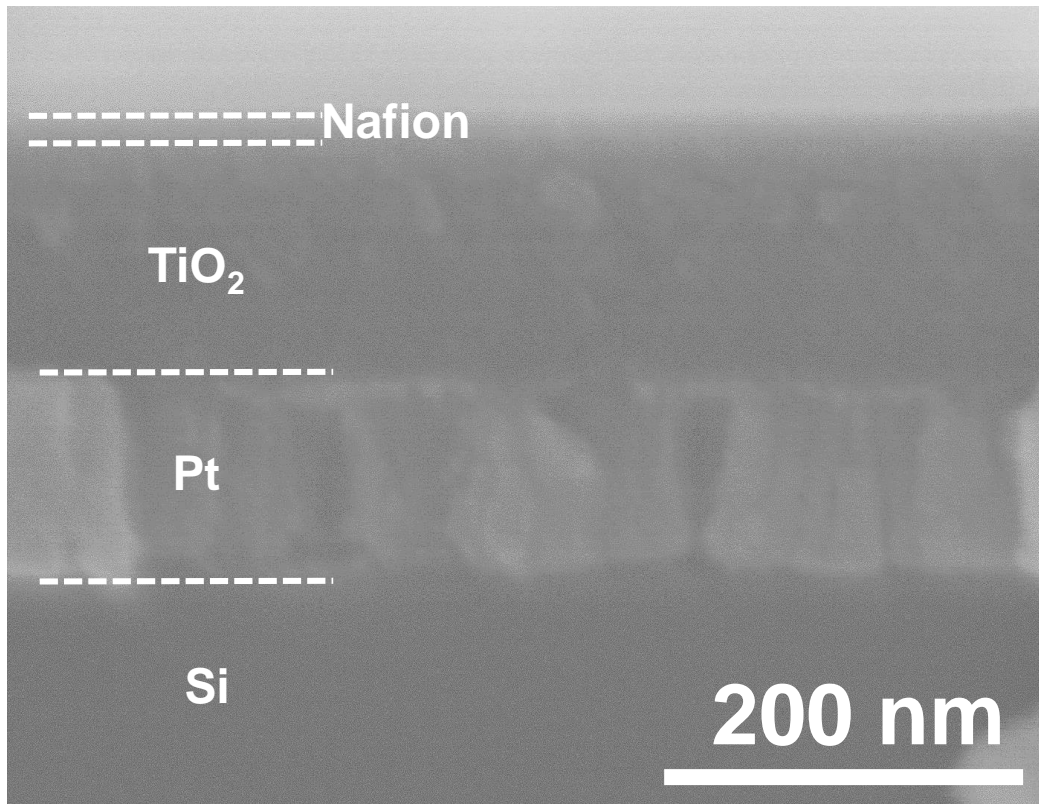
Fig.2-8: Cross section SEM image of a coated multilayered thin films.
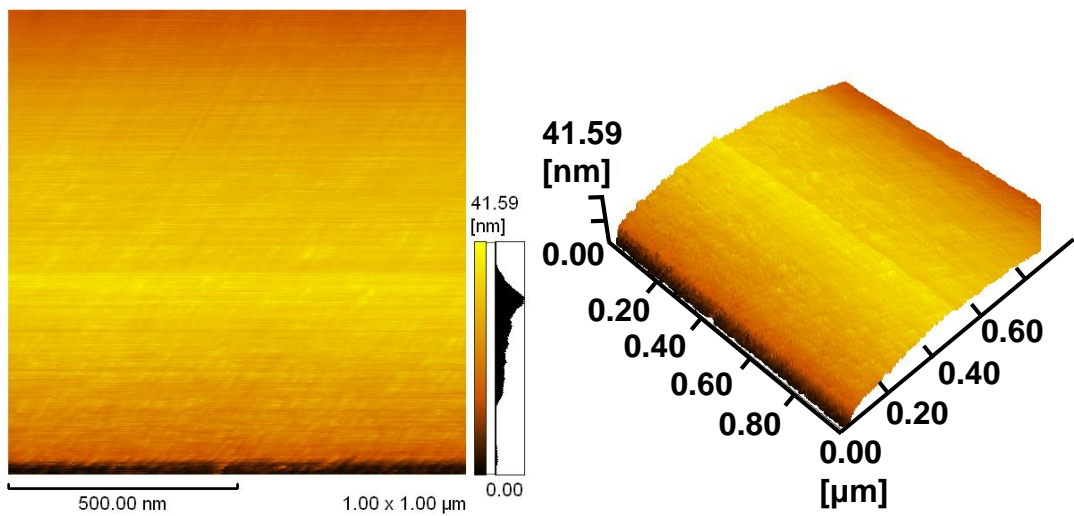
Length X	1000.00 [nm]
Length Y	1000.00 [nm]
Area	1000000.00 [nm²]
Ra	5.676 [nm]
Rz	41.423 [nm]

Fig.2-9: Atomic Force Microscopy(AFM) image of the coated Nafion surface.

Fig.2-10: Contact angles of water droplet on Nafion without voltage applied.

Fig.2-11: Contact angles loaded by DC applied voltage at diffferent polarities
of (a) positive; and (b) negative.

Fig.2-12: Schematic of Nafion branches, (a) without any loading and under different applied voltage of (b) positive DC; and (c) negative DC.

References of chapter 2

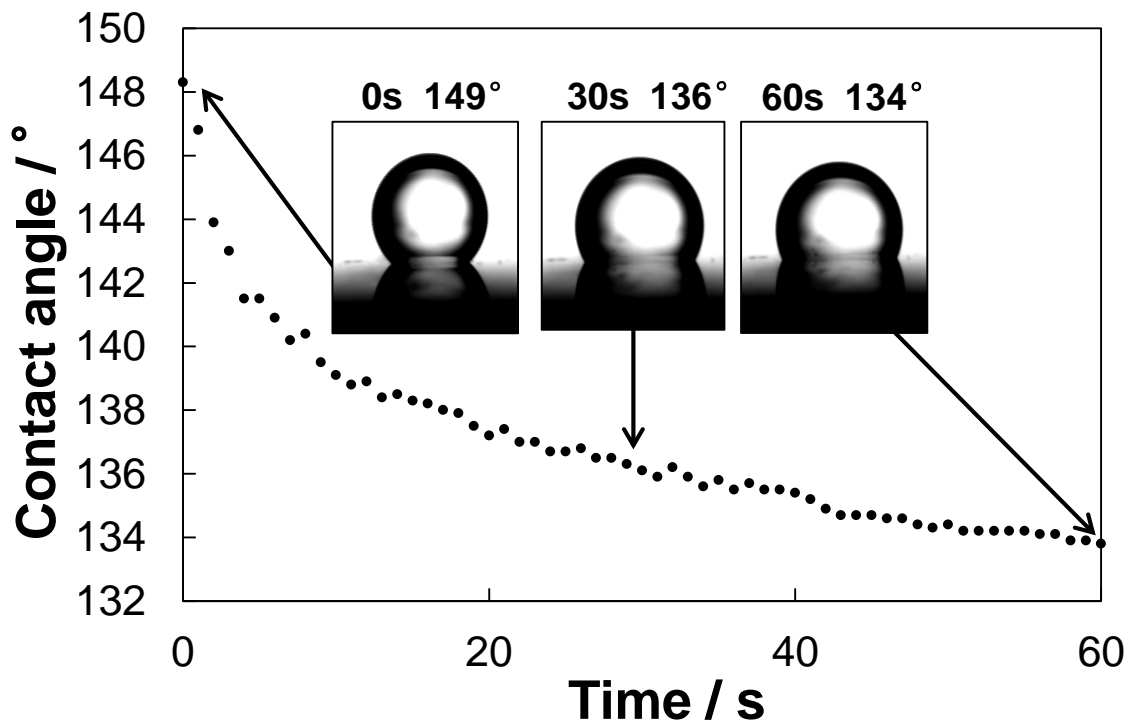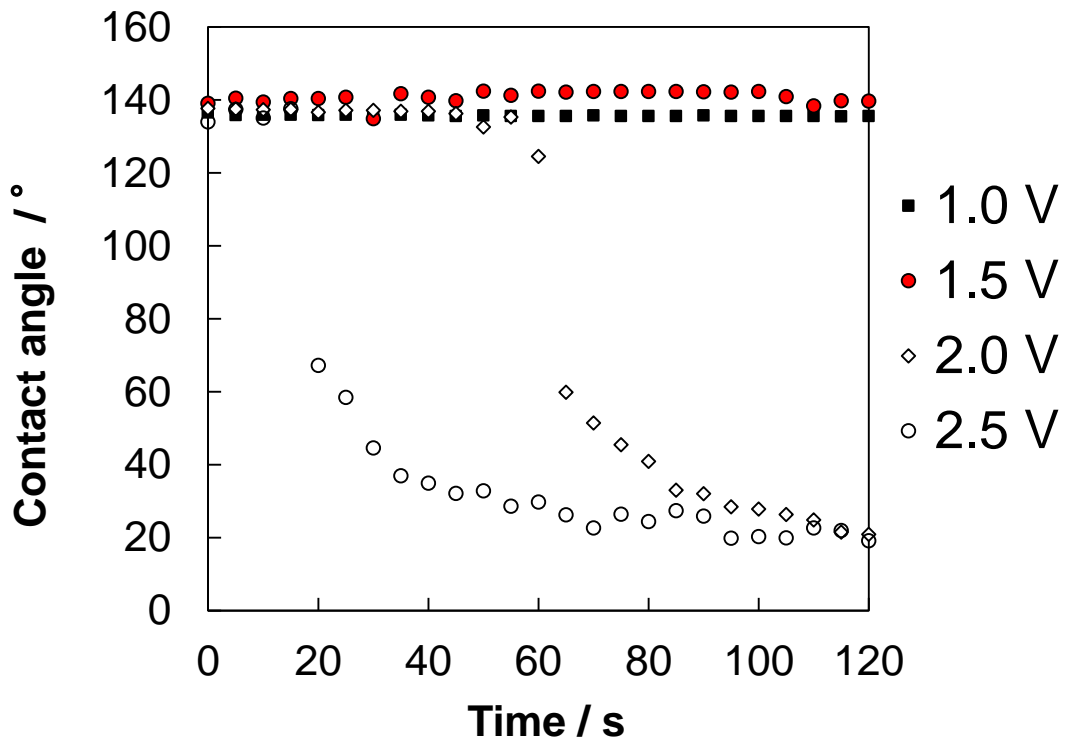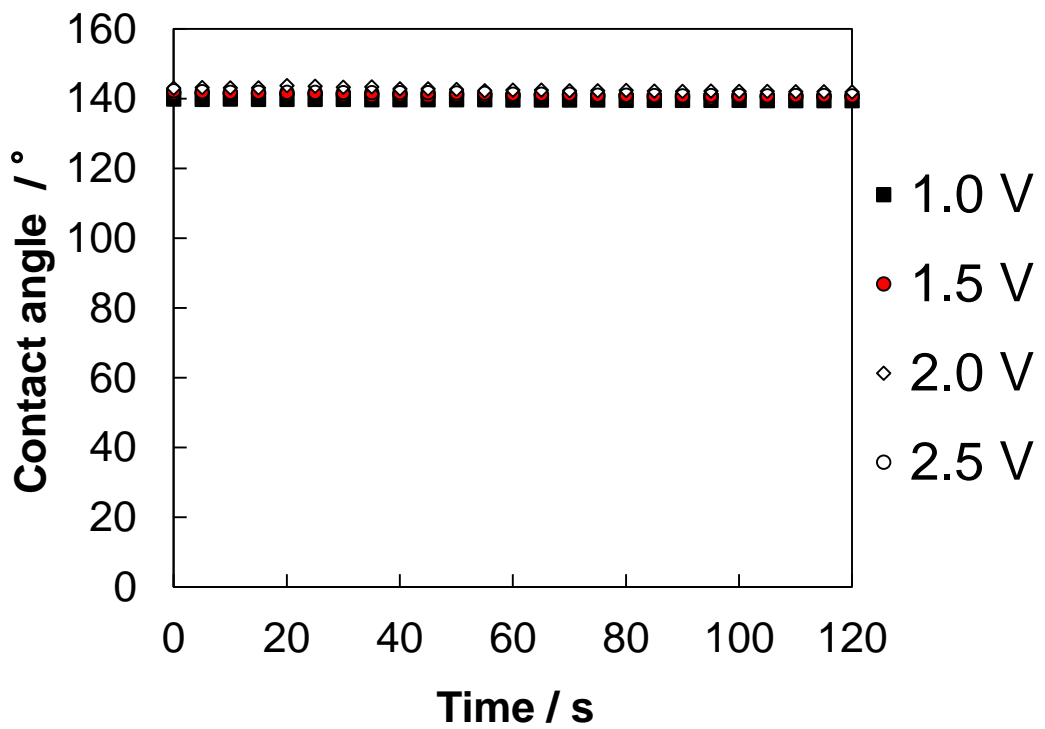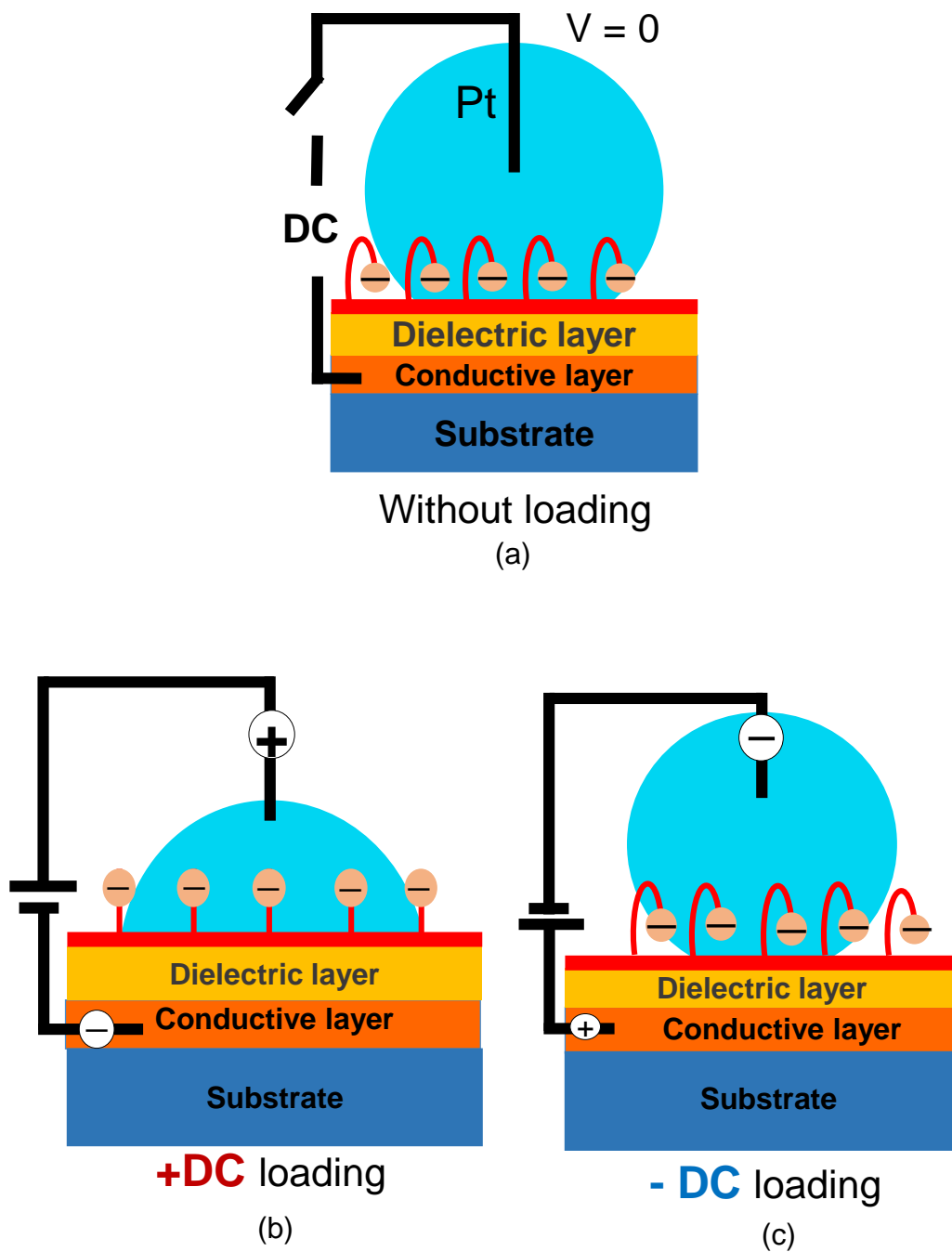| 2-1	Design of a Transparent Hydrophobic Coating, A. Nakajima, Journal of the Ceramic Society of Japan, 112, 533-540 (2004).
2-2	Perspective on Fluorocarbon Chemistry, D.M. Lemal, The Journal of Organic Chemistry, 69, 1-11 (2004).
2-3	Physical Chemistry of Surfaces, A.W. Adamson and A.P. Gast, 808 pages, ISBN: 978-0-471-14873-9, Wiley, USA (1997).
2-4	The Lowest Surface Free Energy Based on -CF$_3$ Alignment, T. Nishino, M. Meguro, K. Nakamae, M. Matsushita and Y. Ueda, Langmuir, 15, 4321-4323 (1999).
2-5	Contact Angles on Chemically Heterogeneous Surfaces, J.N. Israelachvili and M.L. Gee, Langmuir, 5, 288-289 (1989).
2-6	Recent Advances in Perfluorinated Ionomer Membranes: Structure, Properties and Applications, C.H. Wirguin, Journal of Membrane Science, 120, 1-33 (1996).
2-7	State of Understanding of Nafion, K.A. Mauritz and R.B. Moore, Chemical Reviews, 104, 4535–4585 (2004).
2-8	Proton and Water Transport in Nano-separated Polymer Membranes, K.D. Kreuer, M. Ise, A. Fuchs and J. Maier, Journal de Physique IV (Proceedings), 10, 279-281 (2000).
2-9	Organic Synthesis by Catalysis with Ion-Exchange Resins, G. Gelbard, Industrial & Engineering Chemistry Research, 44, 8468–8498 (2005).
2-10	Spontaneous Changes in Contact Angle of Water and Oil on Novel Flip–Flop-Type Hydrophobic Multilayer Coatings, G. Kawamura, T. Ema, H. Sakamoto, X. Wei, H. Muto and A. Matsuda, Applied Surface Science, 298, 142–146 (2014).
2-11	Synthesis and Surface Properties of Novel Fluoroalkylated Flip-Flop-Type Silane Coupling Agents, H. Sawada, Y. Ikematsu, T. Kawase and Y. Hayakawa, Langmuir, 12(15), 3529-3530 (1996).
2-12	Highly Hydrophobic Flip-Flop-Type Ultrathin Coating Films Prepared via Electrostatic Self-Assembly, Y. Daiko, K. Katagiri and A. Matsuda, Journal of Nanoscience and Nanotechnology, 9, 404-407 (2009).

2-13	Transparent Anatase Nanocomposite Films by the Sol-Gel Process at Low Temperatures, A. Matsuda, Y. Kotani, T. Kogure, M. Tatsumisago and T. Minami, Journal of the American Ceramic Society, 83, 229–231 (2000).
2-14	Structural Changes of Sol-Gel-Derived TiO_2–SiO_2 Coatings in an Environment of High Temperature and High Humidity, A. Matsuda, T. Kogure, Y. Matsuno, S. Katayama, T. Tsuno, N. Tohge and T. Minami, Journal of the American Ceramic Society, 76, 2899-2903 (1993).
2-15	Resistance of Solid Surfaces to Wetting By Water, R.N. Wenzel, Industrial & Engineering Chemistry Research, 28(8), 988-994 (1936).
2-16	Wettability of Porous Surfaces, A.N.D. Cassie and S. Baxter; Transactions of the Faraday Society, 40, 546-551 (1944).
2-17	Super-hydrophobic, Highly Adhesive, Polydimethylsiloxane(PDMS) Surfaces, M.M. Stanton, R.E. Ducker and J.C. MacDonald, Journal of Colloid and Interface Science, 367, 502-508 (2012).
2-18	Low Voltage Electrowetting-on-dielectric, H. Moon, S.K. Cho, R.L. Garrell, and C.J. Kim, Journal of Applied Physics, 92, 4089-4087 (2002).
2-19	Amorphous Fluoropolymers as Insulators for Reversible Low-voltage Electrowetting, E. Seyrat and R.A. Hayes, Journal of Applied Physics, 90, 1383-1386 (2001).

Chapter 3

Electrowetting and the fabrication of liquid lens

3.1 Introduction

3.1.1 Theory of reversible and low voltage electrowetting

Basically, electrowetting is a technology which can change the wettability of a solid surface, by loading an applied voltage to the conductive droplet on it. In 1875, announced by Gabriel Lippmann, the studies of electro-capillarity described that it was possible to manipulate the height of mercury by the application of a voltage between the mercury droplet and the electrode [3-1,2]. In the early 1990s, Bruno Berge suggested that a thin layer of insulating material between the solid metallic surface and conducting liquid droplet to overcome the electrolysis problem [3-3]. Today this system has come to be known as electrowetting on dielectric (EWOD).

The theory how an applied voltage drives a droplet is given in [Fig.3-1]. The electrowetting effect has been defined as "the change in solid-liquid contact angle due to an applied potential difference between the solid and the electrolyte". The phenomenon of electrowetting can be understood that the forces of the applied electric field change the surface tension [3-4,5]. When the voltage is loading to the droplet and the substrate, the free charges are gathering on the surface of the insulating layer, turns it into an analogous plate capacitor. Because of the gathering charges, the surface

tension of the solid-liquid interface changes:

$$\gamma_{sl}^* = \gamma_{sl} - \frac{CV^2}{2}$$

-Eq. 3-1

$$C = \frac{\varepsilon_r \varepsilon_0}{d}$$

-Eq. 3-2

Here, γ_{sl} is the original surface tension of solid-liquid; γ_{sl}^* is the surface tension after the applied voltage loaded; C is the capacitance of the film; V is the voltage applied. $\varepsilon_r \varepsilon_0$ is the dielectric constant of the insulating layer and d is its thickness. When it into Young's equation [Eq. 2-4], the cosine of contact angle ($cos\theta_v$) changes to:

$$cos\theta_v = \frac{\gamma_{sl} - \gamma_{sv} - \frac{CV^2}{2}}{\gamma_{lv}}$$

-Eq. 3-3

While, $\frac{\gamma_{sl} - \gamma_{sv}}{\gamma_{lv}}$ is the cosine of original CA ($cos\theta_0$). So we can get that the cosine of CA under the applied voltage:

$$cos\theta_v = cos\theta_0 - \frac{CV^2}{2\gamma_{lv}} = cos\theta_0 - \frac{\varepsilon_r \varepsilon_0 V^2}{2d\gamma_{lv}}$$

-Eq. 3-4

[Eq. 3-4] is called **Lippmann-Young's equation**. It interprets that applied voltage V is the only external cause which can change the CAs in EWOD. While the dielectric constant of the material of the insulating layer

and its thickness also decide the variation of CAs.

Technically, the CAs of a conductive liquid droplet on any dielectric solid surface can be controlled by applied electric field. However, when the applied voltage was removed, most of them cannot restore to the original state, which means the decrease of CAs is permanent. Because when the voltage loaded the surface energy has been turned to low level. Then after the voltage unloaded, the high adhesion force between liquid and solid became a great drag. Thus, when on a solid material which has a high surface tense, it is difficult for the contact angle to reverse [3-6]. Till now only few materials have been found to be adequate on reversible electrowetting. Cytop® and Teflon® are most commonly used. Both of them are amorphous fluoropolymers which have quite low surface tension. Relatively, it is easy for the liquid droplets to overcome the adhesion drag on these solid surfaces [3-7].

According to the Lippmann-Young's equation (-Eq.6), in order to have an obvious contact angle change, a high enough applied voltage is required. However, on a thin-film capacitor, it is easy to be electric breakdown when it is over loaded. The primary challenge for the EDOW technique is to reduce the required applied voltage. Among all the early studies, all of the EWOD systems require to be loaded with around 70 V to 120 V to drive the liquid droplet. That limited the application of EWOD in mobile devices. It is difficult to achieve the high voltage without the aid of

an external power source. However, researchers on low voltage EWOD have proved that, in comparison to a single dielectric layer, multilayered dielectric films lead to a lower required level of applied voltage to make the CAs have the same decrease [3-8,9]. Double-layered insulating film was introduced, with one layer of high dielectric strength (Si_3N_4, SiO_2, Al_2O_3, etc.) and another with a high dielectric constant (TiO_2, $Ba_xSr_{1-x}TiO_3$) [3-10~12]. So that, the electric breakdown can be prevented, also the whole system can still hold a high level on dielectric constant to apply enough surface charges when the voltage is loaded.

3.1.2 Application on liquid lens

EWOD has been utilized in several optical applications such as; reflection-type displays [3-13,14], smart windows [3-15] and liquid lens [3-16~19]. Among them, due to its quick response time, simple fabrication methods, forcing liquid lens driven by EWOD has significant potential to serve in micro-cameras instead of the traditional solid lens in our mobile devices. In recent years, some researchers have already designed different structures on the EWOD liquid lens. For example, by controlling the curvature of the water-oil interface between two transparent thin plates, Atsushi Takei created a micro focusing system which had a function on slanting view [3-17]. EDOW liquid lens can be also achieved on flexible polymer substrate such as polydimethylsiloxane (PDMS), as being reported in a paper by Chenhui Li [3-18].

The advantage of liquid lens can be explained as follows: in optical photography, to shoot a clear image, the object distance (d_1), image distance (d_2) and focal length (f) must obey the Gaussian imaging formula [Eq.3-5]. In the case of a traditional solid lens, its focal length was determined when being manufactured [Fig.3-2]. So it is necessary to adjust image distance inside the camera which requires sophisticated and complicated moving parts on the mechanism. That would increase manufacturing costs, especially for a large number of micro-camera modules used in mobile devices. Whereas, due to the EWOD liquid lens'

ability to change its focal length with only adjusting the applied voltage, there would be no requirement to change the image distance anymore. As a result, it becomes possible to simplify the manufacturing process.

$$\frac{1}{d_1} + \frac{1}{d_2} = \frac{1}{f}$$

-Eq. 3-5

Fig.3-3 gives the working principle of the EWOD liquid lens. When two immiscible liquids (normally aqueous solution and oil) are injected into a small tube, owing to the different surface tensions of these liquids, a curved interface presents between the two phases. Ordinarily, oil has a higher refractive index than water, so the type of lens (convex or concave) would be the same as the shape of the oil phase. In [Fig.3-3 (a)], in oil atmosphere, at the triple point and without applied voltage, water has an original contact angle (θ_0) higher than 90°. As the interface is presenting a plano-concave lens, light passing though it would be spread and it gives a negative focal length. Furthermore, using EWOD technique, the contact angle can be reduced by an applied voltage. Exhibiting in [Fig.3-3(b)], at a particular voltage, the contact angle(θ_v) can be reduced down to 90°. At this specific applied voltage, the interface appears to be flat. At this voltage, the passing light is not being refracted, hence the lens has a focal length to be infinity. Moreover, if the voltage increases, as showing in [Fig.3-3(c)], the contact angle becomes lower than 90° and the interface converges the passing light, similar as what a plano-convex lens does.

In order to get the relationship between the applied voltage and focal length, a theoretical calculation is given as follows: For a plano-convex/concave lens, the focal length satisfies Lensmaker's Formula [Eq.3-6], where f is the focal length of the lens; R is the radius of curvature; N is the relative refractive index which is a ratio of the absolute refractive index for oil (N_{oil}) and water (N_{H_2O}).

$$\frac{1}{f} = \frac{N-1}{R} \qquad (N = \frac{N_{oil}}{N_{H_2O}})$$

-Eq. 3-6

Here, R can be obtained by a simple geometric calculation in Fig.1 (c), where D is the inner diameter:

$$cos\theta_v = \frac{D}{2R}$$

-Eq. 3-7

The relation between applied voltage (V) and instant contact angle (θ_v) is showing in the Lippmann-Young's equation [Eq.3-4].

By combing all the mentioned formulas together, an integrated theoretical equation of an EWOD liquid lens can be established in [Eq.3-7]. Thus, it is obvious that after being fabricated, the applied voltage is the only external cause which affects the focal length[Eq.3-8].

$$f = \frac{D}{2(\frac{N_{oil}}{N_{H_2O}} - 1)(cos\theta_0 - \frac{V^2\varepsilon_r\varepsilon_0}{2d\gamma_{wo}})}$$

-Eq. 3-8

3.2 Experimental

3.2.1 Films Preparation

The method of dip coating of sol-gel and chemical solution deposition was carried out to coat each following thin layer. In the coating process, the thickness of each film was controlled by adjusting withdrawal speeds or just repeating each coating procedures.

Conductive bottom ITO layer:

ITO (indium tin oxide) glass (Rs<10 Ω/sq) was used when the test was taken on a flat substrate. However, to form the lens we need its inner wall being coated by ITO. So that we used a kind of nano-suspension liquid of ITO purchased from Mitsubishi Materials Electronic Chemicals Co, Japan. The coated layer was heated at $500^{\circ}C$ for 30 minutes to make it conductive enough.

Barrier layer of Al$_2$O$_3$:

In order to prepare alumina sol, Aluminum-tri-sec-butoxide (Al(O^{s}Bu)^3) and isopropanol (IPA) were used to be the starting material and solvent, respectively. First of all, Al(O^{s}Bu)^3 was mixed with IPA for 10 min by an electromagnetic stirrer. Then, being used as the stabilizer, ethyl acetoacetate (EAcAc) mixed with IPA was added into the precursor solution. After stirring for 1 h, IEW mixed with IPA was added drop by drop to start the hydrolysis reaction slowly. After stirring for 2 h, stable and homogeneous sol was prepared. The total molar ratio of each chemical was

Al(OsBu)^3 : EAcAc : IPA : IEW = 1:1:20:2. Before coating, the sol was filtered by a PTFE filter with pore size of 0.45 μm to remove the tiny solid impurity. Coating procedure was taken by a dip-coater which can control its withdrawal speed. To get the information of the film thickness against the withdrawal speed, several groups of films have been coated with different withdrawal speed from 0.1 to 2.0 mm/s. Then, heat treatment was taken to these coated films. All the specimens have been annealed at 500°C for 1h in air atmosphere with a step preheat treatment of 10 °C/min[Fig.3-5]. In this preparation, all chemicals are produced by Wako$^©$.

Dielectric layer of TiO$_2$

The TiO$_2$ layer with a thickness of 120 nm was prepared from a sol-gel method. Detailed procedures are showing in chapter 2.1.1 and Fig.2-5.

Top hydrophobic layer of Teflon AF

The solution was prepared by dissolving Teflon$^®$ AF 1600(produced by DuPont$^©$) into FC$^®$-75(produced by 3M$^©$). First, they were mixed with a concentration of 1 wt%. Because the solubility of Teflon AF is poor and FC-75 is easy to evaporate, the solution had to be stirred at 45 C° for 8 h inside a sealed container until the solid was completely dissolved. After cooling to room temperature, the solution was filtered by a polyamide (PA) filter with pore size of 0.45 μm (PTFE filter was used because it would swell in FC$^®$-75). The dip coating step was also taken with different withdrawal speed to get different film thickness. Teflon AF 1600 has a

glass transition temperature (Tg) around 160°C. It starts to decompose at 300 °C. So the temperature during heat treatment was decided to be 285°C for 30 min. That would increase the adhesion between Teflon AF to the substrate. Otherwise the Teflon layer could peel off easily.

3.2.2　Contact angles and leakage currents measurement

The set-up to test contact angles is slimmer with what in 2.2.2 and Fig.2-6. But for EDOW, we added a leakage current testament in the system. A nano-current analysis meter (8340A, ADCMT©) was cascaded in to the set-up in Fig.3-6. The aqueous droplet was formed by water within sodium dodecyl sulfonate (SDS, from Sigma-Aldrich©) 0.1 wt% and 0.1 M sodium chloride (NaCl, from Wako©). NaCl was added to make the droplet conductive so that under an applied voltage, there would be enough charge carriers on the solid-liquid interface. SDS is a kind of surfactant. It was used to reduce the surface tension of water, in order to have a lower original CA. Thus, CA can be reduced lower when being loaded by an specific voltage.

During the test, the applied voltage was increased until the dielectric breakdown occurred which manifested in a jump of leakage current. Contact angle measurements were performed by observation of the droplets though a CCD camera on a contact angle analyzer (Drop Master 200, Kyowa©). In addition, to test the stability of the device, on-off cycles (-10 V DC 1s / off 1s) for 1800 periods have been loaded on. Contact angles from several key frames were analyzed when the voltage was being loaded on and off.

3.2.3 Liquid lens fabrication and performance test

The procedures used for the lens fabrication are illustrated in Fig. 3-7. A glass tube with an inner diameter of 4 mm and length of 10 mm was used as the substrate [Fig. 3-7(a)]. By using the dip coating method, both the inside and outside of the tube were coated. Additionally, the coating area was determined by selecting the section of the tube immersed into the solution. Firstly, around 80% of the tube was coated with ITO [Fig.3-7(b)]. Then, from the opposite side of the tube, also 80% of the tube was coated with the layer of Al_2O_3, TiO_2, and Teflon in sequence [Fig.3-7(c)]. Therefore, on some areas on the outside of the tube, the coated ITO layer makes it conductive to the inside and the exposed section of the tube would be easy to connect with the power supply. After that, at the opposite side of the tube, a piece of ITO glass was affixed, which functions as a counter electrode to apply voltage to the aqueous phase. Next, the aqueous solution and silicon oil (KF-56A, Shin-Etsu©) were injected into the tube successively. Finally, after being sealed by a cover glass on the top and connected two ITO electrodes to the power supply, the fabrication of the EWOD liquid lens was accomplished [Fig. 3-7(d)].

Focal length of liquid lens was tested by change the distance of the object to the lens with different applied voltage [Fig.2-8]. A CCD camera was used to shoot the side view in order to observe the change of water-oil

interface and test the CAs. Meanwhile, we used a tiny CMOS camera to shoot the top view of the object. The original lens of the camera was replaced by our liquid EWOD lens. So that the image length (d_2) was determined. During the measurement, at one specific applied voltage, the object length (d_1) was adjusted and recorded when the top view camera shows the clearest image. By Gaussian imaging formula [Eq.3-2], the focal length of the EDOW lens at this specific voltage can be measured.

However, at some voltage the lens was concave. That means the focal length is negative and it is impossible to give a clear image at any object length. To test the focal length at this situation, an auxiliary solid convex lens was added underneath the liquid lens. So that the total focal length of the lens group turns to be positive and testable. Finally, the focal length of concave liquid lens can be calculated.

3.3 Results and discussion

3.3.1　Electrowetting on multilayered films

Fig.3-9 is the cross-sectioned SEM image of the multilayered films coated on ITO glass. From the image, it is easy to get the thickness of Al_2O_3 and TiO_2 layer, which are 80 nm and 120 nm, respectively. However, the top layer of Teflon AF is a kind of polymer which shrinks a lot when being illumined by electron beam. That leads the measurement of thickness became difficult by SEM. Finally, by ellipsometer, we found that the top layer of Teflon has a thickness of 40 nm.

The ITO conductive layer on the inner wall of glass tube was formed by the nano-particle suspension (produced by Mitsubishi Materials Electronic Chemicals Co.) [Fig.3-10(a)]. The dip coating from this suspension at a withdraw speed of 2 mm/s could form a film with a thickness around 400 nm [Fig.3-10(b)]. The resistance Rs was tested to be around 550 Ω/sq. Thus, the ITO layer formed by this method is not as conductive as the ITO glass. Because that in this case the grain size of ITO is to small and there the compactness is poor, compare with the ITO film made by sputtering. However, being used as a base electrode in EWOD, this level of conductivity is enough. After all, the increase of resistance can be omitted owing to the much larger resistance in the insulating layer.

Fig.3-11 (a) gives the CAs and the leakage currents versus with DC applied voltages loaded to the droplet. When the voltage was 0 V, the

original contact angle was 155° (Fig.3-11 (b)), which should be reduced by the effect of SDS (pure water has a contact angle of 175° on Teflon in oil atmosphere). The reason to add SDS was to reduce the interfacial tension of the aqueous phase so that the contact angle would have a large change range [3-20]. When the applied voltage was on, it was obvious that with an increase in voltage the contact angle decreased with a quadratic function (the broken line in Fig.3-11(a)), that corresponds with the Lippmann-Young equation [Eq.3-4]. In the voltage range between -10 V and 9 V, the leakage current was stable at a very low level (less than 100 nA). The contact angle could be reduced to 67 ° at -10 V with a tiny leakage current of 28 nA, (Fig.3-11 (c)). However, as the voltage kept increasing, the contact angle stoped decreasing and a drastic increase in the leakage current was observed which manifested in the dielectric breakdown of the multilayered dielectric films. This phenomenon has been reported and discussed by Papathanasiou [3-21]. The minimum contact angle was 52° with the applied voltage of -14 V, and the leakage current was quite large, 1020 nA. In Fig.3-11 (d), some tiny bubbles can be observed, which were generated by the water electrolysis caused by the large current. As being reported by some researchers, the dielectric breakdown in EWOD causes significant and irreversible damage to the system such as the electrolysis of the water, the loss of contact angle reversibility, etc. [3-22,23].

Another phenomenon to be noticed from Fig.3-11(a) is that the

EWOD could withstand a larger negative DC voltage compared to a positive voltage. The minimum contact angle reached 52 ° for -14 V, but it was 59 ° for +14 V. The leakage current also jumped sharply when the positive DC was applied. Similar results were reported in Moon and Schultz's work that the negative DC was connected to lower EWOD hysteresis and higher lifetime, which is possibly attributed to less charge trapping [3-10,24]. It has also been proved that negative DC voltage shows better reversibility than positive DC and AC [3-11]. Therefore, in this work, negative DC was chosen to be used as the applied voltage and the maximum working voltage was fixed at -10 V.

Fig.3-12 shows the contact angles when the voltage was loaded for the 1st and the 1800th periods on a square wave with 50% duty factor at -10 V. For both of them, the contact angles started to reduce immediately as soon as the voltage was loaded. It took 100 ms for the contact angles to reduce to the steady loading-level. However, when the loading was removed, 200 ms was needed for the contact angles to increase back to steady unloading-level. This is because when the applied voltage was unloaded, aqueous phase needs to overcome the high viscosity resistance of the oil phase [Table 3-1]. What is more, for the 1800th period, the uploading contact angle was 4 ° less than that in the 1st period (from 155 ° to 151 °). The difference remained after the cycle test was finished. This behavior might be caused by the morphological or structural changes

which could not be observed in each single period. Still, the loading contact

angle did not change too much, so the device is relatively stable.

3.3.2　Performance of liquids lens

In our case, the type of oil being used in EWOD liquid lens must satisfy a range of conditions. Firstly, the oil must possess abundant transparency for visible light. Secondly, its viscosity should not be too high, otherwise it would decrease the response time. Then, in order to make its focal length close enough, the refractive index of the oil should be as high as possible. Finally, by eliminating the effect of gravity to allow the interface to present a perfect circular curved surface but not an ellipsoid one, the density of the oil must be slightly less than water. Dodecane is often used as the oil phase in EWOD. However, with respect to all of the particular requirements mentioned above and after comparing the various properties, we finally chose a silicon oil known as KF-56A to act as the oil phase [Table 3-1]. Even though its kinematic viscosity is much higher than dodecane, the tested response time was still at an acceptable level. (17 ms in dodecane, 204 ms in KF-56A).

Fig.3-13 gives the change of the oil-aqueous interface curvature inside the glass tube. The inner diameter of the tube is 4 mm. The images were taken before (a,b) and after (c,d) -10 V was applied. When the voltage was turned off, the original contact angle, θ_0, was 155 ° [Fig.5 (a)]. That makes the interface a concave lens which has a minus focal length meaning that the object cannot be well focused on [Fig.3-13(b)]. After an applied voltage of -10 V was loaded, the contact angle reduced to be 67 ° [Fig.3-13 (c)].

The interface turns into a convex lens, so the positive focal length, object distance and image distance could satisfy the Gaussian lens formula [Eq.3-2] giving a clear image [Fig.3-13 (d)].

A tiny camera with a prime lens was used to test the EWOD lens's focal length by adjusting the object distance with different applied voltages until it showed the clearest image. Also, the Numerical aperture (NA) of the lens can be calculated by the following formula:

$$NA = Ncos\theta$$

<div align="right">-Eq. 3-9</div>

N is the relative refractive index which is a ratio of the absolute refractive index for oil (N_{oil}) and water (N_{H_2O}). θ is the maximal half-angle of the cone of light that can enter or exit the lens. It equates to the CA in this case.

The result is shown in Fig.3-11. The focal length started from a negative value around -2 mm. NA was 0.21 at that time. As the voltage negatively increased, the focal length became -51 mm at -8 V and jumped to 17 mm at -9 V. According to the contact angle results in Fig.3-11(a), it should become exactly 90 ° somewhere in the range between -8 V to -9 V, with the maximum NA of 1.498. Thus, the focal length should become infinity at that point. Then, with the voltage rising, the focal length becomes 9 mm at -10 V. NA also reduced to 1.38 at that voltage.

3.4 Conclusion

The low voltage EWOD system was made from ITO–Al_2O_3–TiO_2–Teflon multilayered thin films. The sol–gel / CSD dip coating method was used in the film preparation. In an oil atmosphere, a droplet of conductive aqueous solution containing NaCl and SDS showed contact angles changing from 155 ° to 67 ° when -10 V DC was applied, with a negligible leakage current of 28 nA. Using the same multilayers coated inside a tiny glass tube, a low voltage driven liquid zoom lens with diameter of 4 mm was fabricated. Under the safe working voltage range of 0 to -10 V, its focal length could be adjusted from -2 mm to infinity then to 10 mm. The NA of the lens changed from 0.21 to 1.498 then down to 1.38. After being loaded for 1800 periods, the focusing function was still stable.
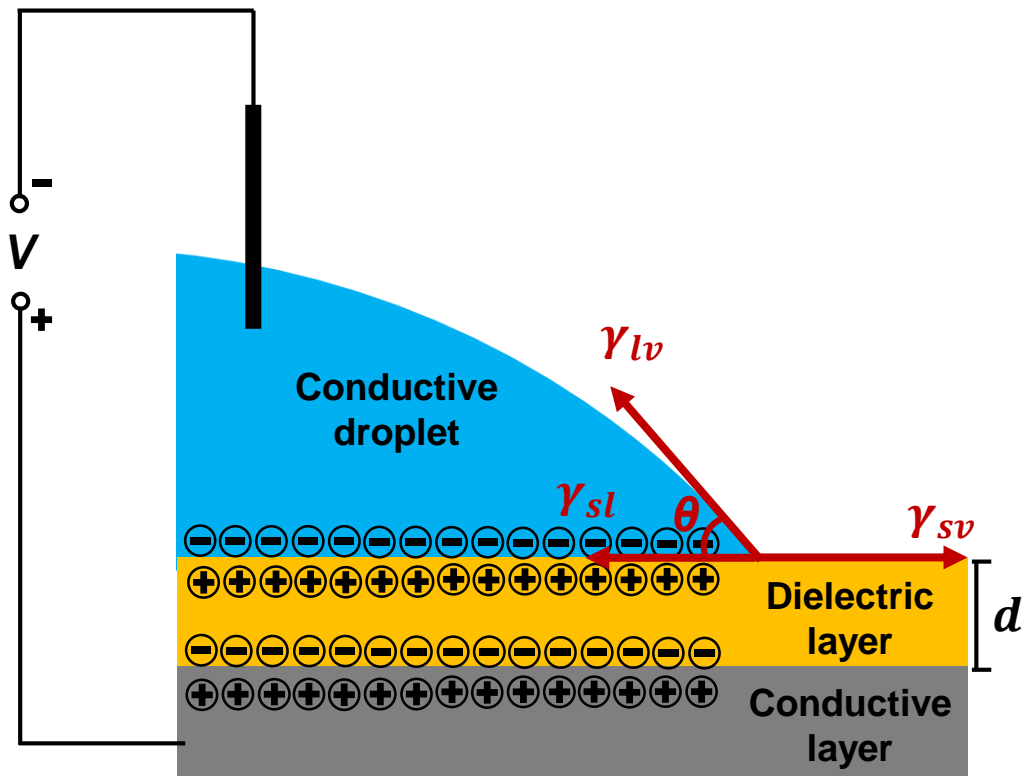
Fig. 3-1: Schematic of theoretical electrowetting on dielectric.

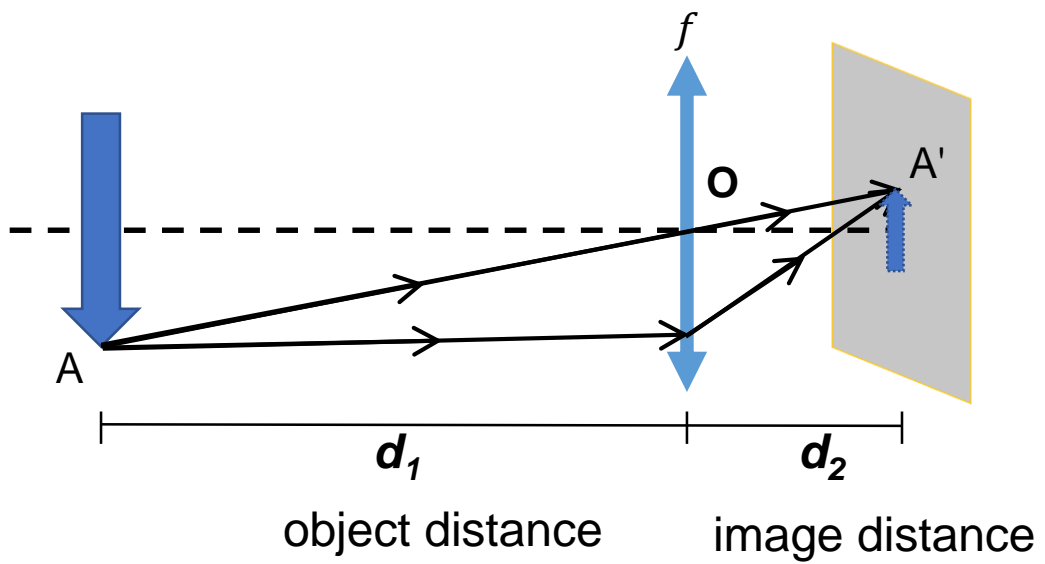**Gaussian imaging formula:** $\dfrac{1}{f} = \dfrac{1}{d_1} + \dfrac{1}{d_2}$
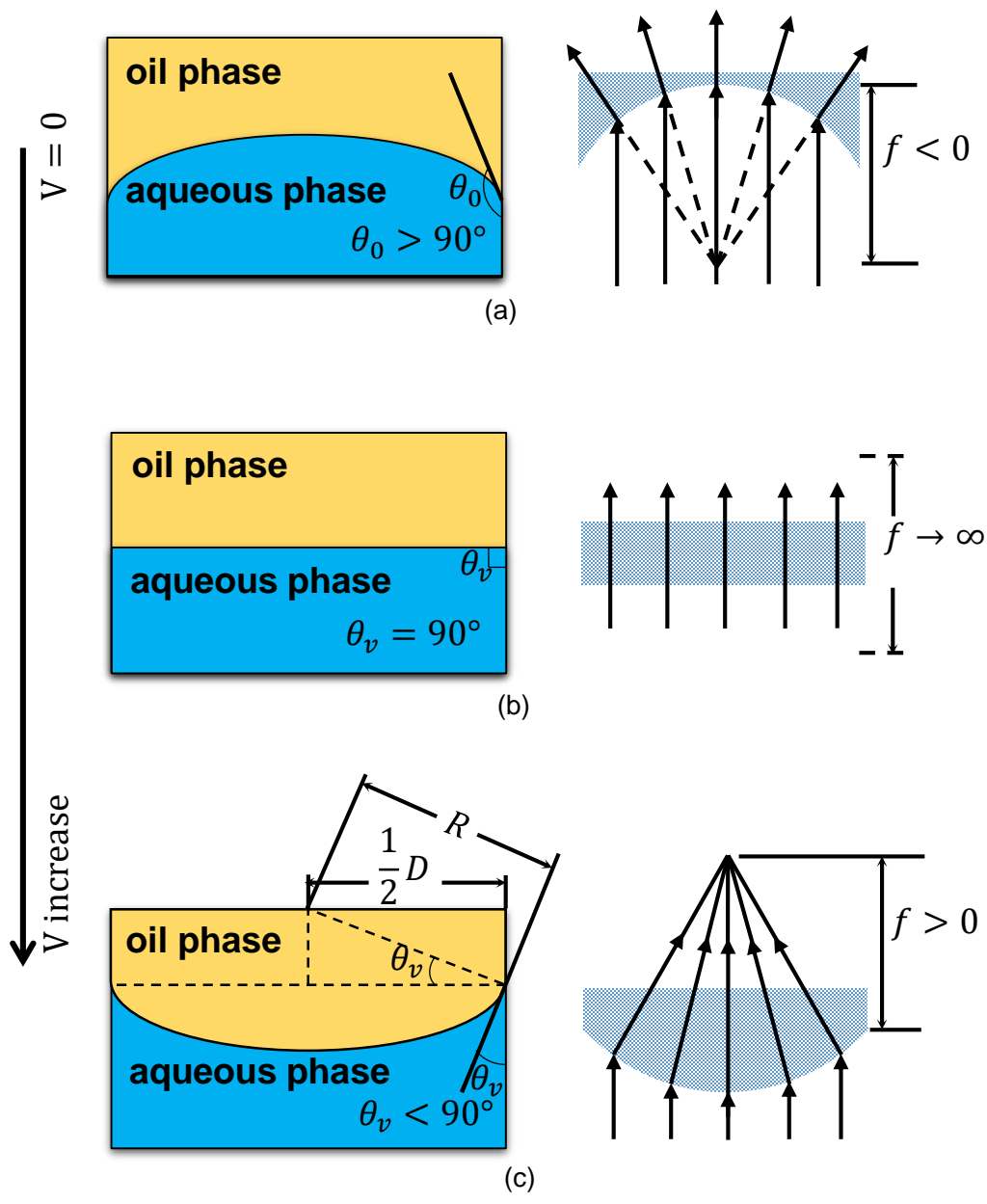

Fig. 3-2: Principle of Gaussian imaging formula.

V = 0

oil phase

aqueous phase θ_0

$\theta_0 > 90°$

$f < 0$

(a)

oil phase

aqueous phase θ_v

$\theta_v = 90°$

$f \to \infty$

(b)

V increase

$\frac{1}{2}D$ R

oil phase θ_v

aqueous phase θ_v

$\theta_v < 90°$

$f > 0$

(c)

Fig.3-3: Working principle of the EWOD water-oil liquid lens.
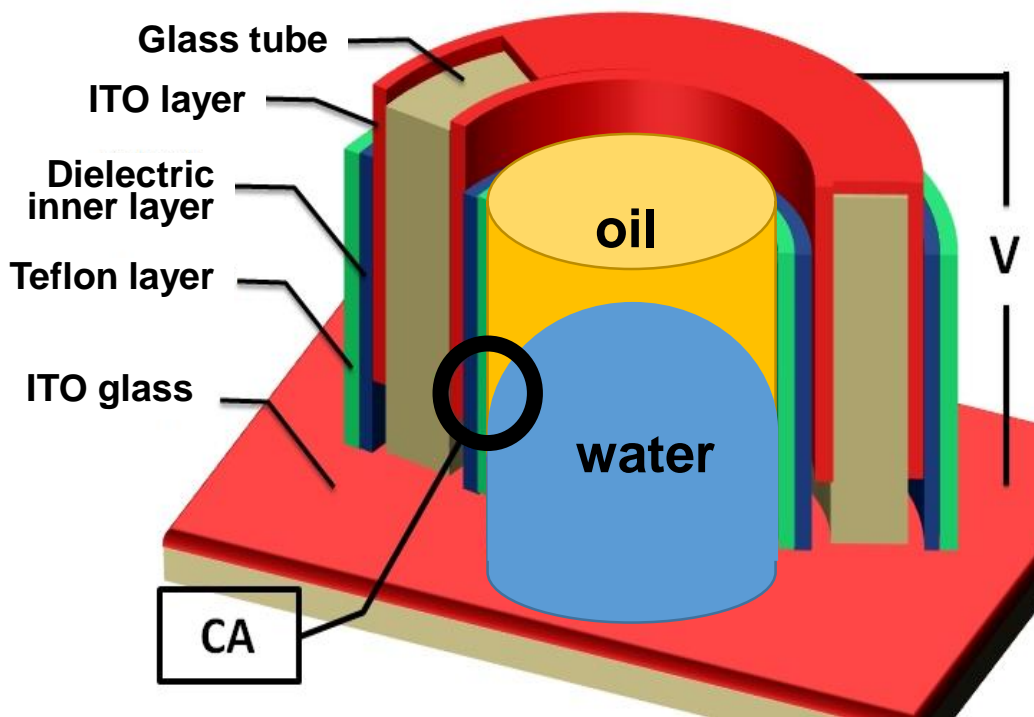
Fig.3-4: Illustration of the EWOD focal lens' structure.

```
                    ┌──────────────────────────────────┐
                    │   Al(OˢBu)³ + IPA                 │
                    └──────────────────────────────────┘
                                    │
                    ┌──────────────────────────────────┐
                    │ Stirring for 10 min at 500 rpm   │
                    └──────────────────────────────────┘
                                    │              ┌──────────────────────────┐
                                    │◄─────────────│     EAcAc + IPA          │
                                    │              └──────────────────────────┘
                    ┌──────────────────────────────────┐
                    │ Stirring for 10 min at 500 rpm   │
                    └──────────────────────────────────┘
                                    │              ┌──────────────────────────┐
                                    │◄─────────────│     IEW + IPA            │
                                    │              └──────────────────────────┘
                    ┌──────────────────────────────────┐
                    │  Stirring for 2 h at 500 rpm     │
                    └──────────────────────────────────┘
                                    │
                    ┌──────────────────────────────────┐
                    │        Al₂O₃ Sol                 │
                    └──────────────────────────────────┘
                                    │
                    ┌──────────────────────────────────┐
                    │           Filtered               │
                    └──────────────────────────────────┘
                                    │
                    ┌──────────────────────────────────┐
                    │      Dip coating 1 mm/s          │
                    └──────────────────────────────────┘
                                    │
                    ┌──────────────────────────────────┐
                    │ Heat treatment 500 °C 1h in      │
                    │       air atmosphere             │
                    └──────────────────────────────────┘
                                    │
                    ┌──────────────────────────────────┐
                    │       Al₂O₃ thin film            │
                    └──────────────────────────────────┘
```
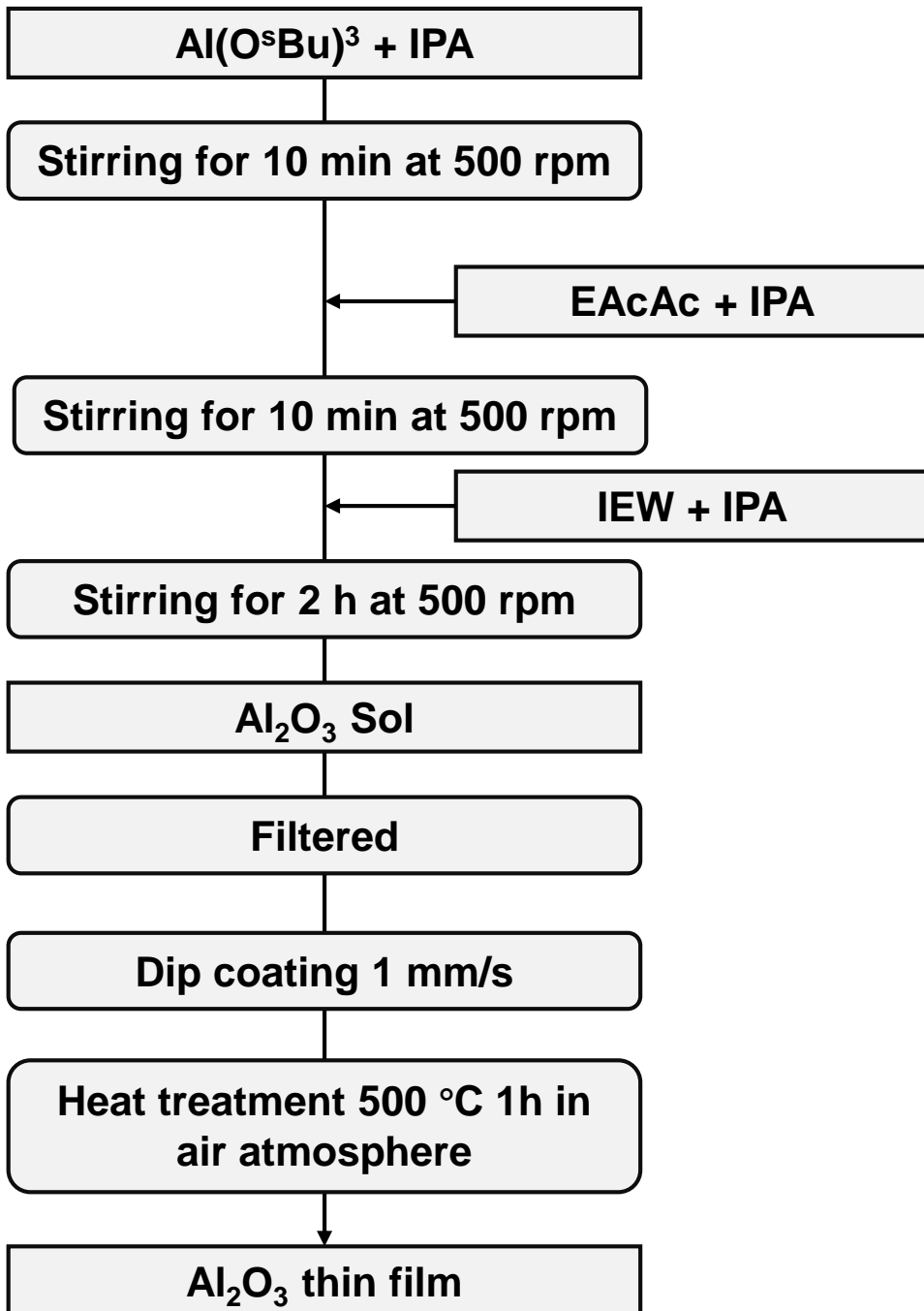
Fig. 3-5: Flow-chart of Al_2O_3 thin films formation prepared by sol-gel dip coating process with the molar ratio of $Al(OsBu)^3$: EAcAc : IPA : IEW = 1:1:20:2.
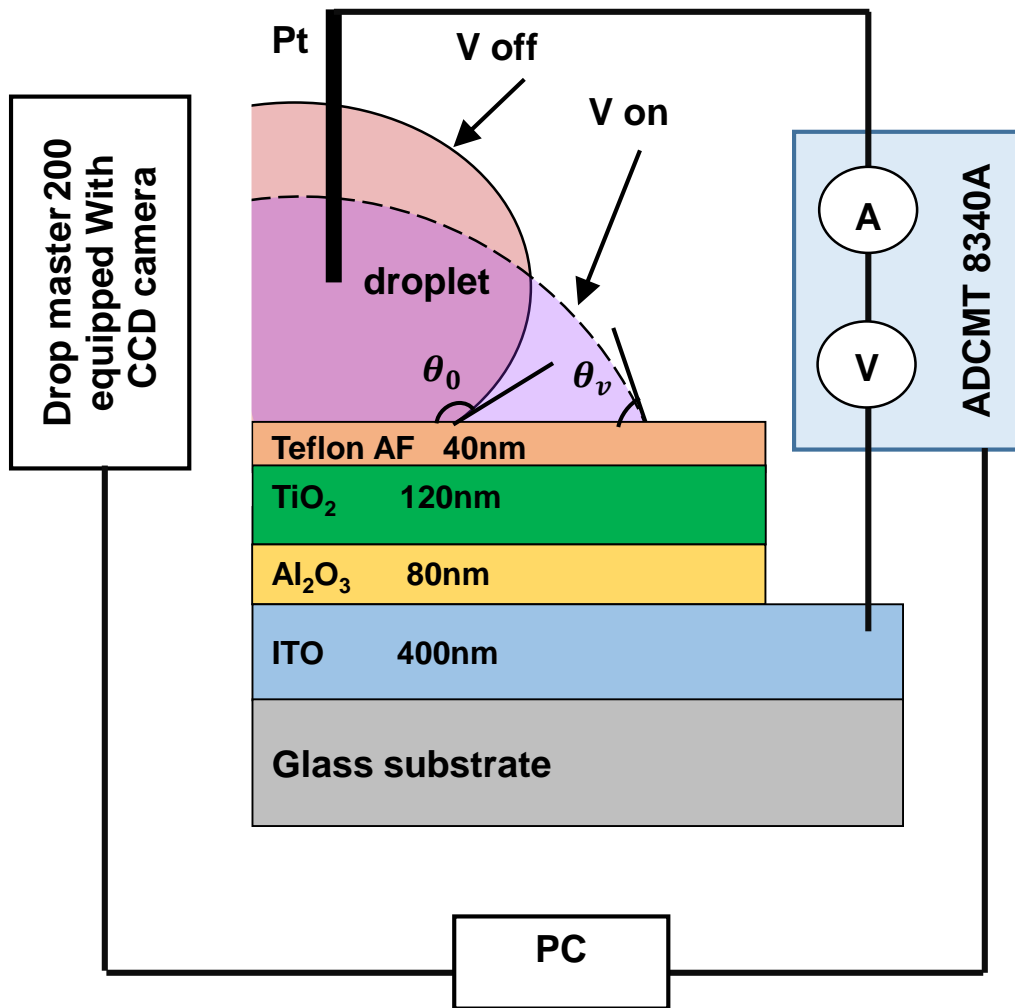
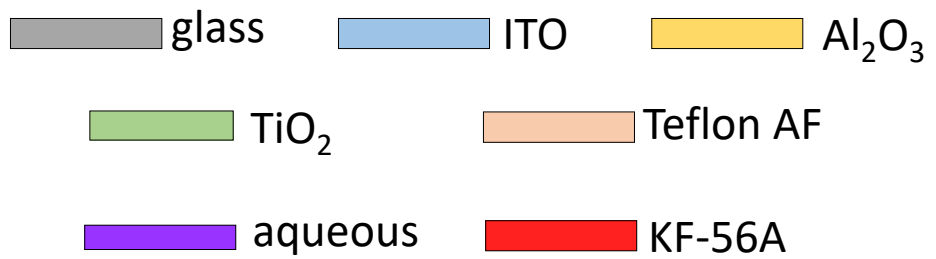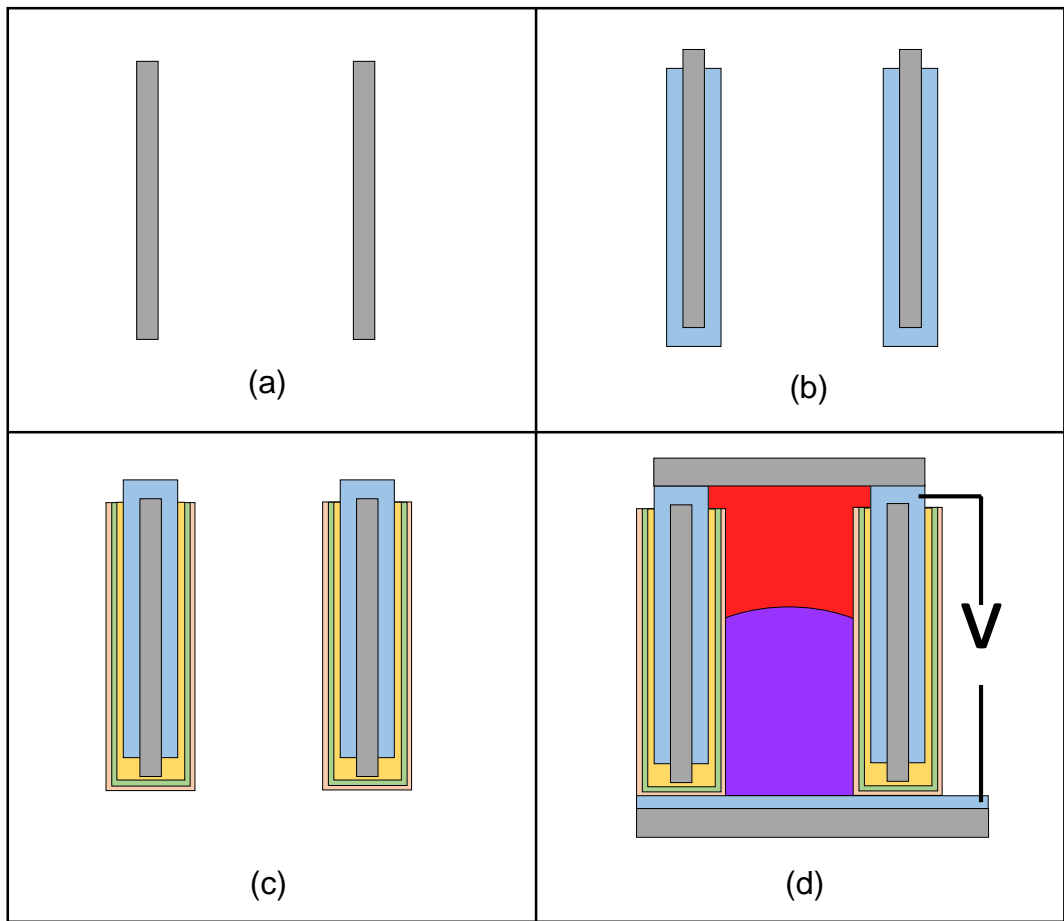Fig. 3-6: Illustration of contact angle measurement set-up.

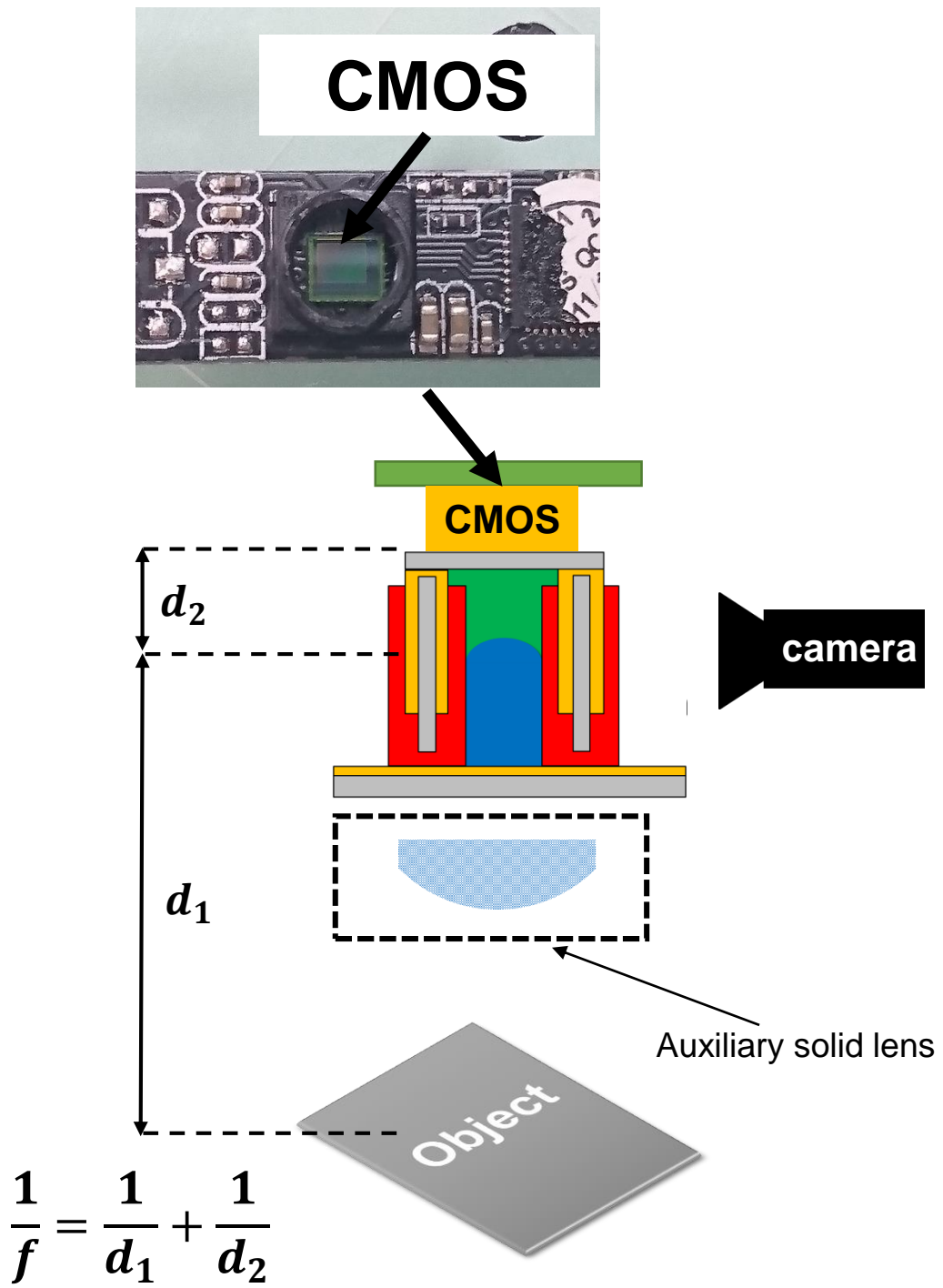Fig. 3-7: Schematic of the EWOD lens fabrication processes.

$$\frac{1}{f} = \frac{1}{d_1} + \frac{1}{d_2}$$

Fig. 3-8: Schematic of focal length test set-up.

Teflon AF 40 nm

TiO$_2$ 120 nm
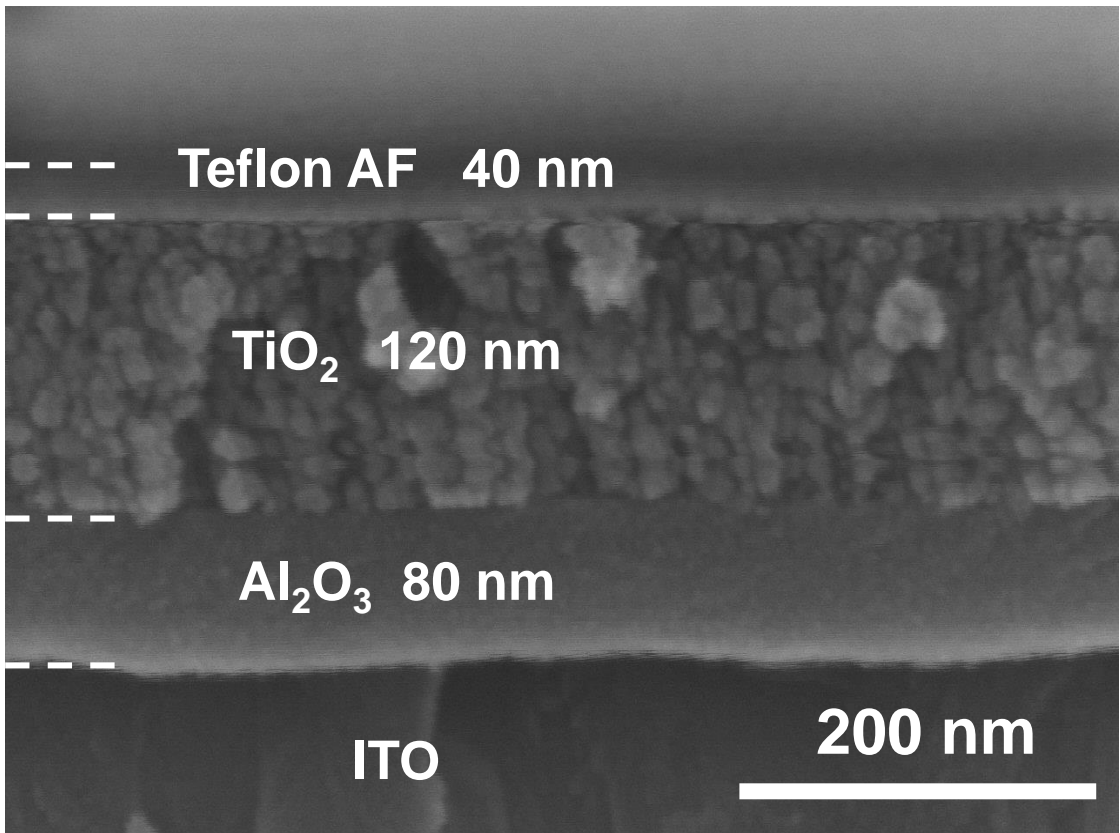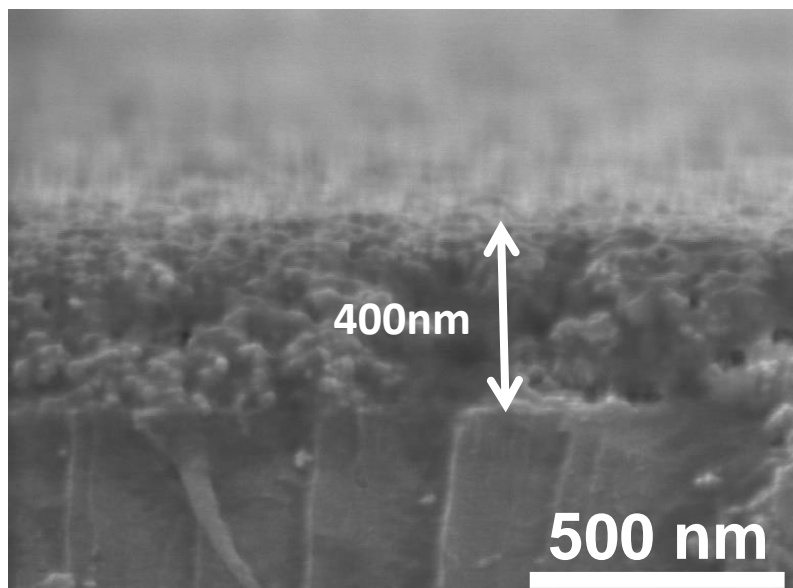
Al$_2$O$_3$ 80 nm

ITO

200 nm

Fig. 3-9: Cross-sectioned SEM image of the multilayered films used on EWOD.

(a)

400nm

500 nm

(b)

Fig. 3-10: (a) Image of the ITO suspension used for the coating of the conductive layer (produced by Mitsubishi Materials Electronic Chemicals Co.); (b) SEM image of the ITO layer coated on the inner wall of the glass tube.
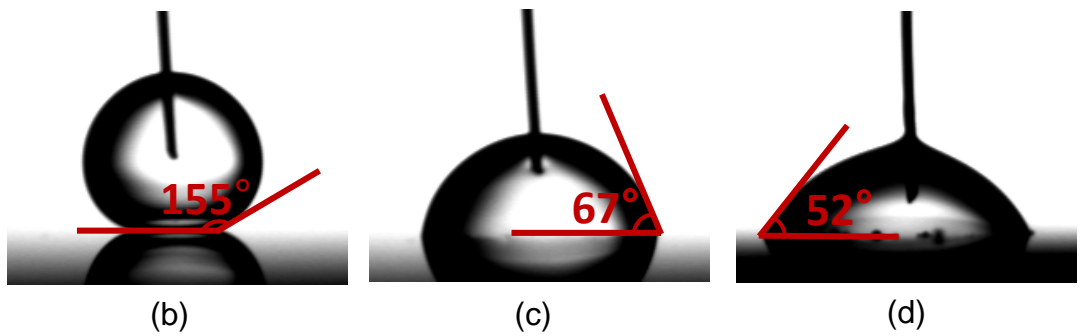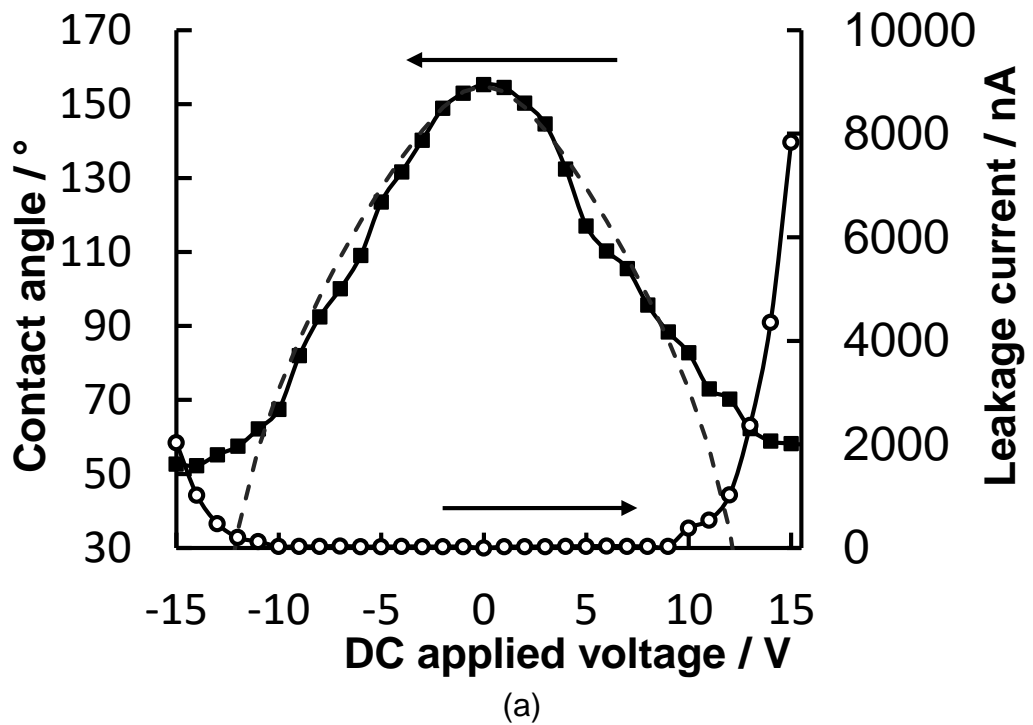
Fig.3-11: (a) CAs and leakage currents obtained under different DC applied voltage (the broken line represent the simulation from Eq.3-4). The corresponding images of the droplet at loadings of (b) 0 V, (c) -10 V and (d) -14 V are also shown.
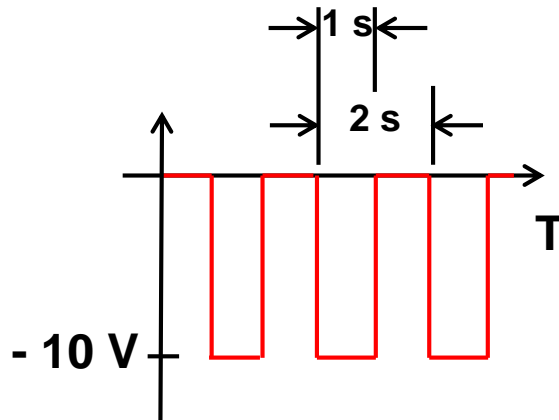
(a)
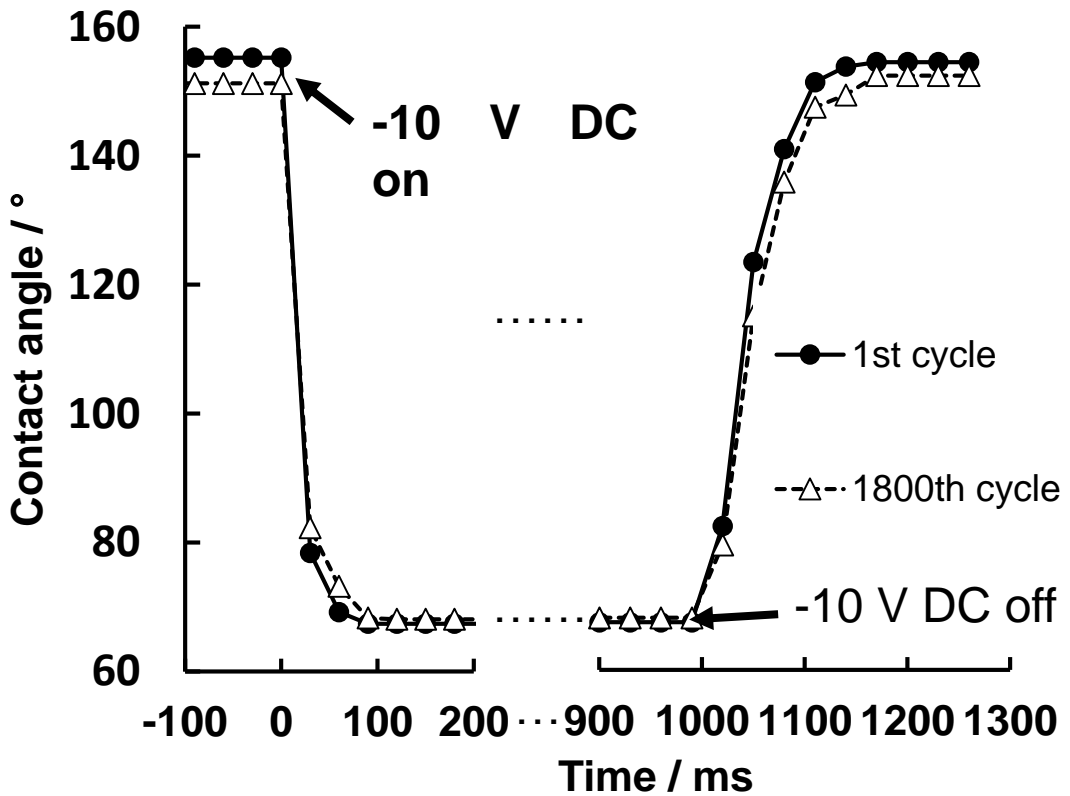
(b)

Fig.3-12: (a) Square wave applied on the lens during the life time test and (b) contact angles for the 1st and 1800th period loading using -10 V DC.
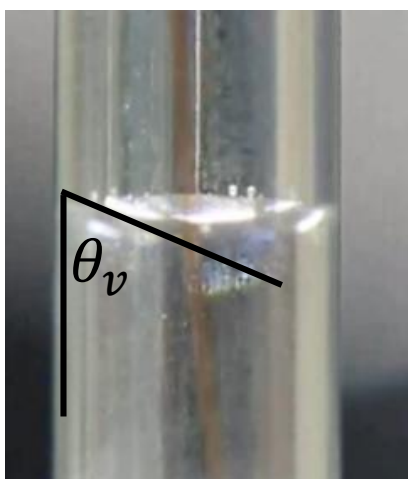
Table 3-1: Properties of dodecane and KF-56A.

	Dodecane	FK-56A
Kinematic viscosity (mm^2/s)	1.266	15
Density (g/ml)	0.7495	0.995
Refractive index	1.421	1.498
Tested response time (ms)	17	204
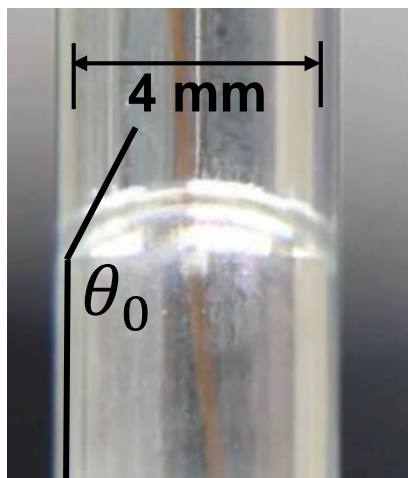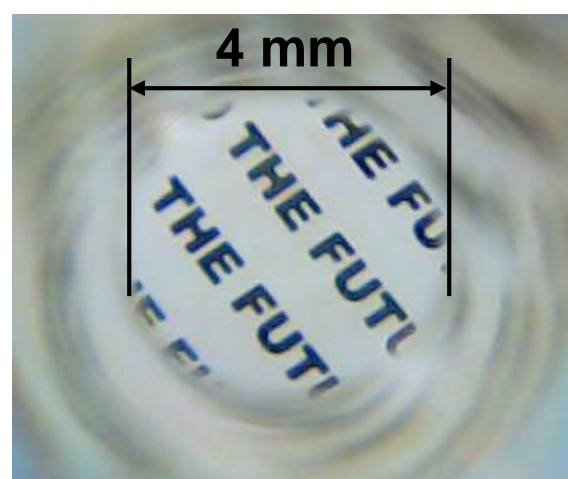
Fig.3-13: (a) Side and (b) top views of oil-aqueous interface before applying DC voltage. (c) and (d) are the corresponding views with applied voltage of -10 V is used.
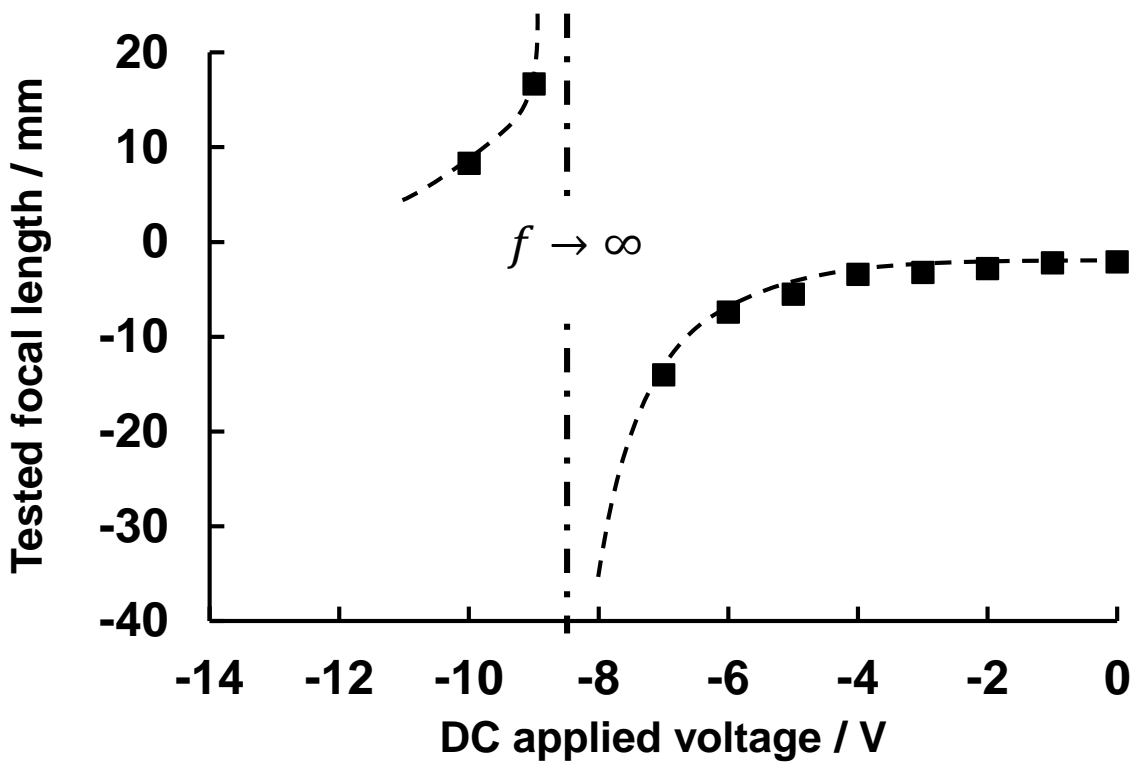
Fig.3-14: Tested focal length with different applied voltage.

References of chapter 3

3-1	Relations Entre Les Phénomènes Électriques et Capillaries, M.G. Lippmann, Annales de Chimie et de Physique, 5, 494-459 (1875).
3-2	Electrowetting: From Basics to Applications, F. Mugele and J-C. Baret, Journal of Physics: Condensed Matter, 17, 705-774 (2005).
3-3	Study of Electrocapillarity in Dielectrics Using Palm Oil, B. Berger, Comptes Rendus de l'Académie des Sciences, 317, 157-163 (1993).
3-4	Micro- and Nanoscale Fluid Mechanics: Transport in Microfluidic Devices, B.J. Kirby, 563 pages, ISBN: 978-1-107-61720-9, Cambridge University, USA (2013).
3-5	Using EWOD (electrowetting-on-dielectric) Actuation in a Micro Conveyor System, I. Moon, and J.W. Kim, Sensors and Actuators A: Physical, 130-131, 537-544 (2006).
3-6	Electrostatic Stabilization of Fluid Microstructures, F. Mugele, and S. Herminghaus, Applied Physics Letters, 81, 2003-2305 (2002).
3-7	Electrowetting on Paper for Electronic Paper Display, D.Y. Kim, and A.J. Steckl, ACS Applied Materials & Interfaces, 2, 3318-3323 (2010),
3-8	Low Voltage Electrowetting-on-Dielectric, H. Moon, S.K. Cho, R.L. Garrel, and C.J. Kim, Journal of Applied Physics, 92, 4080-4087 (2002).
3-9	Dynamics of Self-Excited Droplet Oscillations in Electrowetting, J.C. Baret, D. Steinhauser, R. Seemann, and S. Herminghaus, 4th Int. Discussion Mtg on Electrowetting, TN-2003-00985, Blaubeuren, Germany (2004).
3-10	A Material System for Reliable Low Voltage Anodic Electrowetting, M. Khodayari, J. Carballo, and N.B. Crane, Materials Letters, 69, 96-99 (2012).
3-11	Dielectrically Stabilized Electrowetting on $AF1600/Si_3N_4/TiO_2$ Dielectric Composite Film, J.K. Lee, K.W. Park, H.R. Kim, and S.H. Kong, Sensors and Actuators B: Chemical, 160, 1593-1598 (2011).
3-12	Superior Performance of Multilayered Fluoropolymer Films in Low Voltage Electrowetting, D.P. Papageorgiou, A. Tserepi, A.G Boudouvis, and A.G. Papathanasiou, Journal of Colloid and Interface Science, 368, 592-598 (2012).

3-13	Electrowetting Displays, G. Beni, and S. Hackwood, Applied Physics Letters, 38, 207-209 (1981).
3-14	Electrofluidic Displays Using Young-Laplace Transposition of Brilliant Pigment Dispersions, J. Heikenfeld, K. Zhou, E. Kreit, B. Raj, S. Yang, B. Sun, A. Milarcik, L. Clapp, and R. Schwart, Nature Photonics, 3, 292-296 (2009).
3-15	Versatile Electrowetting Arrays for Smart Window Applications - From Small to Large Pixels on Fixed and Flexible Substrates, H. You, and A.J. Steckl, Solar Energy Materials & Solar Cells, 117, 544-548 (2013).
3-16	Variable-Focus Liquid Lens for Miniature Cameras, S. Kuiper, and B.H.W. Hendriks, Applied Physics Letters, 85, 1128-1130 (2004).
3-17	A Thin Electrowetting Controlled Optical System with Pan/Tilt and Variable Focus Functions, A. Takei, K. Matsumoto and I. Shimoyama, Sensors and Actuators A, 194, 112-118 (2013).
3-18	Electrowetting-Driven Variable-Focus Microlens on Flexible Surfaces, C. Li, and H. Jiang, Applied Physics Letters, 100, 231105(1-3) (2012).
3-19	Fabrication and Demonstration of Electrowetting Liquid Lens Arrays, N.R. Smith, L.L. Hou, J.L. Zhang, and J. Heikenfeld, Journal of Display Technology, 5, 411-413 (2009).
3-20	Optofluidic Solar Concentrators Using Electrowetting Tracking: Concept, Design, and Characterization, J. Cheng, S. Park, and C.L. Chen, Solar Energy, 89, 152-161 (2013).
3-21	Illuminating the Connection between Contact Angle Saturation and Dielectric Breakdown in Electrowetting through Leakage Current Measurements, A.G. Papathanasiou, A.T. Papaioannou, and A.G. Boudouvis, Journal of Applied Physics, 103, 034901(1-3) (2008)
3-22	Ion and Liquid Dependent Dielectric Failure in Electrowetting Systems, B. Raj, M. Dhindsa, N.R. Smith, B. Laughlin, and J. Heikenfeld, Langmuir, 25, 12387-12392 (2009).
3-23	Reliable and Low-Voltage Electrowetting on Thin Parylene Films, M. Dhindsa, S. Kuiper, and J. Heikenfeld, Thin Solid Films, 519, 3346-3351 (2011).
3-24	Charge Injection in Dielectric Films during Electrowetting Actuation under Direct Current Voltage, D. Thomas, M.C. Audry, R.M. Thibaut, P. Kleimann, F. Chassagneux, M. Maillard, and A, Brioude, Thin Solid Films, 590, 224-229 (2015).

Chapter 4

Surface charged silver nanoparticles used in electrophoretic deposition to form dye-sensitized solar cells

4.1 Introduction

In this chapter, we present a new method to prepare nano-composite materials by electrophoretic deposition (EPD). We individually discussed the preparation and characterization of silver nanoparticles and anodized TiO_2 nanotubes. Then their composites are made by EPD with a unique acetone vapor treatment. Finally, (dye-sensitized solar cells) DSSCs made by TiO_2 nanotubes (TNTs)-Silver nanoparticles (Ag NPs) are assembled. The results showed that the adding of Ag NPs is effective to enhance the performance of DSSCs.

4.1.1 Zeta potential on silver nanoparticles

Normally, Zeta potential (ζ-potential) is used to evaluate the surface charge of dispersed particles in a suspension. Basically it is the electric potential difference at the interface between the suspended particles and the dispersion medium around them [4-1].

Fig. 4-1 shows the theory of Zeta potential. When a particle with negative surface charge is being suspended into dispersion medium, for the electrostatic adsorption, there is an interfacial double layer generated by the electrified body attached on the surface of the particle. The double layered structure can be explained by the theory of Stern double layered adsorption model [4-2]. The electrified body is normally made by single ions or long chain polymers. In this case, the slipping plane gives a high positive Zeta potential for the high concentration of positive electrified body adsorbed at the slipping plane.

Zeta potential can be measured by different method such as electro kinetic and electro acoustic phenomena [4-3,4]. With a unit of mV, it is a very important index to value the stability of suspension. For the Zeta potential at 0 mV ~ ±10 mV, the suspension is considered has no stability which mains the particles in suspended would reunite and subside immediately. When it is ±10 mV ~ ±30 mV, the suspension has little stability to hold the uniformity for minutes or hours. If the Zeta potential is higher than ±40, the suspension is very stable. Without any effect from

outside, the coefficient of dispersion can keep at a high level for days or even weeks. In addition, increase the Zeta potential is not only for make stable suspension but also have important meanings in electrophoretic deposition (EPD).

For the case of dispersion medium is water or organic solvent such as ethyl alcohol or isopropanol, the ionization is too weak to generate enough electrified body to form a Stern double layered. To increase the Zeta potential, the most common way is to add surfactant into the suspension. Surfactant is normally made by electrolyte such as sodium stearate which has a hydrophobic/hydrophilic groups at each sides.

4.1.2 Electrophoretic deposition

EPD, short of electrophoretic deposition, is a coating method by using a DC applied voltage loading between the electrode and conductive substrate inside a suspension [**Fig.4-2**]. By the driving force of the electric field, the surface charged particles are pushed moving forward and finally attached on the surface of substrate to form a coating layer[4-5].

For the principle of EPD, it is necessary to get a suspension with high Zeta potential. It is important to choose surfactant and particles in the suspension. Also, when the EPD is taken in an aqueous suspension, selection of the suitable applied voltage to prevent the electrolysis of water is necessary. Otherwise the oxygen gas and hydrogen would respectively generate from anode and cathode electrodes:

Anode: $2H_2O \rightarrow O_2(gas) + 4H^+ + 4e^-$

Cathode: $4H_2O + 4e^- \rightarrow 4OH^- + 2H_2(gas)$

To solve the problem, changing the applied voltage from DC, to a AC+DC pulse current is one advisable method [4-6]. Also in some cases the dispersion medium can be exchanged from water to organic solvents like isopropanol [4-7,8].

4.1.3 Anodized TiO$_2$ nanotubes

Titanium dioxide (TiO$_2$) is an n-type semiconducting material with prominent properties such as chemical stability, sample preparation and environmentally harmlessness. It is now being widely used in the areas of pigment, UV blocking material, photocatalyst and semiconductor [4-9~11].

When being used as a photocatalyst (in our case is the photo anode in DSSCs), it is necessary to provide a high specific surface area. So that the preparation of nano-sized TiO$_2$ has been taken into study. For now, there are many ways to make nano-sized TiO$_2$, such as using sol-gel to make nanoparticles of TiO$_2$[4-12]; using hydrothermal method to make TiO$_2$ nanorods [4-13] and using anodization to prepare TiO$_2$ nanotubes(TNTs) [4-14]. Among all the preparation, anodization is one common method to prepare TNTs. In the last two decades, due to the improvement of the technique, the anodized TNTs with high-performance can be easily made by simple electrochemical set-up [4-15,16].

Anodization is a process of electrolytic passivation to create a thick oxide layer on the surface of metal parts. Not only for Ti, other metals like Fe, Zr, Ni and Cu can also be anodized to form a nanotube/pores array layer or a compact oxide layer (depends on the conductions of anodization)[4-17].

The set-up of anodization is given in Fig.4-3. Counter electrode(Pt) and substrate(Ti) are immersed into the electrolyte and being connected to

a DC power supply. Counter electrode is used as cathode meanwhile the substrate is connected to anode. By the driven voltage, the ions in the electrolyte such F^- and O^{2-} are moving forward to the metal substrate. So it forms an oxide barrier layer at the first. Then due to the effect of de-solution, pores appear in the oxide barrier layer and the ions are going deeper though the pores with growth of the oxide layer thicker. Finally, a nanotube/pores array layer is formed on the metal substrate.

The technology and processes of anodization have been well studied in lots of fields such as the composition of electrolyte, working applied voltage and temperatures [4-18~20].

4.1.4 Dye sensitized solar cells made by TiO$_2$ nanotubes-silver nanoparticles

Dye sensitized solar cells (DSSCs) is a new low-cost solar cell belonging to the group of thin film solar cells. Dye-sensitized solar cells (DSSC) are an efficient type of thin-film photovoltaic cell. DSSCs are easy to manufacture with traditional roll-printing techniques, and are semi-transparent and semi-flexible, allowing a range of uses that are not applicable to rigid photovoltaic systems. Most of the materials used are low-cost, however a handful of costly materials are necessary, such as ruthenium and platinum. There is a significant practical challenge involved in designing the liquid electrolyte for DSSCs, which must be able to remain in the liquid phase in all kinds of weather conditions.

The DSSCs made by TNTs arrays are given in Fig. 4-4. When being illumined by solar light, photo electrons are activated in dye molecules. Then, the electrons transfer to TNTs and finally flow in to the Ti metal. On other hand, the holes in dye molecules are filled by the I^- in the electrolyte and I^- lost electros to become I^{3-}. At the counter electrode, I^{3-} get electrons and returns into I^-. These are the full cell cycle of DSSCs.

In our case, the TNTs-Ag NPs are used as the photo anode of DSSCs. Nanoparticles (NPs) of noble metal (such as Ag and Au) can increase the photoelectric conversion efficiency of TNTs due to the phenomenon of localized surface plasmon resonance (LSPR). Such TNTs-NPs composites

have been applied in photocatalysis [4-21,22] and DSSCs [4-23,24]. In order to add Ag NPs into TNT arrays, currently, light degradation of silver nitrate solution is a general method. However, we found it is difficult to generate Ag NPs uniformly inside the TNT arrays. Because the light is firstly being absorbed on the top of the TNTs and Ag NPs generated there. Then, these Ag NPs absorb much light and grow bigger, leaving the deep area being lower illuminated. Therefore, the Ag NPs are just cover the top area and the size is difficult to be controlled. In this study, we invented new technique to deposit Ag NPs into TNT arrays and succeeded to remarkably enhance the efficiency of DSSCs due to the electrophoretic deposition (EPD) method. Frist, TNT arrays and Ag NP suspension were prepared individually. Then, the TNT arrays were immersed into the suspension in an acetone vapor filled atmosphere to remove the air inside the TNTs. After that, TNTs were immersed into Ag NP suspension for EPD with an AC+DC applied voltage, the surface charged Ag NPs were forced to move forward and filled into the TNT arrays. DSSCs fabricated by the Ag NPs filled TNT arrays showed better performance than those without Ag NPs.

4.2 Experimental

4.2.1 Preparation on silver nanoparticles

The preparation of Ag NP suspension began with dissolving 0.17g silver nitrate into 98 ml H_2O which containing 0.025 wt% carboxy methylcellulose. The starting solution was heated up to 95°C in a hot water bath with strong stirring. Then, 2 ml trisodium citrate aqueous solution was added as the reductant. The total mole ratio of Ag and trisodium citrate was 1:1.37. The reaction time was 10 min with keeping the temperature and stirring. In the end, the hot suspension was transferred into an ice-water bath to stop the reaction [4-24]. All chemicals above are produced by Wako©.

The characterization of Ag NPs was taken by SEM(SU-8000, Hitachi©), TEM(JEM-1400 Plus, JEOJ©) and XRD(UltimaIV R185, Rigaku©). The Zeta potential of the suspension was also measured by ELS-Z1NT, Otsuka©.

4.2.2 Preparation on anodized TiO_2 nanotubes

TNTs were prepared by anodizing Ti foils (2 cm x 3 cm x 0.2 mm, Nilaco©) in an electrolyte with 0.3 wt% NH_4F and 2 wt% H_2O in ethyl glycol (all from Wako©), with the temperature being controlled at 23°C. To get a uniform surface morphology, two times anodization was operated [14]. The Ti foil was first anodized for 1 h followed by removing the generated tubes in ultrasonic bath. The 2nd TNTs were generated by anodizing the previous Ti foil for 2 h with the same electrolyte and temperature. Then, heat treatment at 450°C was performed for 2 h to crystallize the amorphous TNTs into anatase phase. The Ti foil was masked to anodize only a certain area of the foil (0.78 cm^2). The characterization of TNTs was performance using SEM, TEM and XRD.

4.2.3 Acetone vapor per-treatment

To get a uniform electric field during the EPD procedure, it is necessary to remove the air from the TNT arrays. Therefore, a vacuum chamber with a lifting structure inside was manufactured, to immerse the specimen into the suspension under low gas pressure [Fig.4-5(a)]. Inside the chamber, the Ti foil with TNTs was hanged over the Ag NPs suspension with an opened bottle of acetone inside. When the chamber was vacuumed, due to its high vapor pressure, acetone began to boil. After a few minutes, the atmosphere in the chamber was replaced from air into acetone vapor [Fig. 4-5 (b)]. Then, with the low gas pressure, in this acetone vapor atmosphere, the TNTs were immersed into the suspension [Fig. 4-5 (c)]. After that, when the chamber was back to air pressure, the acetone vapor inside the TNTs dissolved into the water and the aqueous suspension could fill into the inner space. A Pt counter electrode and the Ti foil were connected to an AC/DC power supply (EC750S, NF©) [Fig. 4-5 (d)].

4.2.4 Electrophoretic deposition with different voltage conductions

By the reason of the negative surface polarity of the Ag NPs (-45mV), the Ti foil was connected to the positive pole and the counter electrode to the negative. Driven by the electric field, the Ag NPs were pushed towards the TNT arrays and filled inside them [Fig.2. (d)]. After taking EPD for 30 min, the specimen was ultrasonically washed by water for 10 s to move away the piled Ag NPs on the top of TNTs. Since the water electrolysis took place when DC > 3 V or AC > 5 V, 2 V DC and 4 V AC were employed for the maximum applied voltages during the EPD. Detail conditions are given in the following in Table 4-1. To measure the exact amount of Ag NPs which have been filled into the TNT arrays, each specimen (cut to be 1 cmx1 cm) has been independently immersed into 100 ml 0.1 M nitric acid at 40°C for 1h with stirring, to dissolve the Ag from metal NPs into ions. Then, the solution was analyzed with Atomic Absorption Spectroscopy (AAS, AA-660, Shimadzu©).

4.2.5 Dye-sensitized solar cells fabrication

Fig.4-6 shows the molecular structure of dye N-719 (<u>Di-tetrabutyl ammonium cis-bis(isothiocyanato) bis (2,2′-bipyridyl-4,4′-dicarboxylato) ruthenium(II)</u>) and the back illuminated DSSCs fabricated by a common method [22-24]. Acting as the photo anode, TNTs/Ag NPs were immersed into dye N-719 solution (0.3 mM in acetonitrile and tert-butanol solution,1:1 volume) for 24 h to absorb dye molecules on the surface. Briefly, Pt sputtering coated ITO glass was used as the counter electrode. The thickness of the Pt layer was a little less than 10 nm for sufficient transmission of incident light. A piece of polymer spacer was melted between the photo anode and the counter electrode for bonding them together to form a cell. Finally, DSSC was accomplished after the I^{3-}/I^- electrolyte containing I^2, LiI, 1-butyl-3-methylimidazolium iodide and 4-tert-butylpyridine, has been injected into the empty cell. The detail of component of the electrolyte is given in Table 4-2, the molecular structure of 1-butyl-3-methylimidazolium iodide and 4-tert-butylpyridine are given in Fig. 4-7. All chemicals above are produced by Wako©.

4.3 Results and discussion

4.3.1 Characterization on silver nanoparticles

SEM of Ag NPs is given in Fig.4-8 (a) with the photo of just prepared Ag NP suspension insect. The average size of Ag NPs is around 25 nm. At this size of the particles, suspension normally shows yellow or blown color (depends on the concentration). Our suspension shows a very dark blown color because the concentration is too high. While it would become yellow when being diluted. It also shows that the Ag NPs have a tested zeta potential of -43.3 mV which made the suspension to be very stable. Fig.4-8(b) is the TEM image of Ag NPs. The size is coincided with the SEM image. Inset of Fig.4-8(b) is the electron diffraction pattern of Ag NP. The well-ordered diffraction pattern proved that each Ag NP is a single crystal.

XRD pattern [Fig.4-9] was measured by spin coating the Ag NP suspension onto a slide glass and well dried. according to the PDF-87-0717 of silver, the mean peaks with the 2θ of 38.1°, 44.3°, 64.4°, 77.5° and 81.5° are all well matched. An impure peak at 36.3° appears which would come from the unreacted material or the aluminum holder of the XRD machine. The result of XRD proved that the product of nanoparticles is almost Ag NPs. Also they are hardly oxidized in the air atmosphere.

4.3.2 Characterization on TiO$_2$ nanotubes

Fig.4-10 gives the SEM images of as prepared TNTs. For the first anodization, the surface of TNT array was very mess [Fig.4-10(a)]. Because before the anodization the surface of Ti metal was not smooth enough. Meanwhile, the 2nd anodized TNTs shown a very beautiful surface morphology [Fig.4-10(b)], with each pore size around 80 nm. The reason can be explained that after being anodized for the 1st time and removed the first generated oxide layer, there leaves array of concaves which are used to be the interface between the metal and TNTs (insect of Fig.4-10(b)). The 2nd anodized TNTs growing on that surface would guarantee that the surface of TNT array shows a thin, well-ordered pore structure. The top view of the array looks more like "pores" but not "tubes". Because during the anodization, there was a porous layer generated on the top of the nanotubes. In our case the thickness of the layer was very thin (around 20 nm) [4-25]. Additionally, the pores were all big enough ($\approx$80 nm) for Ag NPs to pass through. So the top layer was considered to be inoffensive. The thickness of TNT array was approximately 13 μm judging from the image of Fig.4-10(c). The diameter of TNT was around 100 nm [Fig.4-10(d)].

Crystallization of TNTs were tested by XRD, [Fig. 4-11]. Before being heat treated, the XRD pattern only shows the peaks of Ti metal, with 2θ of 35.1°, 38.4°, 40.2°, 53.0°, 62.9° and 70.7°. No peaks of TiO$_2$ can be tested out. That means the as prepared TNTs are amorphous state. After

being heated at 450 °C for 2 h, in the XRD pattern, strong peaks of anatase appeared, with 2θ of 25.0°, 37.0°, 37.9°, 38.6°, 48.2°, 54.2°, 55.2° and etc.. All the peaks on the XRD pattern completely match the PDF-card of anatase and Ti phase. That means there is no rutile phase of TiO_2 generated, The temperature during the heat treatment is not high enough for the anatase to transfer into rutile (normally the anatase transfer into anatase above 700 °C)

4.3.3 Results of electrophoretic deposition

Fig.4-12 is the Ag NPs filled TNTs array (sample a. in Table.1) from top and cross view (mechanically cut by a scissor), respectively. Inset image of Fig.4-12(a) is a EDX spectrum of TNTs-Ag NPs. It can be clearly observed that of Ag NPs have been achieved both on the top layer and inside the TNT array. According to the EDX measurement, peaks of silver can be observed at 3.1 eV. The peaks of silver are weak because the total amount of silver relatively low comparing to the TiO_2.

Fig.4-13 is the TEM images of Ag NPs filled TNT arrays with different magnification. In Fig.4-13(a), all the Ag NPs are attached on the wall of nanotubes, which proved that the particles are not only filled outside the tube wall but also inside each nanotube. Fig.4-13(b) shows that both TiO_2 and Ag NPs are crystalline.

To test the distribution of Ag NPs in TNTs, TEM-EDX mapping is shown in Fig. 4-14. As a result, at the different area of TNTs, the signal of Ag can be test out from the mapping. That means by using the EPD method, the Ag NPs can reach the bottom of the TNT arrays.

Calculated Ag amount per unit area of TNT arrays for different EPD conditions is given in Fig. 4-15. From the results of sample b., c. and d., when the AC voltage increased, more Ag NPs were filled into TNT arrays. Since the free space is very narrow for Ag NPs to passing through, frictional resistance from each tubes and the water viscous resistance are

attempting to drag all the particles. Thus, for sample c, when AC voltage was added, particle movement was accelerated periodically to carry higher kinetic energy to overcome the resistance. For the particles which stuck inside the TNTs, if AC voltage is higher than DC, such as sample b., there should be a "withdraw" movement in each period. That may help the particles escape from the jammed locations and try to move forward again. Meanwhile, effect coming from frequency can be judged from samples b, e and f, which share same volt but different frequency. As a result, applied voltage with lower frequency showed to be more effective than higher ones. The reason can be explained that voltage with lower frequency would have longer time working on particles in each period. Therefore, these particles would have higher speed to move deeper. Same explanation can be applied for the reason why square wave was better than sinusoidal wave (samples a and b). For square wave, much kinetic energy can transfer into particles for its geometrical difference from sinusoidal wave. As the AAS results showed that sample a was the one which carried most Ag NPs, it was decided that sample a would be used as a typical TNTs-Ag NPs for future analysis. Meanwhile, sample g, which was not pretreated by acetone vapor, gave the lowest Ag amount. Thus, the acetone pretreatment was proved to be necessary before EPD process.

4.3.4 Performance of dye-sensitized solar cells

Abs(absorption) spectra of samples applied at DC 2V + square waved AC 4V with different EPD time (15 min, 30 min, 60 min) was evaluated by the of UV-vis measurement, shown in Fig.4-16. After being filled with Ag NPs, in the range of 410 nm to 540 nm, there was a conspicuous increase in the Abs. As the EPD time increasing, more Ag NPs were attached on TNTs. So the absorption peak became more obviously around 490 nm due to the LSPR of Ag NPs. After the dye adsorption, highest visible light absorption sample was the one with 30 min EPD. When EPD time increased to 60 min, the Abs. decreased. The reason may because that too many Ag NPs on the TNTs would decrease the surface area of TiO_2. Therefore, less dye molecules were adsorbed.

Photocurrent-voltage characteristics of the DSSCs separately using TNTs-Ag NPs at applied voltage of DC 2V + square waved AC 4V with different EPD time are exhibited in Fig.4-17. Their performance parameters were measured and given in Table 4-3. It is clear that compared with the one without Ag NPs, after being filled with Ag NPs, the short-circuit photocurrent per unit area (J_{sc}), open-circuit photo-voltage (V_{oc}), power conversion fill factor (FF) and efficiency (ɳ) were all increased. The one with EPD time of 30 min showed highest efficiency of 5.01%, which is a relatively high level for back illuminated DSSCs [4-26~28]. That was a 35% performance improvement than the one without Ag NPs.

Higher performances DSSCs made by TNTs/Ag NPs can be attributed to following reasons: first, the increase of J_{sc} was attributed to the enhanced light absorption (given in Fig.4) due to the LSPR. That means the dye molecules can be more stimulated to generate more charge carriers. Besides, the Schottky barrier at the interface of Ag and TiO_2 prevents the recombination of photoelectrons inside TNTs and oxidized species (I^{3-}) in the electrolyte. Therefore, the transfer of electrons inside the TNTs would be benefited. Also, the V_{oc} increased due to the slowdown of electron-oxide recombination. In addition, the Ag NPs can make the photo anode system has larger electron storage capability for the quasi-Fermi energy of Ag/TiO_2 tends to shift to negative level comparing with pure TiO_2, which leads to a higher V_{oc}. However, in the case of the one with 60 min EPD, although its J_{sc} and V_{oc} still increased, the efficiency decreased to 4.62%. The reason can be attributed to the less light absorption in Fig. 4-16. Also it can be expanded that too many Ag NPs inside the TNT array could block the circulation of I^{3-}/I^- electrolyte and caused uneven concentration of it. Thus, it gave lower efficiency and lower fill factor than the one with less Ag NPs.

4.4 Conclusion

Suspension of Ag NPs with the average size of 25nm and Zeta-potential of -43.3mV was prepared. Ag NPs filled TNTs were prepared by the EPD method. TNT arrays with a thickness of 13μm were achieved by anodizing Ti foils. Ag NPs were made by chemical reduction of silver nitrate. During the EPD process, DC 2V + square waved AC 4V with frequency of 1 Hz was proved to be most effective applied voltage according to the results of AAS quantitative analysis. Meanwhile, an acetone vapor pretreatment was necessary before EPD. Back illuminated DSSCs were fabricated by the TNT arrays with different EPD time. With addition of Ag NPs, J_{sc} and V_{oc} were increased due to the LSPR and slowdown the charge recombination. Meanwhile, the efficiency increased to 5.01% with 30 min EPD time. It decreased to 4.62% for the excess Ag NPs when the EPD time was 60 min. Therefore, using EPD to make TNTs-Ag NPs was approved to be a promising method to enhance the performance of DSSCs.
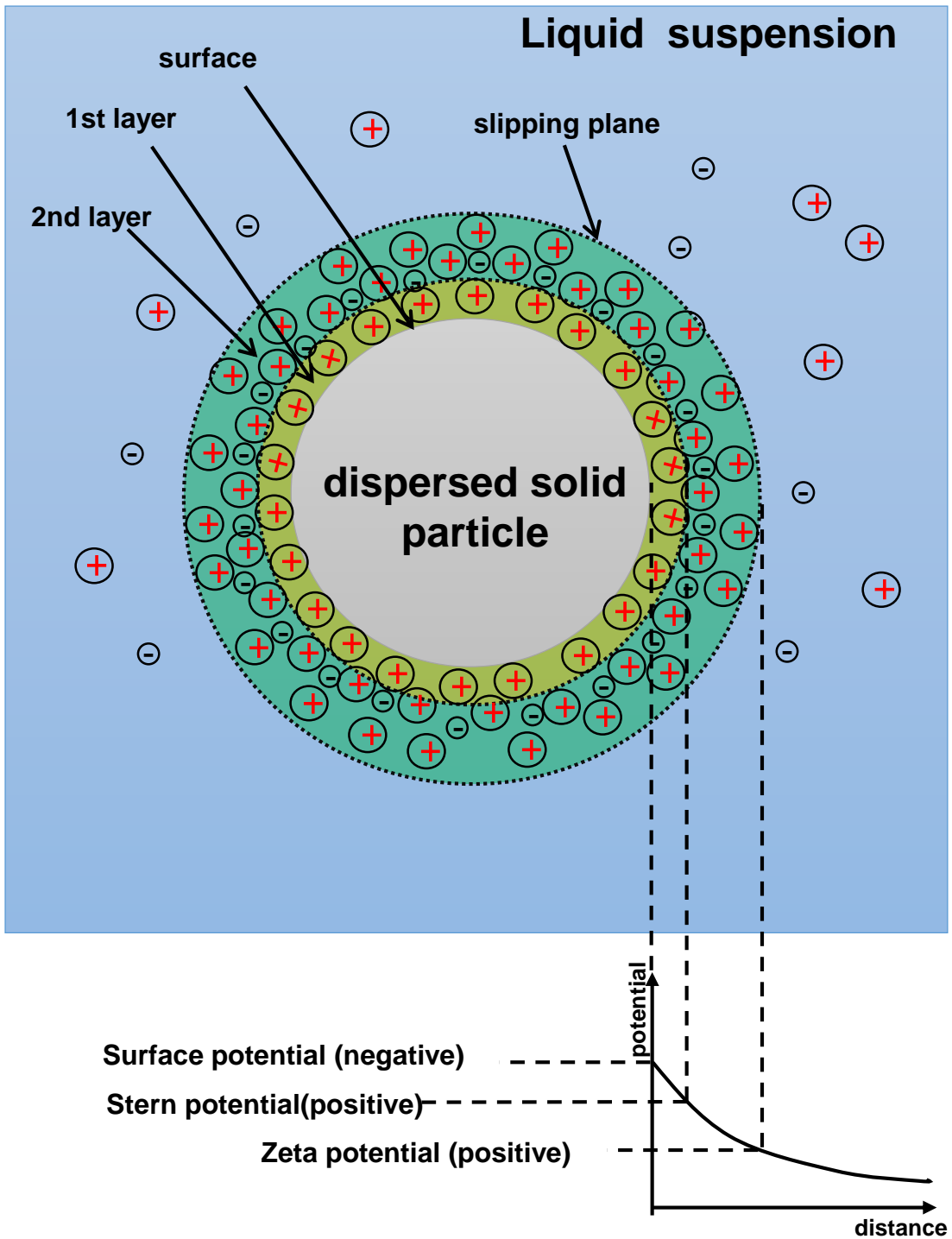
Fig.4-1: Diagram of a suspended particle with a positive Zate-potential.
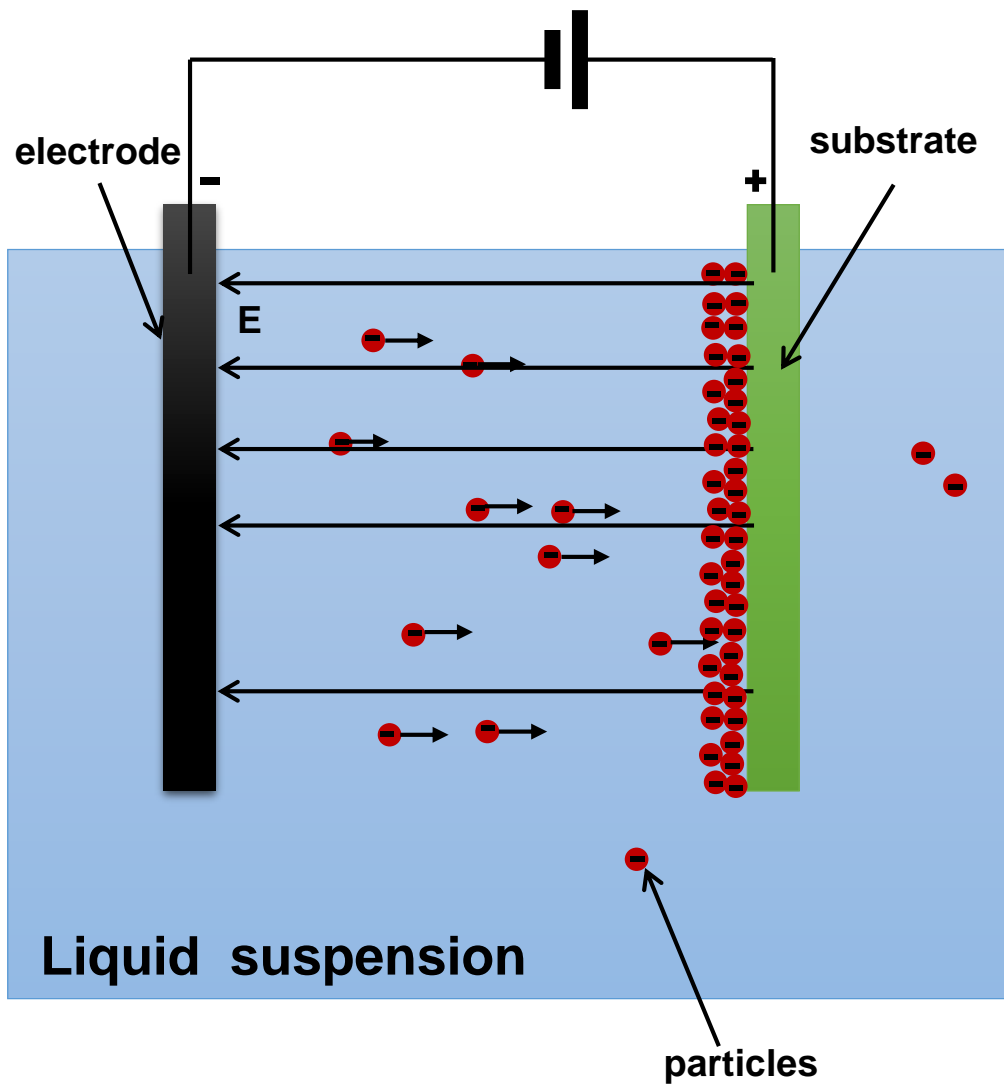
Fig.4-2: Schematic of electrophoretic deposition.
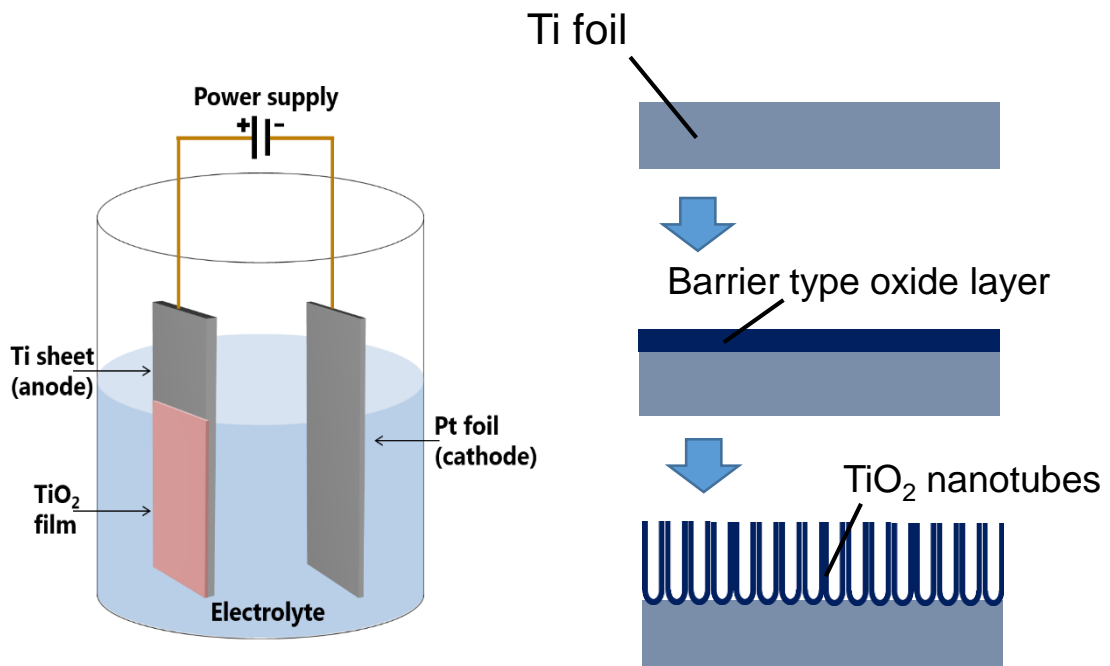
Fig.4-3: Schematic of the anodization method used to form TNTs.
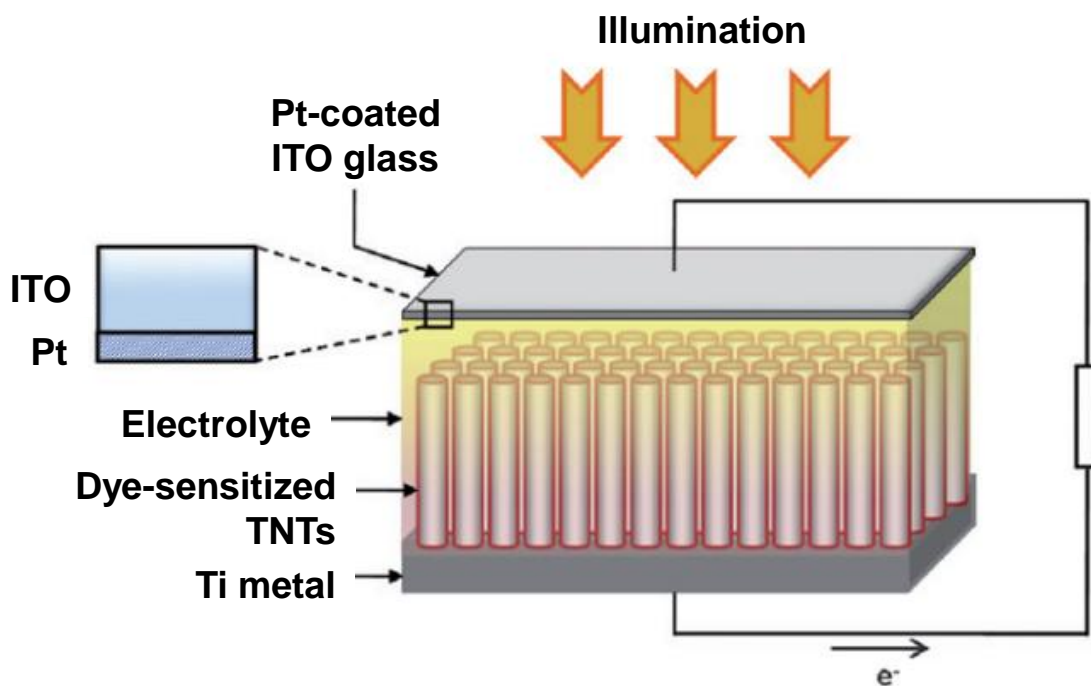
Fig.4-4: Schematic of the DSSCs assembly that consisted of by anodized TNTs.
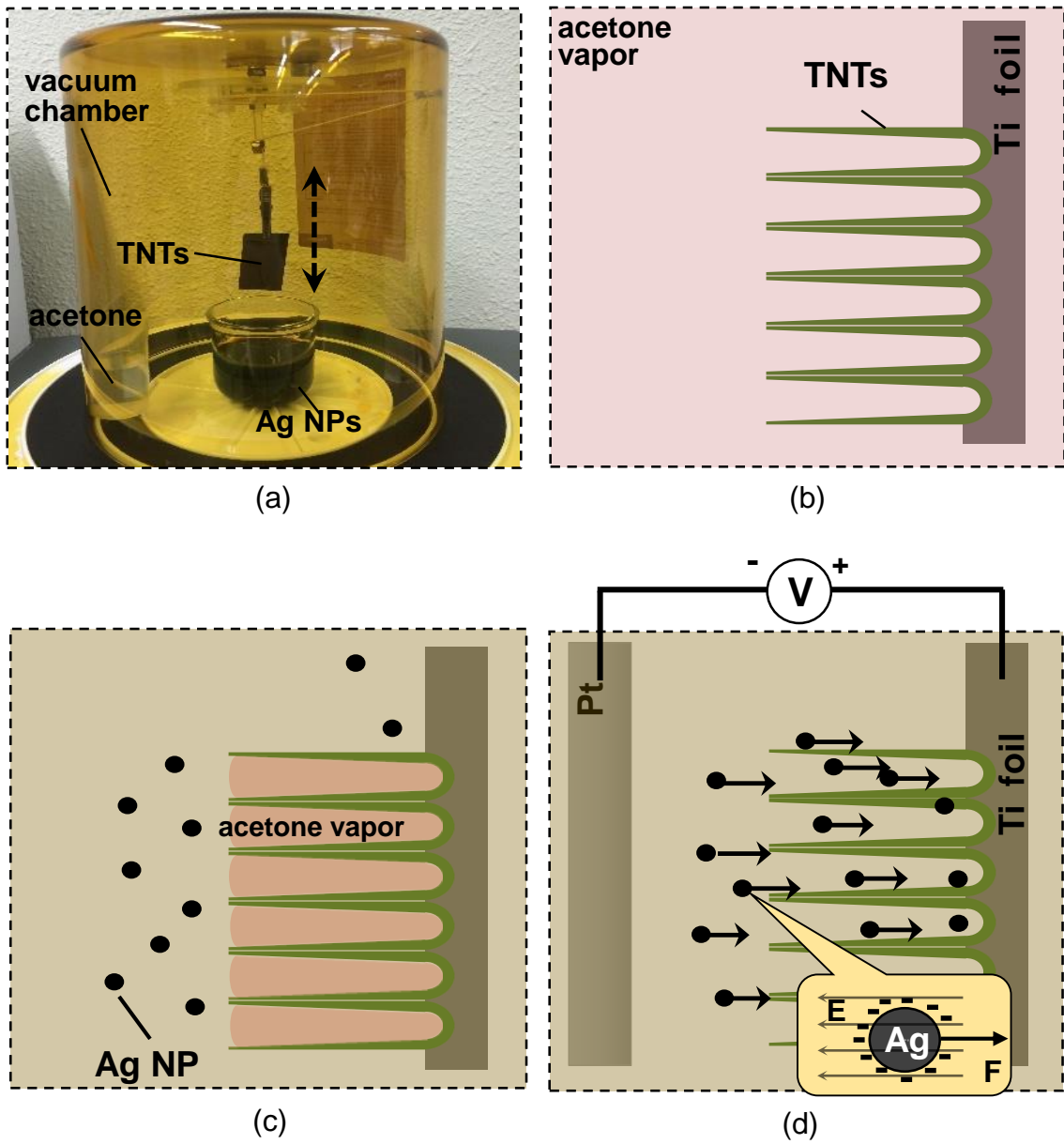
Fig.4-5: (a) Image of vacuum chamber for acetone vapor pre-treatment; (b,c) schematic diagrams of the pre-treatment and (d) EPD of Ag NPs.

Table 4-1: EPD conductions for 30 min with different applied voltage.

Samples \ Conditions	DC (V)	AC (V)	Wave type	Freq.(Hz)
a	2	4	square	1
b	2	4	sine	1
c	2	2	sine	1
d	2	0	sine	1
e	2	4	sine	2
f	2	4	sine	10
g (without acetone vapor pretreated)	2	4	square	1

Dye N-719
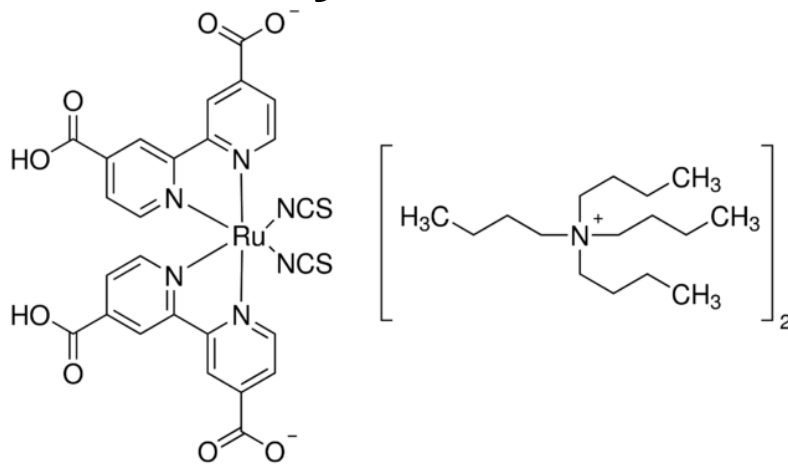
Di-tetrabutylammonium cis-bis(isothiocyanato)bis(2,2′-bipyridyl-4,4′-dicarboxylato) ruthenium(II)

(a)

Electrolyte

ITO glass

Spacer

TNTs

Ti

Ø =1.2 cm
A = 0.9 cm²
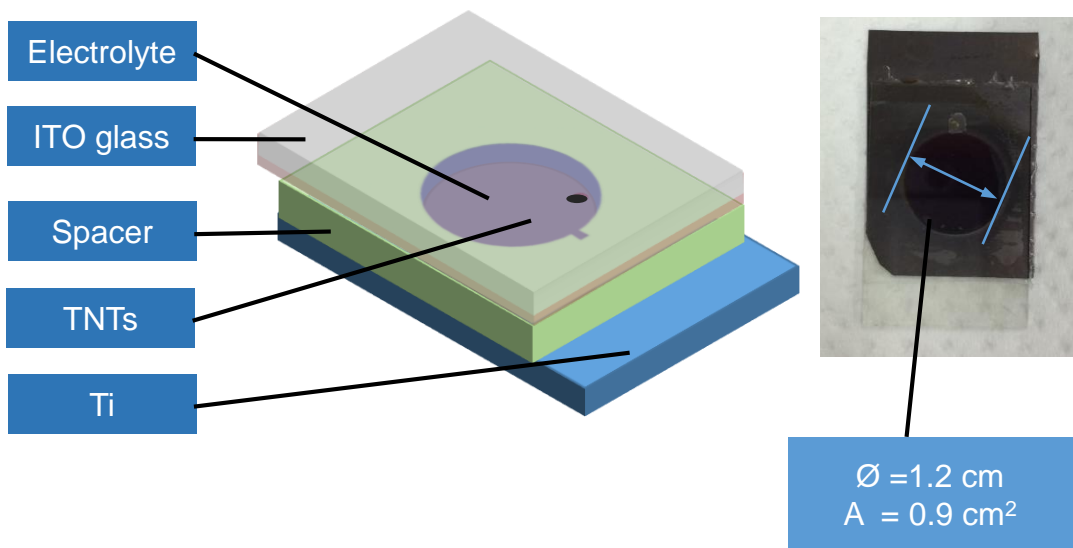
(b)

Fig.4-6: (a) Molecular structure of dye N-719 and (b) back illuminated DSSCs that consisted of anodized TNTs (b).

Table 4-2: Composition of the electrolyte.

Chemical	Concentration (mol/L)
I_2	0.05
LiI	0.1
1-butyl-3-methylimidazolium iodide	0.6
4-tert-butylpyridine	0.5
Solvent: Acetonitrile	
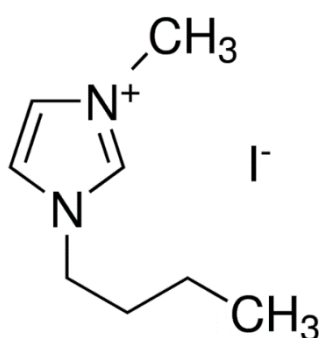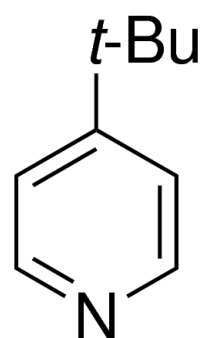
1-butyl-3-methylimidazolium iodide   4-tert-butylpyridine

Fig.4-7: Molecular structure of 1-butyl-3-methylimidazolium iodide and 4-tert-butylpyridine.
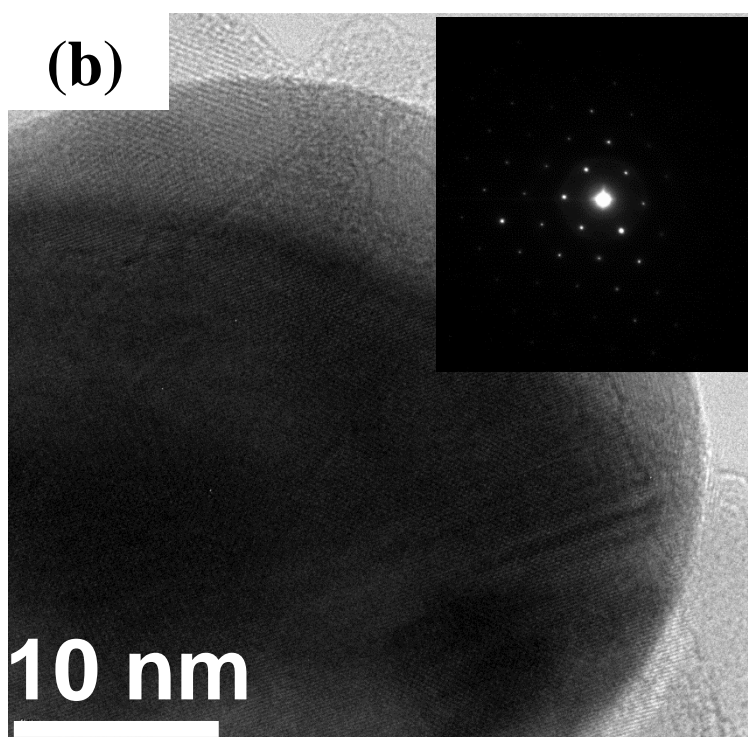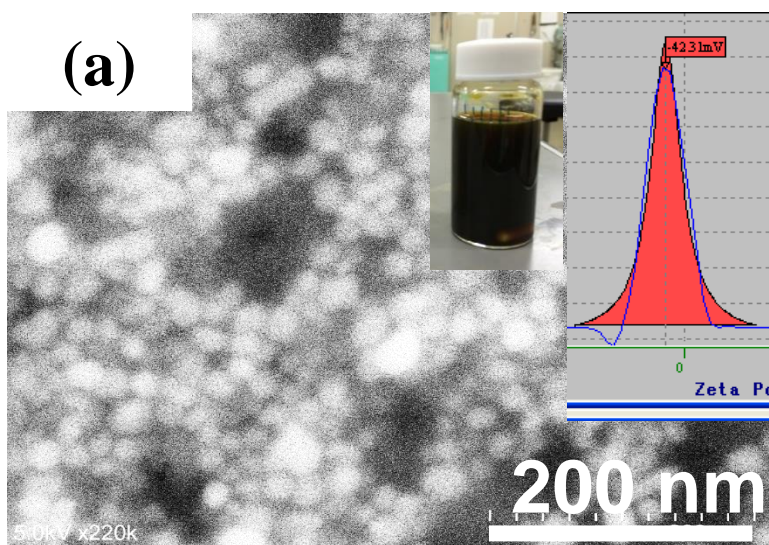
Fig.4-8: (a) SEM and (b) TEMimages of Ag NPs, inset of (a) is the image of the as-prepared Ag NPs suspension and tested Zeta potential, while inset of (b) is the electron diffraction pattern of a Ag NP.
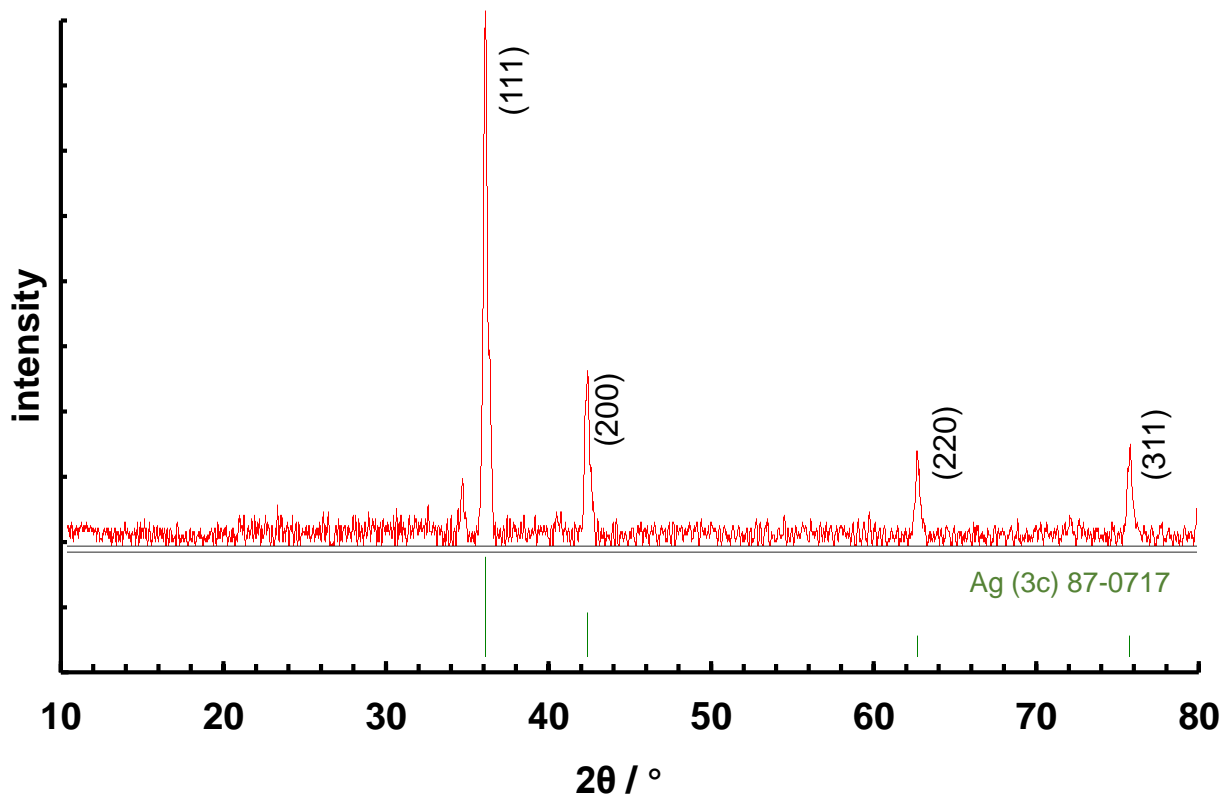
Fig.4-9: XRD pattern of Ag NPs.
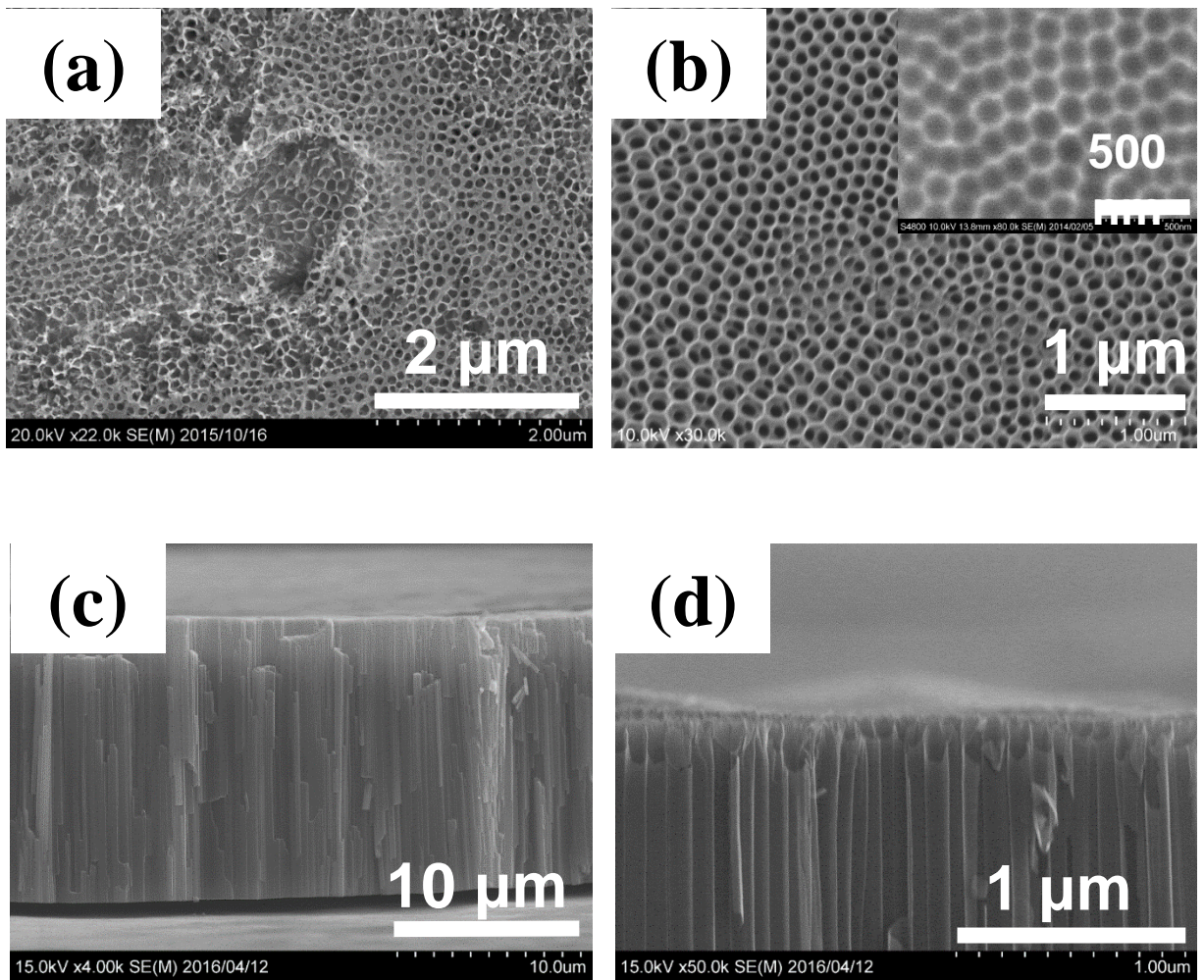
Fig.4-10: Top view of the TNT arrays obtained after the (a) 1st and (b) 2nd anodization step; (c) cross section of the TNT film on Ti foil; (d) top area of the TNT film (inset of (b) is the surface of Ti metal after the removal of 1st TNTs.)
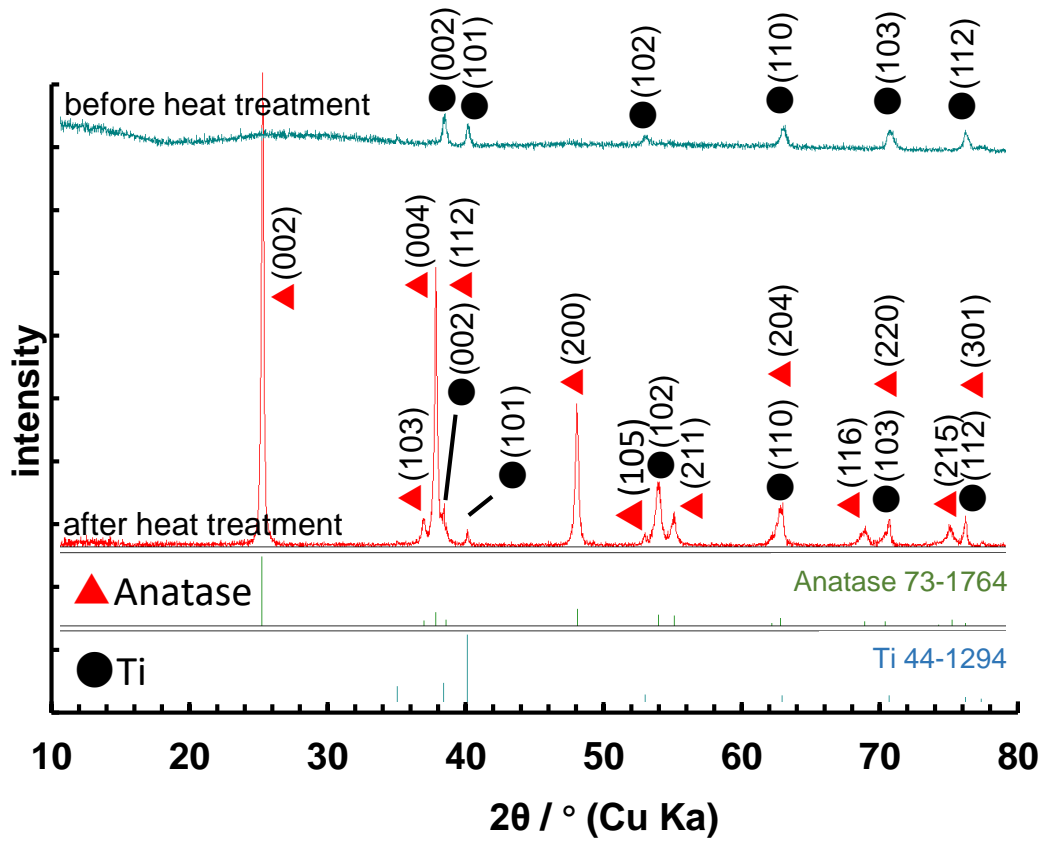
Fig.4-11: XRD patterns of TNTs before and after heat-treatment at 450°C for 2h. (standard pattern of anatase and Ti are also included)
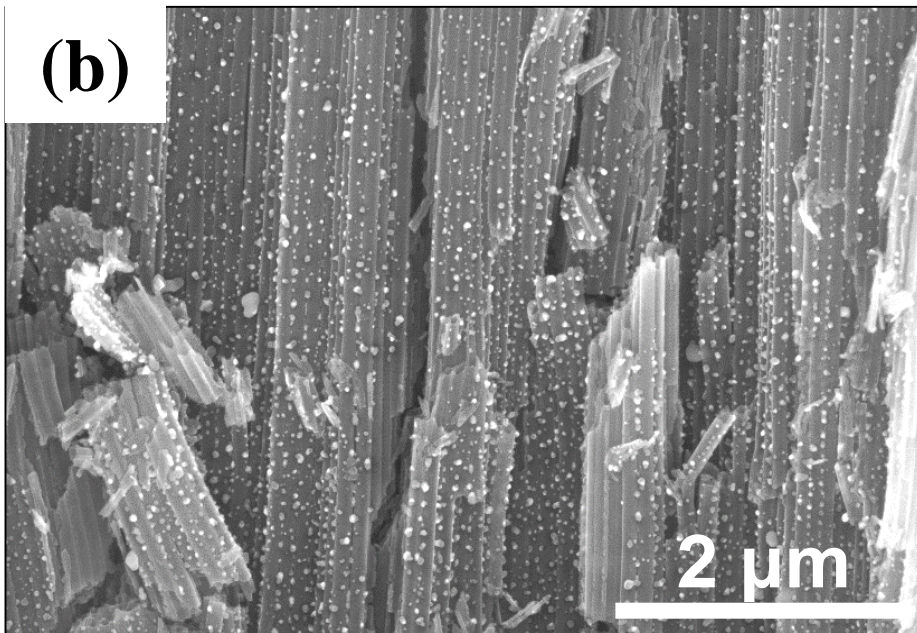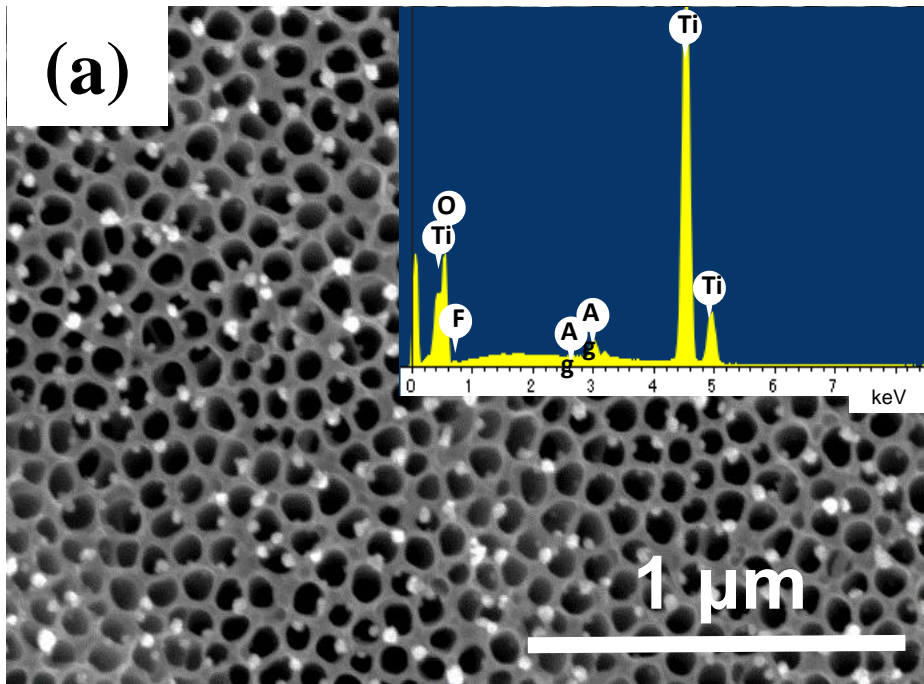
Fig.4-12: SEM images of TNTs - Ag NPs obtained by EDP with DC 2V + AC 4V, 1Hz, square wave for 30min (sample a in Table 4-1), (a) top view and EDX results(inset) and (b) cross-sectional view.
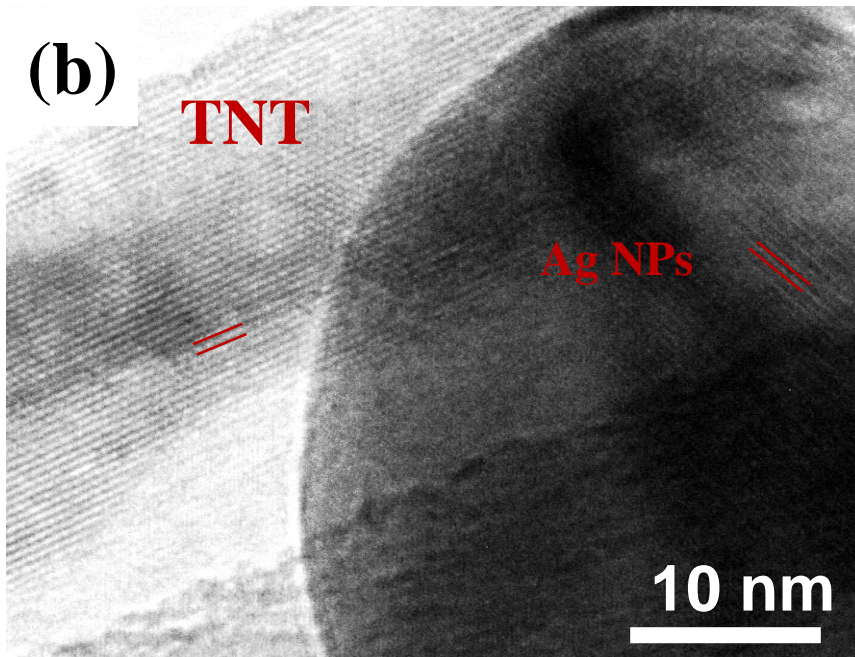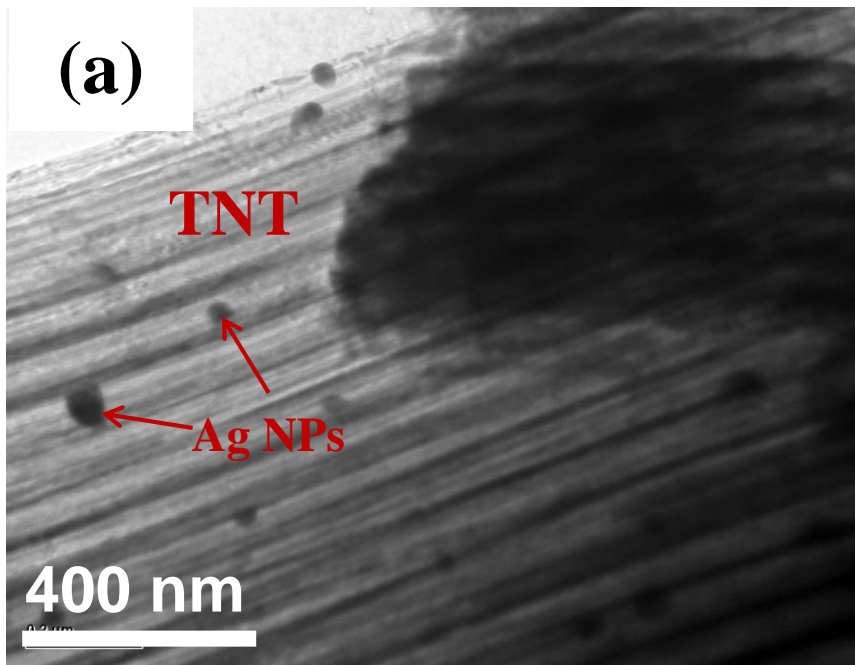
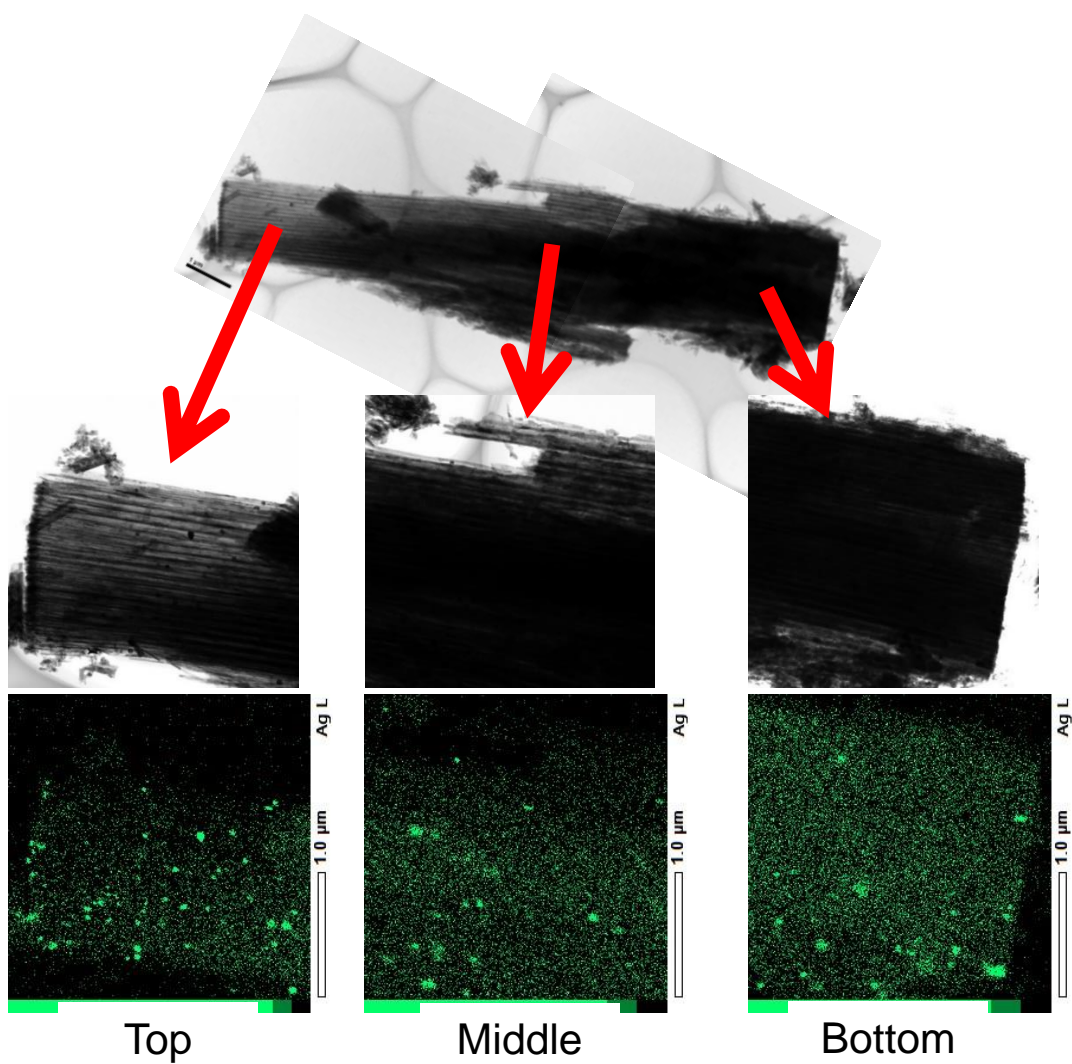Fig.4-13 TEM images of TNTs - Ag NPs with different magnification.

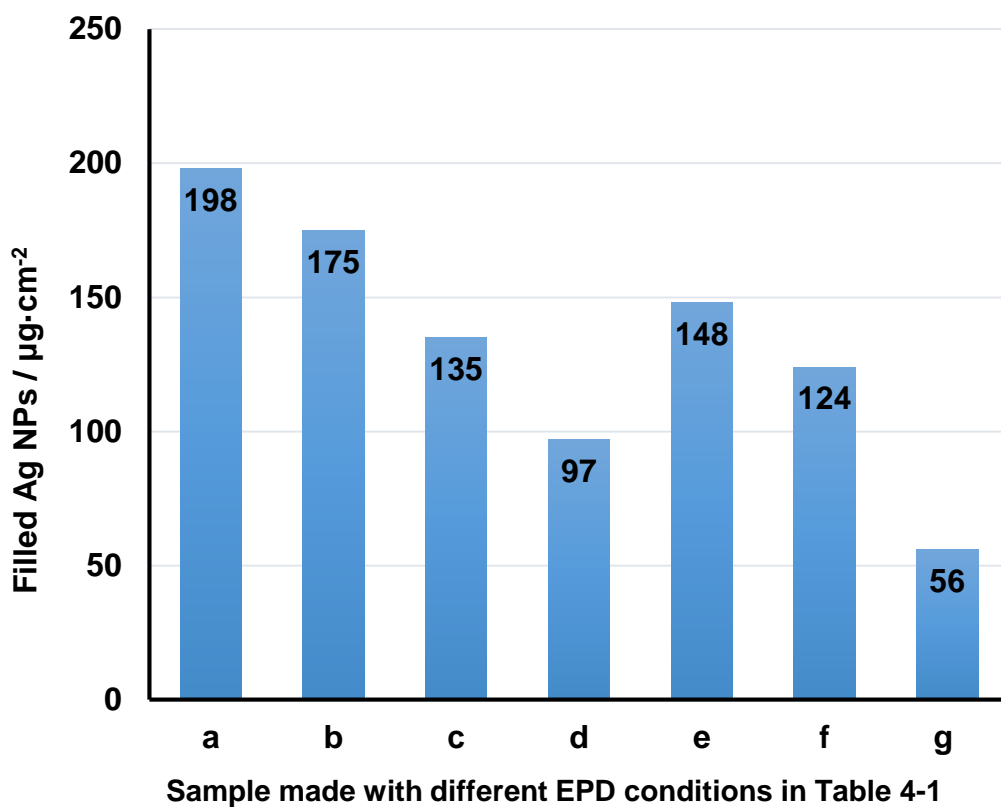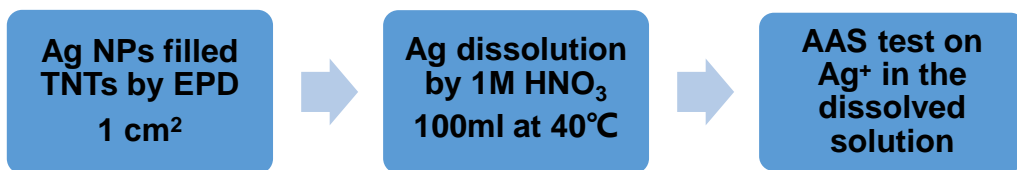Fig.4-14: TEM-EDX mapping of different area of the Ag NPs filled TNTs.

Fig.4-15: AAS quantitative analysis procedures and results for samples obtained by different EPD conditions as in table 4-1.
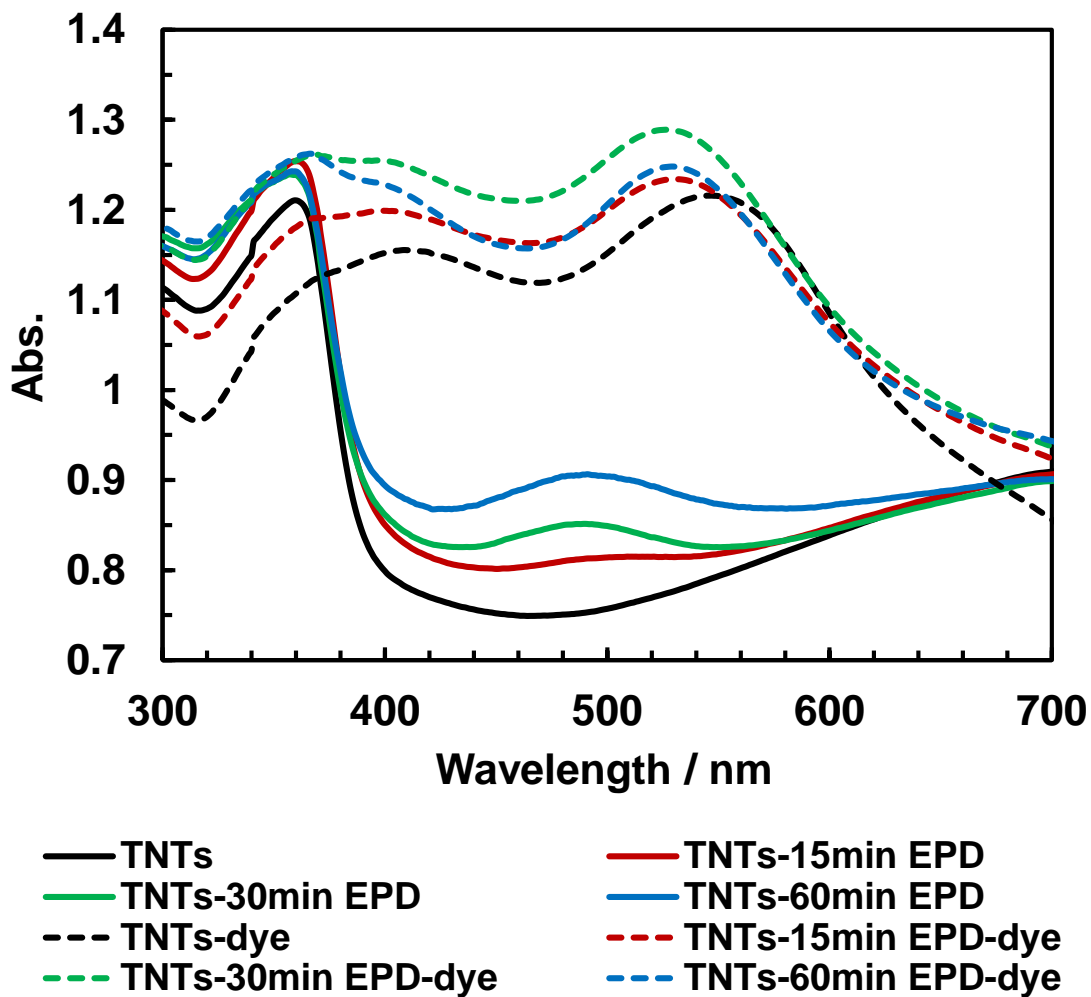
Fig.4-16: UV–Vis absorption spectra of TNTs/Ag NPs with different EPD time by applying 2V DC + 4V AC, before (solid line) and after (dash line) dye adsorption.

Table 4-3: Tested performance parameters of DSSCs with different EPD time with the applied voltage of 2V DC + 4V AC.

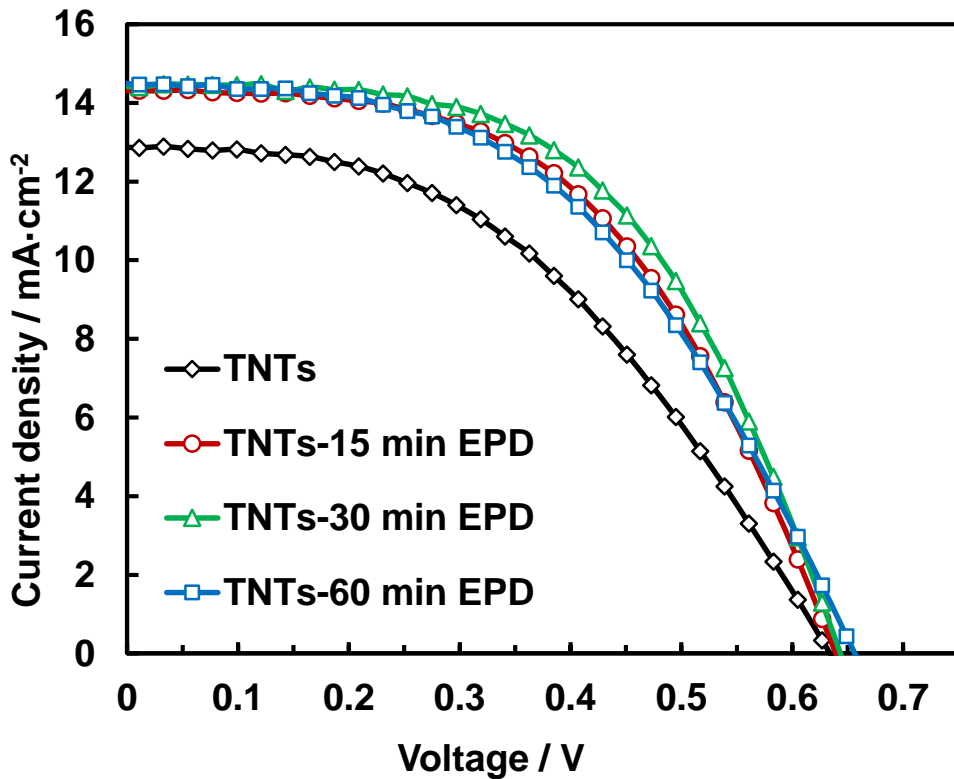| DSSCs made by:	J_{sc} (mA/cm^2)	V_{oc} (V)	FF (%)	η (%)
TNTs	12.87	0.634	0.45	3.7
TNTs-15min EDP	14.31	0.639	0.52	4.76
TNTs-30min EDP	14.42	0.643	0.54	5.01
TNTs-60min EDP	14.49	0.656	0.49	4.62

Fig.4-17: Photocurrent-voltage characteristics of the DSSCs using TNTs-Ag NPs with different EPD time with the applied voltage of 2V DC + 4V AC.

References of chapter 4

4-1	IUPAC. Compendium of Chemical Terminology, 2nd ed.(the "Gold Book"), A. D. McNaught and A. Wilkinson, 464 pages, ISBN: 0-9678550-9, Blackwell Scientific Publications, USA (1997).
4-2	Ueber einige Gesetze der Vertheilung elektrischer Ströme in körperlichen Leitern mit Anwendung auf die thierisch-elektrischen Versuche, H. Helmholtz, Annalen der Physik und Chemie, 165 (6), 211-233 (1853).
4-3	Effect of Short Chain Aliphatic Carboxylic Acids for Sorption of Uranyl on Rutile Zeta Potential and in situ ATR-FTIR Studies, B.K. Singh, F.M. Bion, G. Lefevre, and E. Simoni, Journal of Industrial and Engineering Chemistry, 35, 325-331 (2016).
4-4	Influence of Shrinkage and Water Transport Mechanisms on Microstructure and Crack Formation of Tile Adhesive Mortars, A. Wetzel, M. Herwegh, R. Zurbriggen, and F. Winnefeld, Cement and Concrete Research, 42, 39-50 (2012).
4-5	Electrodeposition of Coatings, Editor(s): G.E.F. Brewer, American Chemical Society, ISBN: 978-0-8412-0161-3 (1973).
4-6	Glucose Microbiosensor Based on Glucose Oxidase Immobilized by AC-EPD: Characteristics and Performance in Human Serum and in Blood of Critically Ill Rabbits, M. Ammam, and J. Fransaer, Sensors and Actuators B: Chemical, 145, 46-53 (2010).
4-7	Decomposition of Formaldehyde by EPD Photocatalyst Filters in HVAC, C.C. Chen, C.S. Jwo, and T.P. Teng, Particuology, 9, 497-501 (2011).
4-8	Paint and Coating Testing Manual (14th Edition), K.V. Joseph, 950 pages, ISBN: 978-0-8031-2060-0, ASTM International, USA (1995).

4-9	Preventing Sodium Poisoning of Photocatalytic TiO_2 Films on Glass by Metal Doping, M.E. Kurtoglu, T. Longenbach, and Y. Gogotsi, International Journal of Applied Glass Science 2, 108-116 (2011).
4-10	Discovery and Applications of Photocatalysis - Creating a Comfortable Future by Making Use of Light Energy, A. Fujishima, Japan Nanonet Bulletin Issue 44, page.72-150 (2005).
4-11	The Electrical Conductivity of Titanium Dioxide, M.D. Earle, Physical Review, 61, 1-2 (1942).
4-12	Preparation of N-Functionalized TiO_2 Particles Using One-Step Sol–Gel Method and Their Photocatalytic Activity, I. Jang, H.J. Leong, H, Noh, T. Kang, S. Kong, and S.G. Oh, Journal of Industrial and Engineering Chemistry, 37, 380-389 (2016).
4-13	Defect Study of TiO_2 Nanorods Grown by a Hydrothermal Method through Photoluminescence Spectroscopy, M. Rajabi, S. Shogh, and A.I. Zad, Journal of Luminescence, 157, 235–242 (2015).
4-14	Formation of Double-Walled TiO_2 Nanotubes and Robust Anatase Membranes, S.P. Albu, A. Ghicov, S. Aldabergenova, P. Drechsel, D. LeClere, G.E. Thompson, J.M. Macak, and P. Schmuki, Advanced Materials, 20, 4135-4139 (2008).
4-15	Different TiO_2 Nanotubes for Back Illuminated Dye Sensitized Solar Cell: Fabrication, Characterization and Electrochemical Impedance Properties of Dsscs, M.M. Momeni, and M.G. Hosseini, Journal of Materials Science: Materials in Electronics, 25, 5027-5034 (2014).
4-16	A 4.2% Efficient Flexible Dye-Sensitized TiO_2 Solar Cells Using Stainless Steel Substrate, M.G. Kang, N.G. Park, K.S. Ryu, S.H. Chang, and K.J. Kim, Solar Energy Materials and Solar Cells, 90, 574-581 (2006).
4-17	TiO2 Nanotubes: Synthesis and Applications, P. Roy, S. Berger, and P. Schmuki, Angewandte Chemie International Edition, 50, 2904-2939 (2011).

4-18	Effect of Electric Field Strength on the Length of Anodized Titania Nanotube Arrays, L. Sun, S. Zhang, X.W. Sun, and X. Dong, Journal of Electroanalytical Chemistry, 637, 6-12 (2009)
4-19	Magnetic Properties of Fe Deposited into Anodic Aluminium Oxide Pores as a Function of Particle Size, D. AlMawlawi, N. Coombs, and M. Moskovits, Journal of Applied Physics, 70, 4421 (1991).
4-20	Tracer Investigation of Pore Formation in Anodic Titania, D.J. LeClere, A. Velota, P. Skeldon, G.E. Thompson, S. Berger, J. Kunze, P. Schmuki, H. Habazaki, and S. Nagata, Journal of The Electrochemical Society, 155, C487-494 (2008).
4-21	A Novel Approach to Titania Nanowire Arrays as Photoanodes of Back-Illuminated Dye-Sensitized Solar Cells, R.H. Tao, J.M. Wu, H.X. Xue, X.M. Song, X. Pan, X.Q. Fang, X.D. Fang, and S.Y. Dai, Journal of Power Sources, 195, 2989-2995 (2010).
4-22	Photo-Electrochemical Cells, M. Grätzel, Nature, 414, 338-344 (2001).
4-23	Photocatalytic Events of CdSe Quantum Dots in Confined Media Electrodic Behavior of Coupled Platinum Nanoparticles, C. Harris, and P.V. Kamat, ACS Nano, 4, 7321-7330 (2010).
4-24	High Performance Dye-Sensitized Solar Cells (Dsscs) Achieved via Electrophoretic Technique by Optimizing of Photoelectrode Properties, M. Hamadanian, A. Gravand, and V. Jabbari, Materials Science in Semiconductor Processing, 16, 1352-1359 (2013).
4-25	Reparation and Enhanced Properties of Dye-Sensitized Solar Cells by Surface Plasmon Resonance of Ag Nanoparticles in Nanocomposite Photoanode, K. Guo, M. Li, X. Fang, X. Liu, B. Sebo, Y. Zhu, Z. Hu, and X. Zhao, Journal of Power Sources, 230, 155-160 (2013).
4-26	Highly Defined and Ordered Top-Openings in TiO_2 Nanotube Arrays, S.P. Albu, and P. Schmuki, Physica Status Solidi, 7, 151-153 (2010).

4-27	An Insight into the Optical Properties of Cdse Quantum Dots during Their Growth in Bovine Serum Albumin Solution, A. Singh, M. Ahmed, A. Guleria, A.K. Singh, S. Adhikari, and M.C. Rath, Journal of Luminescence, 179, 122-131 (2016).
4-28	Photoassisted Platinum Deposition on TiO_2 Powder Using Various Platinum Complexes, J.M. Herrmann, J. Disdier, and P. Pichat, The Journal of Physical Chemistry A, 90, 6028-6034 (1986).

General conclusion

The main motivation of this research work is to investigate the controllable wettability/surface potential and application in optical and electrochemical devices. This controllable wettability/surface potential has a great prospect in the application of new surface technology. By using sample preparation methods such as sol-gel coating, EPD, and anodization, specimens with nano-sized structure (multilayered films or nano-tubes) were prepared. Based on the results obtained from various tests on these specimens, stable liquid lens driven by EWOD and DSSCs made from Ag NPs-TNTs are fabricated. Their performances were also evaluated and analyzed.

The results and discussion are summarized as follow:

In the first study, the wettability of Nafion film was found to be controllable by the applied voltage: CA could be reduced when the water droplet was loaded with a positive DC due to its "flip-flop" property. To study the effect of the applied voltage on this phenomenon, we used multilayered thin films of 67 nm Nafion / 150 nm TiO_2 / 110 nm Pt coated on silicon wafer by sol-gel dip coating. The results showed that when a water droplet was loaded on positive DC with voltage higher than 2 V, due to the strong attraction force towards the sulfonic top groups, unwinding of the branched chains in the polymer film becomes enhanced. A decrease

in CA to a minimum of 20° could be obtained in two minutes. Conversely, a negative DC voltage inhibits the "flip-flop" property by giving repulsive force towards the sulfonic groups. This controllable "flip-flop" property would be useful in many applications. For example, the switchover of hydrophilic/hydrophobic surface can be used in oil-water separation inside water pollution treatment facilities. Also, as Nafion is now being commonly used as an ion exchange material, it has potential to control the ion permeability by changing its wettability,

In the second study, electrowetting property on dielectric multilayered thin films was investigated. Multilayered thin films of 50 nm Teflon / 160 nm TiO_2 / 80 nm Al_2O_3 / on ITO glass prepared by sol-gel methods were used as the basic EWOD solid films. TiO_2 layer and Al_2O_3 layer were added to increase the dielectric constant and dielectric strength, respectively. By measuring the CAs with different applied voltages, we found that negative DC was more stable than positive DC. In addition, by testing the leakage current during the electrowetting, the most suitable working voltage was obtained to be -10 V DC. In dodecane atmosphere, the CA of a water droplet on Teflon surface was controlled from 155° to 67° by loading with -10 V DC without any electric breakdown. It was also proven that under this voltage, the stability could reach over 1800 loading periods. Based on those results, a liquid lens was assembled by coating

the same multilayers on the inner wall of a tiny glass tube (inner diameter: 4 mm). The curvature of the water-oil interface inside the tube can be adjusted using applied voltage. So that the focal length could be controlled by applying different voltage. When the voltage changed from 0 V to -10 V, the focal length changed from -2 mm to +10 mm, with the numerical aperture changed from 0.21 to 1.38. Until now, an EWOD liquid lens which has such focal length changing range under low necessary working voltage is unusual. In addition, sol-gel dip coating process is not only a simple manufacture method, but it also makes it possible to achieve uniform coating on the inner wall of the tube. EWOD liquid lens has good potential to be used in mobile device replacing traditional solid lens.

In the final study, Ag NPs modified by carboxy methylcellulose with high Zeta-potential of -43.3 mV were prepared. At same time, the TNTs with a thickness of 13 μm were grown by anodizing Ti foils. A unique pretreatment using acetone vapor was taken to remove the air inside the nano-structures. Then, EPD was employed to fill the TNT arrays with Ag NPs. A combination of +2 V DC and square waved 4 V AC with a frequency of 1 Hz is found to be the most effective applied voltage for EPD according to the results obtained by quantitative analysis of deposited Ag NPs. Results of SEM and TEM-EDX mapping showed that the distribution of Ag NPs was relatively uniform inside the TNT arrays.

By using this nano-composite as the photo anode, back illuminated DSSCs were fabricated. Due to the surface plasmon resonance effect, the efficiency of DSSCs increased from 3.70% to 5.01% after filled with Ag NPs obtained by 30 min of EPD time. The increment is relatively high for a back illuminated DSSCs. These simple solar cells which can be easily manufactured with low cost have a promising future to replace the expensive Si-based solar cells that are commonly used today. In addition, these methods (acetone vapor treatment and EPD) not only could be used as steps to enhance the performance of solar cells but also to make other nano-composite materials. For example, it would be possible to make new kinds of solid electrode/electrolyte in battery by filling nano-sized catalyst particles into porous matrix.